Multimodal Sensory Control of Exploration by Walking *Drosophila melanogaster*

Thesis by

Alice Anne Pennoyer Robie

In Partial Fulfillment of the Requirements

for the Degree of

Doctor of Philosophy

California Institute of Technology

Pasadena, California

2010

(Defended May 5, 2010)

to my grandfathers

R T Pennoyer (1907-2004)

J W Robie (1919-2001)

whose intellectual curiosity was an inspiration

Acknowledgments

First, I would like to thank my advisor, Michael Dickinson, without whom this thesis would not have been possible. His scientific curiosity and guidance allowed me to navigate largely uncharted waters and he encouraged me to discover my own path.

I would like to thank the rest of my committee, David Anderson, Mark Konishi, Mark Frye, and for a time Gilles Laurent, for their time and keen scientific feedback.

I would particularly like to thank Andrew Straw, whose scientific generosity and range of skills continue to amaze me and without whose dedication to software development for behavioral experiments this work would not be possible. I would also like to thank my collaborators on the multiple fly tracking project, Kristin Branson and Pietro Perona, who reminded me that other people could be interested in walking flies and opened up a whole new world of behavior analysis to me.

This work would not have been accomplished without the all the members of the Dickinson laboratory over the years, who created an environment of intellectual richness, rigor and camaraderie. In particular, I would like to thank the early Caltech crew who introduced me to the world of power tools, Matlab and fly wrangling, Seth Budick, Mike Reiser, Rosalyn Sayamon, Will Dickson and Mark Frye; Martin Peek who provided assistance at the beginning with arena building and at the end with

the gluing of fly antennae under a microscope; Andrew Straw, Gaby Maimon and Wyatt Korff who were always willing to answer a 'quick' question that turned into an hour long discussion; my fellow graduate students, Gwyneth Card and Jasper Simon, whose fellowship and scientific suggestions and discussions were excellent and greatly appreciated; Allen Wong who was generous and patient teaching genetics to me; Akira Mamiya for his quiet expertise; and last, but certainly not least, the new school: Peter Weir, Marie Suver, Floris van Fleugel and Francisco Zabala, my late night lab companion, who all provided fresh perspective and enthusiasm to the lab.

Additionally, I would like to thank Michael Dickinson, Andrew Straw, Kristin Branson, Gaby Maimon, Allen Wong, Akira Mamiya, Francisco Zabala, Holly Beale and Susan Robie for feedback on and assistance with the production of this dissertation.

Finally, my parents who created the foundation from which everything becomes possible and who have shown unwavering support and patience overs the years.

This work was supported by the National Institutes of Health.

Abstract

Walking fruit flies, *Drosophila melanogaster*, use visual information to orient towards salient objects in their environment, presumably as a search strategy for finding food, shelter or other resources. Less is known about the role of vision or other sensory modalities in the evaluation of objects once they have been reached. In order to study these behaviors, I developed a large arena in which I could track individual fruit flies as they walk through either simple or more topologically complex landscapes. Flies use visual cues from the distant background to stabilize their walking trajectories. When exploring an arena containing objects, flies actively orient towards, climb onto, and explore the objects, spending most of their time on the tallest, steepest object. A fly's behavioral response to an object's geometry depends upon the intrinsic properties of each object and not an assessment relative to other nearby objects. Further, the preference is due to a change in locomotor behavior once a fly reaches and explores the object's surface. Specifically, flies are much more likely to stop walking for long periods on tall, steep objects. Both the visual and the antennal mechanosensory systems provide sufficient information about an object's geometry to elicit the observed change in locomotor behavior. Only when both these sensory systems are impaired do flies not show the behavioral preference for the tall, steep objects. Additionally, I

examined the locomotor and social behaviors of large groups of flies. In order to do these studies, I assisted in the development of automated software for tracking and maintaining the individual identity of large groups of flies and for the quantification of individual flies' locomotor and social behaviors. Behavioral differences between individuals are consistent over the time of the trials and are sufficient to predict a fly's gender (male vs. female), genotype (wild type vs. *fruitless*), or sensory environment (with vs. without visual cues). During encounters, males approach other flies more closely than do females and are most often located behind the other fly. The software developed is publicly available and represents a new level of automated quantification in behavioral studies of flies.

Contents

List of Figures

List of Tables

Acronyms

2D 2-dimensional.

3D 3-dimensional.

AC alternating current.

AMMC antennal mechanosensory and motor center.

CCD charge-coupled device.

CPG central pattern generator.

CPU central processing unit.

CX central complex.

fps frames per second.

GUI graphical user interface.

HR high-resolution.

IR infrared radiation.

JO Johnston's organ.

LED light-emitting diode.

LR low-resolution.

PID proportional-integral-derivative.

TE thermoelectric.

TRP transient receptor potential.

UV ultraviolet.

Chapter 1

Introduction

The distribution of organisms in the environment is not uniform or normal. This is because resources, essential to the survival and reproduction of organisms, are found in patches (Bell, 1991). Organisms use cues from the environment to find and utilize these clustered resources. Indeed, the need to search effectively for resources has undoubtedly been a major selective pressure in the evolution of sensory systems and behavior (Bell, 1991; Nation, 2008).

Dusenberry provides a useful framework in which to consider the study of behavior that he calls the 'hierarchical pyramid' (Dusenbery, 1992); this is the idea that the behavior of an individual can be studied at many levels. Figure 1.1 extends Dusenberry's pyramid to include the modern focus on the cellular, molecular, chemical and physical levels in the study of nervous systems. Dusenberry states, 'At any given level, questions about mechanism have answers referring to the next lower level, and questions of function have answers referring to the next higher level.' The work in this thesis generally falls under sensory ecology; it is largely concerned with resource localization, for which we look to the 'locomotion' level for mechanisms and 'survival and reproduction' level for function. My purpose in studying behavior is to gain insight into how the nervous system produces behavior.

Drosophila melanogaster, the fruit fly, is an excellent model organism in which to study behavior for a variety of reasons. It is an insect, and insects are highly successful; they represent more than half of all known living organisms. They have evolved a large array of sensors with which to transduce information from the environment into their nervous system, and they will readily behave in the laboratory in

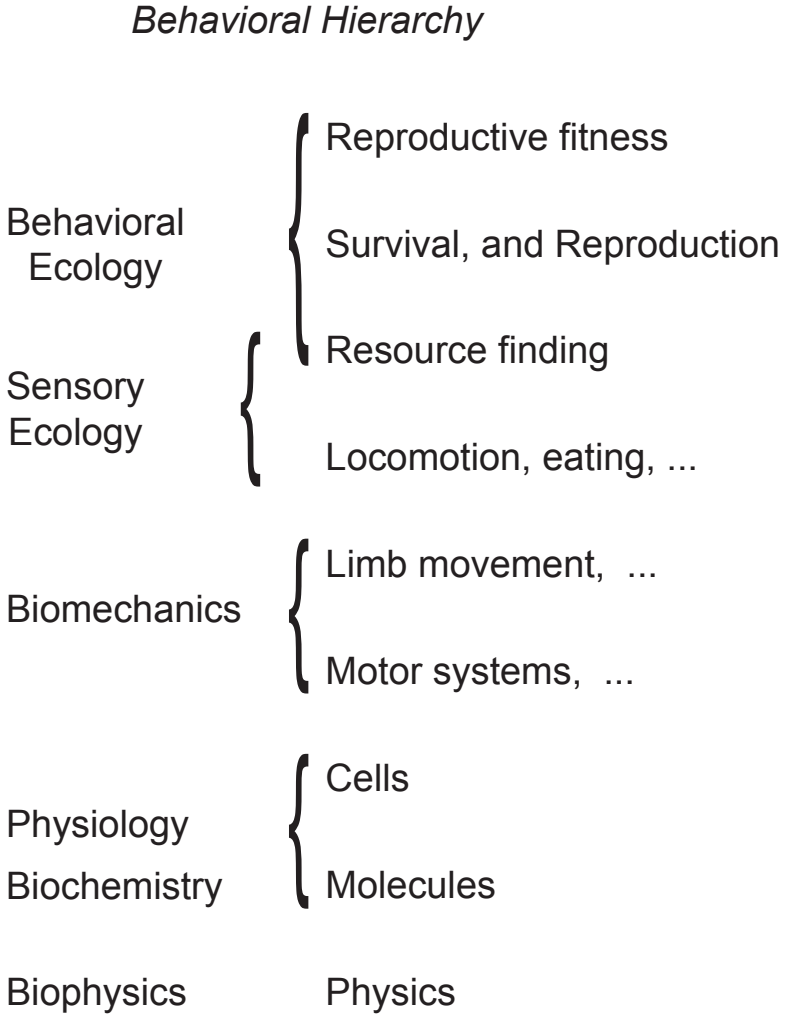

Figure 1.1: The scales at which behavior can be studied. Modified from Dusenbery (1992).

reduced sensory landscapes. Extensive research has been done on the nervous system of *Drosophila*, which is relatively simple compared to that of a vertebrate and contains identifiable neurons that can be studied across individuals. The fruit fly became a model system because of its small size, a fast generation time, behavior in the laboratory setting, and its amenability to genetic manipulations. Genetic manipulation is what catapulted it into the 'excellent' model organism category. The genetic toolkit available to map and manipulate circuits in the nervous system in the fly is unprecedented. The current state-of-the-art of these tools was recently reviewed by Holmes et al. (2007), Simpson (2009), and Zhang et al. (2007). The development of electrophysiological preparations in the brain of intact adult flies (Wilson et al., 2004) during behavior (Maimon et al., 2010) only increases its utility. For these reasons I chose to study the exploratory behavior in the fruit fly.

1.1 Resource localization

'Resources' can mean many things to a fruit fly including food, mates, oviposition sites or refugia. These resources provide many different cues the flies can use to improve their exploration success. These stimuli have different qualities of spatial extent, directionality, intensity, etc. A recurrent theme in exploratory behavior is the use of different sensory modalities for different stages of the search sequence. For example, olfactory or visual cues may guide an animal toward a goal over a long distance whereas tactile and gustatory cues are more important once an animal is in contact with a potential resource. Directed movement in response to a stimulus is

termed taxis whereas non-directional change in movement patterns is termed kinesis (Fraenkel and Gunn, 1961). Goal directed search behaviors such as object fixation or tracking an odor plume are taxes. Local search, by contrast often includes kinesis. For example, walking, hungry flies that have encountered a sucrose patch decrease their forward velocity and increase their rotational rate (Bell, 1985). Local search can, however, also involve taxes. For example, a male fly that sees a another fly will orient visually towards it and then tap in order to sense female cuticular hydrocarbons with the gustatory sensors on his tarsi (Ritchie, 2008). In the absence of any cues, animals may perform ranging search, which can consist of a random walk in which turn and distance between turns may be randomized, or straight line search where animals move in a straight line for a randomly determined length of time (Bell, 1991). These search behaviors would have to be internally generated if indeed no sensory cues were available in their environment. Götz and Beiesinger reported an increase in mean free path length in walking flies exploring an empty arena which was not seen when olfactory, visual or temperature cues were present (Götz and Biesinger, 1985a,b). This increase in path length between turns is consistent with a random walk exploration in the absence of salient cues. Reynolds and Frye (2007) report that during flight inter-saccade intervals, in the absence of cues, are sampled from a Lèvy distribution rather than a Gaussian distribution, which is the assumption of the random walk. Theoretically, sampling from the longtailed Lèvy distribution would more efficiently move flies further from their starting point. Flies have been seen to disperse long distances over relatively short time periods in capture-release-recapture

experiments (Coyne et al., 1982), however the mechanisms of this dispersal have not been determined.

In a natural setting, there are many cues about the environment that flies can sense. These include volatile and non-volatile chemicals, light, temperature, humidity, gravity, wind, and sound. Flies can also sense the relative location of their body parts through their proprioceptive neurons and noxious stimuli via nociceptors. I will discuss the role of vision and graviperception in controlling behavior in more detail below, as these are cues I manipulated in my studies of exploration behavior.

1.2 Graviperception and gravity responses

Gravity is a unique environmental cue for motile organisms on Earth, since it provides a constant reference stimulus. Most organisms have evolved sensory systems to detect the gravitational vector and use this information to structure their behavior. All vertebrates, and many marine invertebrates including those of the subphylum Crustacea, sense gravity with a statocyst-type organ. This consists of a field of mechanosensory cells that are deflected by the movement of a mass due to gravity. This statocyst-type mechanism is used in the vestibular system of the inner ear in mammals. Until recently, most invertebrates were thought to sense gravity mainly by means of dispersed sensory bristles and joint position sensors (reviewed by Beckingham et al. (2005) and Bender and Frye (2009)). More recent studies in *Drosophila melanogaster* have demonstrated a role for the Johnston's organ (JO) (a specialized mechanosensory organ located in the antenna) in graviperception (Kamikouchi et al., 2009; Sun

et al., 2009), a role that had been suggested in earlier invertebrate studies (reviewed by Schneider (1964); Armstrong et al. (2006); Baker et al. (2007)). As Beckingham et al. (2005) suggested, I will follow the convention of describing responses to gravity with the prefix 'gravi-,' which correctly refers to the influence of gravitational force rather than 'geo-,' which implies an influence of the Earth.

The walking fruit fly, *Drosophila*, does use gravity to orient its behavior. The earliest report, according to Greenspan (2008), of behavioral responses to stimuli in a *Drosophila* species included negative gravitaxis (Carpenter, 1905). Hirsch and colleagues used gravitational responses of fruit flies in a vertical choice maze to demonstrate the genetic heritability of behaviors (Hirsch, 1959; Hirsch and Eerlenmeyer-Kimling, 1962; Hirsch and Ksander, 1969). Flies are also known to respond to agitation by walking up against the gravitational force (negative gravitaxis) (Beckingham et al., 2005). This has been quantified using numerous apparatus usually resulting in a score of how many flies cross a fixed height on the wall of a cylinder after being tapped to the bottom within a given time period. A more quantitative method measures negative gravitaxis using the countercurrent device (Inagaki et al., 2010). This device was developed by Benzer (1967), in order to fractionate fly populations based on their phototactic response by repeatedly testing the flies' distribution in a tube following mechanical agitation. These assays both convolve abnormal locomotor function and graviperception. However, phototaxis can be used as a positive control for normal locomotion. These assays have been used to successfully gain insight into the flies' gravitational sensory system as discussed below. However, they do not mea-

sure the full range of the flies' response to gravity and more refined assays might be needed to gain insight into the subtleties of neuronal function in gravitation-based behaviors.

It is probable that multiple mechanisms provide walking fruit flies with information about the gravitational vector (reviewed by Beckingham et al. (2005) and Bender and Frye (2009)). The loading of the leg joints due to the body mass is measured by mechanosensory bristles that sense joint position and stretch receptors in the joint cuticle. The deflection of the head-body position due to the mass of the head can be measured by the prosternal organ, a field of mechanosensory hairs between the head and body. More recently it has been proposed that the third antennal segment deflects relative to the second due to gravity and that this is sensed by antennal mechanosensors. This third mechanism has been shown to play a dominant role in the negative gravitaxis behaviors in walking flies. The structure and function of the antennal mechanosensory systems is discussed below.

The insect antennae contain diverse sensory neurons that are involved in sensing sound, wind, gravity, chemicals, temperature and humidity (Schneider, 1964). I will focus on the mechanosensory function of the antennae. All of the winged (subclass Pterygota) and some of the wingless (subclass Apterygota) insects have flagellar-type antennae composed of the scape (first antennal segment or a1), pedicel (second antennal segment or a2) and flagellum (Schneider, 1964). In fruit flies, the flagellum is made up of the funiculus (third antennal segment or a3) and the arista (Fig. 1.2A,B). The scape-pedicel joint can be actively articulated in the both horizontal and vertical

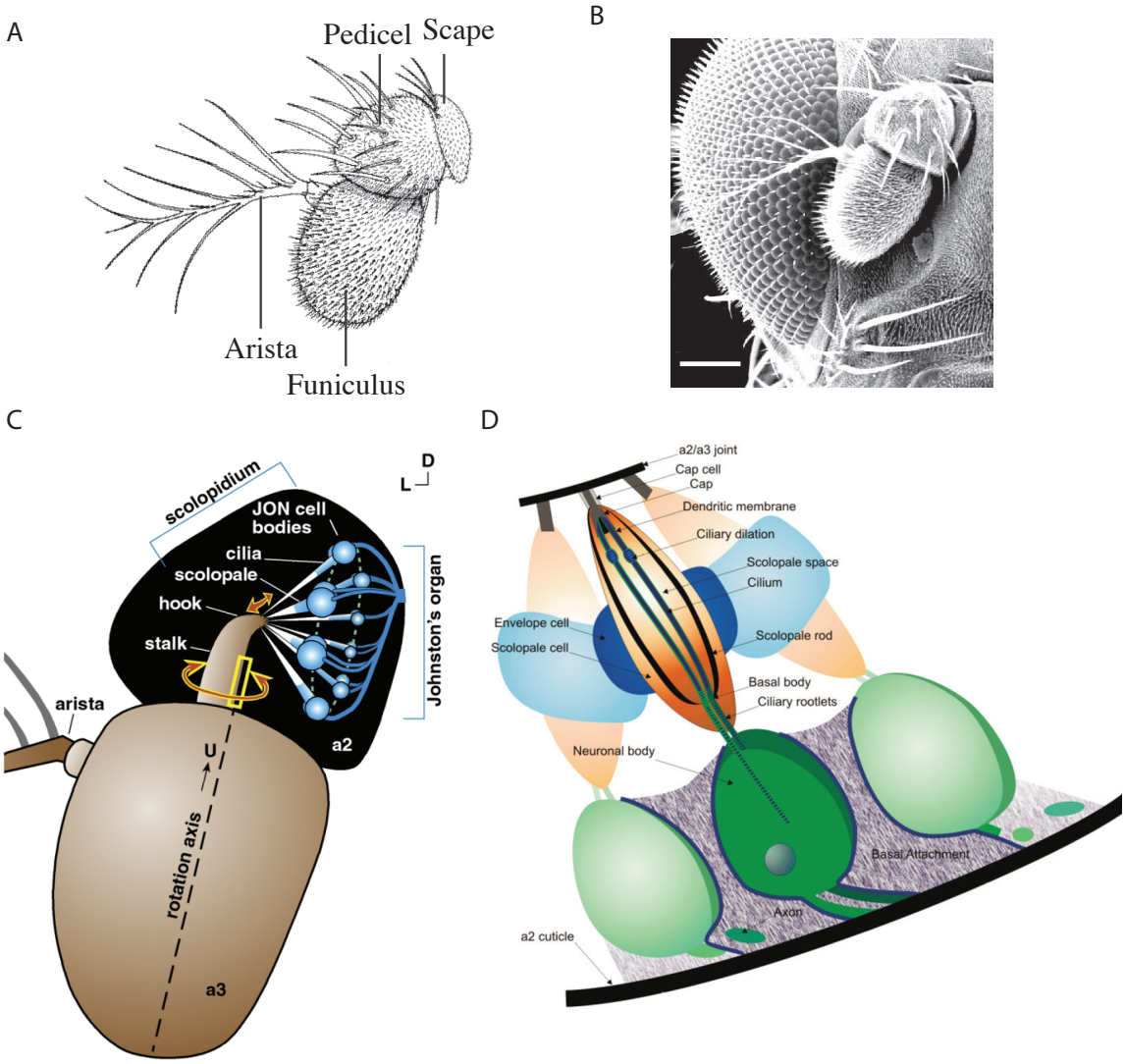

Figure 1.2: Structure of the antenna and Johnston's organ of *Drosophila melangaster*. (A) A schematic drawing of antennal structure and (B) A scanning electronmicrograph (scale bar 0.1 mm) modified from Göpfert and Robert (2002). (C) A schematic drawing of the JO reproduced from Kamikouchi et al. (2006). (D) A schematized drawing of chordotonal organs reproduced from Todi et al. (2004).

planes by two muscles, but the head-scape joint is not mobile unlike most other insects (Taylor and Krapp, 2008). The pedicel-funiculus joint fits together like a 'key and lock' as described by Göpfert and Robert (2002) in a study of anatomical serial sections of *Drosophila melanogaster* (Fig. 1.2C). The proximal end of the funiculus forms a narrow stalk and hook that fit into a deep invagination of the distal end of the pedicel. The hook projects perpendicularly to the longitudinal axis of the funiculus and joins the pedicel's cuticle creating the connection between the pedicel and funiculus (Göpfert and Robert, 2002; Kamikouchi et al., 2006). This anatomy allows both the rotation and deflection of the third antennal segment relative to the second. The arista (a lever arm) and funiculus act as a single mechanical entity that has been demonstrated to transduce air particle movement (near-field sound) such as that produced by the *Drosophila* courtship song into mechanical vibration thus sensing sound (Göpfert and Robert, 2002). This receiver unit is statically displaced by constant velocity air flow and thus can sense steady wind (Yorozu et al., 2009). Calculations based on the receiver's apparent mass suggest gravity could also produce deflections of the receiver (Kamikouchi et al., 2009). However, in what way the third antennal segment moves relative to the second under the influence of gravity has not been shown. Flies with immobilized antennae or those lacking antennae or aristae have shown functional deficits in wind responses (Budick et al., 2007; Mamiya et al., 2008; Duistermars et al., 2009; Yorozu et al., 2009), sound responses (Kamikouchi et al., 2009; Manning, 1967; Yorozu et al., 2009), and gravity responses (Kamikouchi et al., 2009; Sun et al., 2009).

The movement of the third antennal segment relative to the second segment can be sensed by the JO in fruit flies (Ewing, 1978). However, there are also many other mechanosensory cells located in and on the antenna. Bristles located between the head-scape joint and scape-pedicel joint (named Böhm bristles and identified in the order Lepidoptera; reviewed by Schneider (1964)) function as proprioceptors in other insects (Pringle, 1938). Antennal position sensation by the scape-pedicel bristles interacts with active antennal positioning and gravity sensation in walking *Calliphora* (Horn and Kessler, 1975). Additionally, a large campaniform sensilla has been reported in the antenna of *Calliphora*. It is located in the pedicel with its sensory terminal inserted near the pedicel-funiculus joint (Burkhardt and Gewecke, 1965), which makes it likely to provide information about this joint's movement. A large campaniform sensilla has also been identified in the pedicel of *Drosophila melanogaster* (A. Wong, personal communication). However, the JO has been demonstrated to have a clear role in behavioral responses to gravity by fruit flies (Kamikouchi et al., 2009; Sun et al., 2009) and the structure of the fruit fly JO is described in greater detail below.

The basic unit of mechanosensation in the Johnston's organs is the chordotonal organ (also known as a scolopidium), a stretch receptor that is composed of at least one neuron and accessory cells (Fig. 1.2D). Eberl and Boekhoff-Falk (2007) reviewed the development of chordotonal organs. The anatomy is concisely reviewed by Todi et al. (2004), which I will summarize here. The ciliated dendrite of the sensory neuron is enclosed in the scolopale space, which is enriched in potassium ions. The tips of

the cilia are embedded in the dendritic cap (extracellular matrix) and attach to the cuticle of the hook of the funiculus through the cap cell. The neuronal cell body is anchored to the pedicel wall, perhaps via ligaments that connect to apodemes (cuticular extrusions). These apical and basal attachments suspend the chordotonal organ between the exterior wall of the pedicel and the proximal tip of the funiculus such that when the funiculus is displaced relative to pedicel the array of the chordotonal organs comprising the JO are extended or compressed. However, precise orientations of the chordotonal organs attachments to the hook are not known.

The scolopidia of the Johnston's organ predominantly contain two mono-ciliated sensory neurons, however, ∼10% contain 3 neurons (Todi et al., 2004). Kamikouchi et al. (2006) elucidated the Johnston's organ anatomy comprehensively. They counted ∼480 neuronal cell bodies in the JO, which implies that it is comprised of about 227 scolopidia. These cell bodies were described to be arranged as a bottomless bowl, tilted on its side, with the opening facing laterally (Fig. 1.2C). The axons gather and project out of the pedicel at the "bottom" of this bowl whereas the ciliated dendrites (and scolopidia that contain them), are arranged like a cone with its apex at the hook of the funiculus and the base at the bowl of neuronal cell bodies (Kamikouchi et al., 2006). This semi-spherical arrangement and the neuronal sensitivity to both extension and compression suggests the JOs should be able to respond to any possible displacement direction of the third antennal segment relative to second.

Recent calcium imaging studies suggest that extension depolarizes and compression hyperpolarizes the sensory neuron of the chordotonal organ creating the mechanosen-

sory receptor potential (Kamikouchi et al., 2009). The mechanically activated ion channels in cilia are in the TRP family (Venkatachalam and Montell, 2007). Two TRPV channels (Nanchung (Nan) and Inactive (Iav)) are required for mechanosensation by all the JO chordotonal organs (Kim et al., 2003) and may form a heteromultimeric channel (Gong et al., 2004). Additionally, a TRPN ion channel, No mechanoreceptor potential C (NompC), is required in a subset of the chordotonal organ neurons for normal audition but not for sensing gravity (Eberl et al., 2000; Kamikouchi et al., 2006, 2009; Walker et al., 2000; Sun et al., 2009). Conversely, a TRPA ion channel, Painless (Pain), is required in a different subset of the chordotonal neurons for the transduction of gravity but not sound (Sun et al., 2009)[1]. This suggests subgroups of the chordotonal organs in the JO are specialized for sensing different types of movement in the pedicel-funiculus joint that can be caused by different qualities of the mechanosensory stimuli, such as amplitude, frequency and velocity.

Kamikouchi et al. (2006) also established a projection map of JO neurons from the antennae to the antennal mechanosensory and motor center (AMMC). They described five zones (further divided into 19 subareas) of the AMMC that are based on innervation by the JO neurons. They defined types of JO neurons based on their innervation of one of the five zones (A-E) and various combinations of subareas within that zone. The cell bodies of these JO neurons types are organized in the JO in either rings or paired clusters. The resolution of these definitions was limited by the specificity of the GAL4 promotor lines used for this study. However, the structure

[1]I created the transgenetic UAS-Painless flies used in this study during a rotation in the laboratory of Seymour Benzer (Al-Anzi et al., 2006)

is suggestive of functionally diverse types of JO neurons. This is consistent with the expression of different TRP channels in different subpopulations of the JO neurons. In fact, the *nompC TRPN* expressing population of JO neurons, required for hearing, are in the subgroups AB but not in CE (Kamikouchi et al., 2009). The CE subgroups are necessary for wind and gravity sensation (Kamikouchi et al., 2009; Yorozu et al., 2009), however, it has not been demonstrated which anatomically-defined neuronal subgroup contains the Pain TRPA ion channels (required for gravity sensing).

As mentioned above, other mechanosensors of the antenna, beside the JO neurons, are mostly likely involved in antennal position sensing. Neurons from the Böhm bristles are known to project to the AMMC in some insects (Nation, 2008). Kamikouchi et al. (2006) reported having to reject 66 of the 70 GAL4 promotor lines selected in their primary screen for neural fibers projecting through the antennal nerve to the AMMC due to expression in cells other than the JO neurons. Some of these rejections were due to expression in the anterior-dorsal region of the head or possibly motor neurons whose dendrites arborize in the AMMC and innervate the muscles in the antenna. However, it is likely that many of the lines represent mechanosensory neurons of the antenna, outside the JO, that project to the AMMC. It is probable that there are interactions between information from these antennal mechanosensory systems at the level of the AMMC. In fact, the JO-CE (JO-31, NP6250) GAL4 promotor line labels external sensory neurons on the second antennal segment that also project to the C and E zones of the AMMC (Kamikouchi et al., 2006) and have been used in behavioral studies of JO function (Kamikouchi et al., 2009; Yorozu et al.,

2009). A combinatorial approach with GAL4 promoter lines specific to the JO do strongly suggest a functional role for the JO neurons in sensing vibration and deflections of the antennal receiver, but as always experiments using GAL4 lines with nonspecific expression must be interpreted with some caution.

Whereas precise movements of the pedicel-funiculus joint have not been mapped directly to exact deformations of the chordotonal organs in the JO, the experimental evidence is suggestive that flies can sense the change in the relative position of this joint due to gravity. If, as suggested, the JO is the primary tranducer of such movement, it is interesting to consider how the flies would sense gravity with the JO. How could a fly tell it was facing down rather than up on an incline plane? If the fly is standing still, these two different orientations would cause different displacement of the joint due to gravity (ignoring active positioning of the antennae for this exercise). Facing down an incline would cause the third antennal segment to hang farther away from the head whereas facing up an incline would cause it to lie closer to the head. These static displacements of the funiculus would extend and compress opposing sets of the JO chordontal neurons. When the fly is changing inclination, inertia of the antenna receiver relative to the body would cause a transient change in relative motion. This was simulated experimentally using centrifugal forces due to rotation by Sun et al. (2009), who recorded units in the antennal nerve in response to rotation that were abolished by immobilization of the antennae. However, it is likely that graviperception is further complicated by active articulation of the scape-pedicel joint as was described in the responses to gravity of walking *Calliphora* (Horn and

Kessler, 1975).

In conclusion, the antennae of the fruit fly, *Drosophila melanogaster*, sense gravity. The Johnston's organ is a necessary component of gravity sensing as assayed by the bang assay (Kamikouchi et al., 2009; Sun et al., 2009) and the vertical choice maze (Sun et al., 2009). However, it is likely that other antennal and non-antennal mechanosensory neurons also sense gravity. These neurons may mediate gravitational responses not yet identified or play a non-essential role in the known gravitational responses.

1.3 Visual control of behavior

Light, in contrast to gravity, is a dynamic stimulus with many qualities (intensity, direction, frequency, polarization and wavelength) that covey information. Insects use light to control their behavior over a range of time scales. Day-night cycles in light intensity are used to control general activity levels (Konooka and Benzer, 1971). For instance, *Drosophila* has a crepuscular activity pattern; it is most active at dawn and dusk. During periods of active locomotion, flies also use visual information to localize resources. This can consist of directed responses or generalized changes in locomotor pattern (Fraenkel and Gunn, 1961; Götz, 1980). More immediate visual reflexes are involved in the stabilization of locomotion (Taylor and Krapp, 2008; Krapp, 2010).

Throughout this work I will use the terms 'visual system' and 'vision' to refer to the light sensing pathways of both the compound eye and the ocelli unless otherwise specified because, in many behaviors, their roles have not been disambiguated. The

multiple faceted compound eyes have largely been studied with regards to motion detection and processing, but they also sense color and polarization. Briefly, information flows from the retina to the optic lobes, which consist of the lamina, medulla and lobula complex (lobula and lobula plate). The structure and function of the optic lobes have been extensively studied (reviewed by Borst (2009); Nation (2008); Sanes and Zipursky (2010); Taylor and Krapp (2008)).

Projection neurons connect the optic lobes to the central brain. There are different morphologically-defined types of projection neurons that target different optic glomeruli (or foci) in the lateral protocerebrum (Otsuna and Ito, 2006; Strausfeld and Okamura, 2007). One class of projection neuron consists of the well-studied lobula plate tangential cells (LPTCs). These cells are responsive to optic flow caused by self-motion (summarized by Borst and Haag (2007)).

The ocelli are three simple eyes located on the dorsal surface of the head, two lateral and one medial. They are also responsive to visual cues of self-motion. As far as their function is understood by homology with *Calliphora*, they sense intensity differences between large regions of the visual field (Schuppe and Hengstenberg, 1993). The ocellar pathway involves fewer processing steps than the compound eyes and optic lobes pathway and is faster (Parsons et al., 2010).

Due in part to its importance as a genetic model organism, much is known about how the fruit fly uses visual information to control its behavior. Flight stabilization reflexes use information from the visual system, as well as mechanoreceptors located on the antennae, halteres and the wing hinge (reviewed by Taylor and Krapp (2008)).

Important visual course control mechanisms include optomotor responses, which are 'compensatory movements that follow displacement of the whole visual scene,' Wehner (1981). Optomotor responses to wide-field rotations have been successfully studied in tethered flight simulators. Tethered *Drosophila* exhibited changes in wingbeat amplitude in response to wide-field visual motion (Götz, 1968). These reflexes are thought to be mediated by the LPTC system (Krapp, 2010). Walking flies also display rotatory and translatory optomotor responses (Götz, 1975, 1980; Götz and Wenking, 1973; Kalmus, 1964; Katsov and Clandinin, 2008; Zhu et al., 2009).

Visual information is also used to control oriented flight behaviors such as fixation (Wehner, 1981). Tethered flying flies will fixate a vertical edge in a closed-loop flight simulator and do so for extended periods of time (Götz, 1987). Reichardt and Poggio proposed that fixation in flight can be decomposed into optomotor responses, and that it functions as another mechanism of course stabilization (Reichardt and Poggio, 1975). Horn and Wehner, inspired by Reichardt's work, demonstrated that walking *Drosophila* will turn towards and maintain a course towards a prominent visual edge (Horn, 1978; Horn and Wehher, 1975). However, these optomotor reflexes do not explain all visually controlled behavior in walking flies.

Götz and colleagues demonstrated that when choosing between a set of unattainable visual objects, flies show a preference for approaching the nearest object (when background information is available), but do not demonstrate any particular innate preference according to features such as size or shape (Götz, 1994). Flies judge distance using the motion parallax of the object's image on the retina and not expansion

cues (Götz, 1994; Schuster et al., 2002). They will maintain a heading towards an object after it disappears (Strauss and Pichler, 1998), or even return to a course toward an object after it disappears and a distracter object is transiently presented (Neuser et al., 2008). Additionally, walking flies can fixate and track a moving target; in the chase phase of courtship, a male orients towards and follows a female. Male flies without visual information are only able to track females moving at low velocities (Cook, 1980). Together, this work demonstrates the saliency of visual objects in the behavior of walking *Drosophila*.

1.4 Methods for studying locomotor behaviors in walking flies

Many of the older studies of visual control of walking behavior were performed in relatively small arenas, with visual patterns that did not provide motion parallax cues (Götz, 1975, 1980; Götz and Wenking, 1973; Horn, 1978; Horn and Wehher, 1975). Additionally, the quality of the tracking was limited. More recent experiments reliably track individual walking flies within an arena (Neuser et al., 2008; Strauss et al., 1997; Strauss and Pichler, 1998), but they use a water moat to contain the flies, which limits the duration of trajectories that can be continuously recorded. Martin (2004) solved this problem by containing the flies within a chamber, however, its limited size creates a situation where the flies' behavior is dominated by edge effects. The details of locomotor behavior in response to gravity have not been studied, as discussed earlier.

All of these studies have produced insights into fly behavior. However, in order to study the sensory control of locomotor behavior, one would ideally want to be able to track the fly's position and orientation precisely and continuously in a controlled sensory landscape. Quantitative and repeatable behavioral analysis is possible when high-quality data are collected.

For high-throughput but quantitative behavioral analysis, it is necessary to track multiple flies and useful to maintain their identities. Machine vision has shown promise for automating tracking and behavior analysis of *Drosophila* and other animals. Several algorithms have been developed that can successfully track the trajectories of single, isolated flies (Grover et al., 2008; Martin, 2004; Ramazani et al., 2007; Valente et al., 2007). Although useful, tracking only a single fly limits the types of behaviors that can be analyzed as well as the throughput of the system. Several tracking systems can follow multiple, unmarked, interacting animals, but fail when the animals are in close proximity to one another, and thus cannot keep individual identities distinct (Crocker and Grier, 1996; Ramot et al., 2008; Ryu and Samuel, 2002; Soll and Voss, 1997; Tsunozaki et al., 2008; Wolf et al., 2002). The commercially available Ethovision system (Noldus) can track the identities of multiple interacting animals, but requires tagging the animals with colored markers. The problem of tracking individuals within groups has been researched for studies of eusocial insects (ants and bees) (Khan et al., 2005; Veeraraghavan et al., 2008), but robust implementations are not publicly available. Recently, systems were developed to automatically detect components of aggression and courtship behavior in flies (Dankert et al., 2009; Hoyer

et al., 2008), in addition to tracking their positions. However, these systems cannot be used with large populations or unmarked flies, and detectors for new behaviors cannot be created without additional programming.

1.5 Plan for thesis

This thesis examines the behavior of the fly in response to sensory cues in its environment. In Chapter 2, I describe a new behavioral arena that I developed to allow for quantitative analysis of the behavior of freely walking *Drosophila* in a controlled but complex sensory landscape. I document the effect on locomotor behavior when all visual information is removed. I also examine the behavioral response of flies exploring the arena with more complex topology and the effect of removing input from the visual and antennal mechanosensory systems on those behaviors. The results of these experiments have been accepted for publication in the *Journal of Experimental Biology* (Robie 2010, in press). In Chapter 3, I test what aspects of arena topology are sensed by the visual and antennal mechanosensory systems. Some of these results maybe submitted for future publication in a peer-reviewed journal. In Chapter 4, I describe the use of the new behavioral arena (described in Chapter 2) for studying large groups of flies. This work was done in collaboration with the development of software for automated tracking and behavioral analysis of large groups of flies by Kristin Branson. Using my behavioral setup, I performed all the behavioral experiments presented and assisted in the development of the behavior analysis framework. Most of the work presented in Chapter 4 has been published (Branson et al., 2009).

The tracking algorithm and behavior analysis from Branson et al. (2009) are described in Appendix A.

Chapter 2

Object preference is mediated by vision and graviperception

2.1 Introduction

In this study we examine the role of vision and gravity sensation in shaping the exploratory behavior of freely walking fruit flies. Rather than studying the approach of flies to virtual or unattainable objects, we allow them to explore a large arena containing actual 3-dimensional (3D) features while we track their locomotor behavior using a simple machine vision system. We found that while flies are approaching objects they show little preference for different shapes of visual targets. Once reaching the target, however, they demonstrate a clear preference for tall, steep objects. This preference is manifest by much longer residency times on tall, steep objects, which is due to a preponderance of long periods during which they cease walking. Animals lacking either visual information or with impaired gravitational sense still exhibit a preference for tall, steep objects, but animals with both impairments show no preference. These results demonstrate the role of visual and mechanosensory modalities in the exploratory behavior of *Drosophila*.

2.2 Methods

2.2.1 Flies

All experiments were performed on three-day-old mated female fruit flies, *Drosophila melanogaster* Meigen, selected from a laboratory population descended from 200 wild-caught females. The flies were maintained at 25°C and ambient humidity (20–40%) on a 16:8 light:dark cycle. One day before each experimental trial was performed, we

anesthetized the flies on a cold plate held at 4°C. The wings of the flies were clipped between the first and second cross-veins, approximately half the length of the wing. If the flies' gravitational sense was to be impaired, it was done at this time as well by immobilizing the joint between the second and third antennal segments with a UV-cured glue (Budick et al., 2007). The flies were allowed to recover with food overnight and then deprived of food, but not water, 10–14 hours before the experiments were performed. All experiments were performed during the evening peak in their circadian activity cycle (Shafer et al., 2004). The flies were placed into individual vials with a water source and allowed to acclimate to experimental light levels for at least 30 minutes prior to experiments. Each fly was used once and only once, and all trials consist of a single fly recorded for 10 minutes.

2.2.2 Walking arena

In order to study the behavior of flies exploring a topologically complex environment we developed a large, free-walking arena. The arena consisted of a 24.5 cm diameter black disk surrounded by a 24.5 cm tall backlit cylindrical panorama of randomized black squares with a 50% filling probability that provided a background visual stimulus (Fig. 2.1A). As viewed from the center of the arena each square subtended 5°. The paper printed with the panorama was backlit by a circular array of eight 35 W halogen lights (Fig. 2.1B). Flies were maintained within the arena using a thermal barrier, which proved easier to regulate and much more effective than either a water moat or a wall coated with Fluon^{TM}. Most flies approached the thermal barrier and

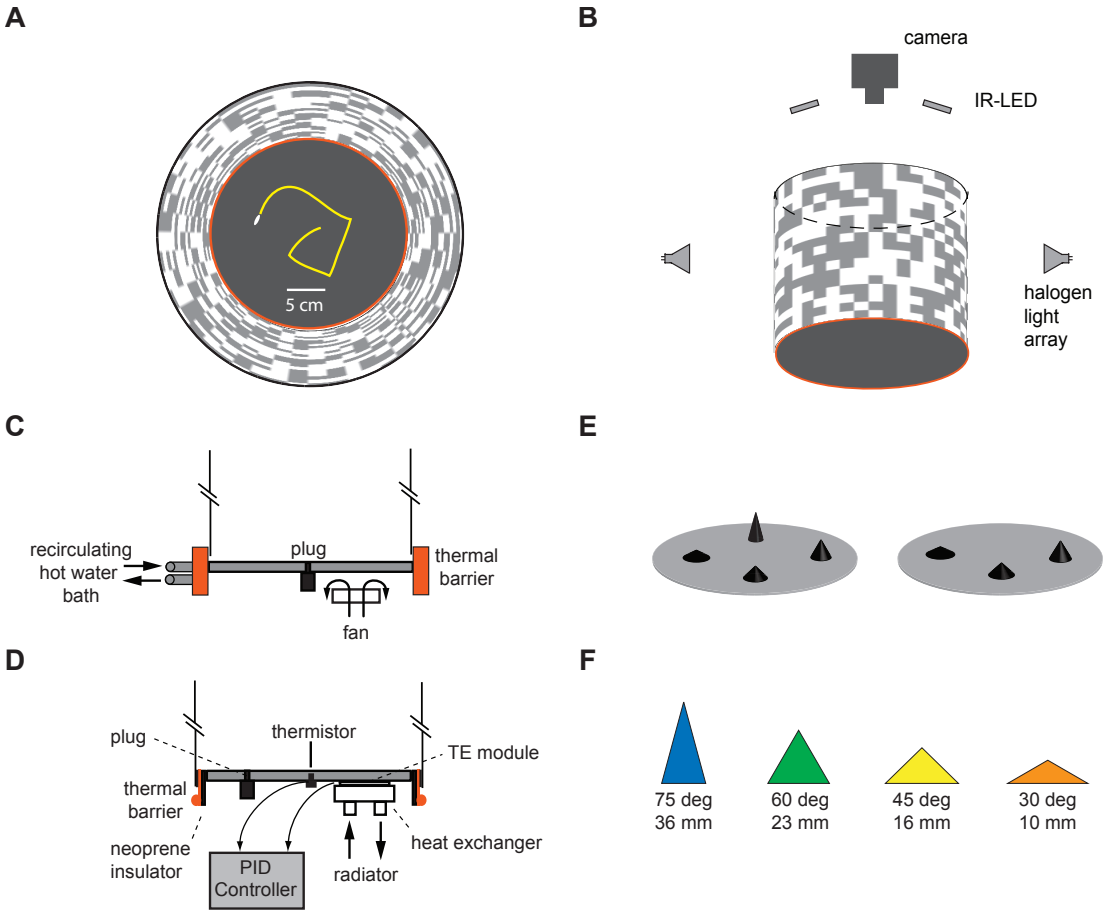

Figure 2.1: Experimental apparatus. (A) Top-down view of the arena with backlit panorama. Thermal barrier is depicted in red. (B) Schematic side view of the fly visualization setup. Two of the eight halogen lights arranged in a circular array are depicted. Near-IR LEDs mounted with the camera above the arena. (C) Schematic cross section of Arena 1 with passive cooling. Recirculating hot water heats the thermal barrier and four CPU fans cool the walking platform (only one is depicted). (D) Schematic vertical cross section of Arena 2 with active cooling. The thermal barrier is strip of galvanized steel wrapped by a rope heater and insulated from the walking platform by a layer of neoprene. The walking platform in actively cooled by a PID controlled array of four thermoelectric modules with water-cooled heat sinks (only one is depicted). (E) The two arrangements of cones in the arena. The arena floor is shown in gray for illustration purposes only; the floor and cones were both painted matte black. (F) The color code convention used for the cones of equal lateral surface area throughout the paper. The angle between the base and lateral surface and the height are noted below each cone.

turned away; rare experiments in which flies did escape over the barrier before the end of the 10 min trial were discarded. Two versions of the arena were used in the majority of these experiments simply due to methodological improvements that were made during the course of the study. Arena 1 was equipped with a water-heated thermal barrier and a passive cooling system (Fig. 2.1C) whereas Arena 2 was equipped with an electrically heated thermal barrier and an active cooling system (Fig 2.1D). Although both systems worked, the active electrical system is easier to fabricate and permits more precise control of surface temperature. All trials were performed in Arena 2 unless noted otherwise. In all cases in which identical treatments were performed in Arenas 1 and 2, we verified the data were indistinguishable and the results were pooled in subsequent analysis. A third arena, Arena 3, was similar in design principle to Arena 2, but had a dynamic visual display (Fig. 2.2).

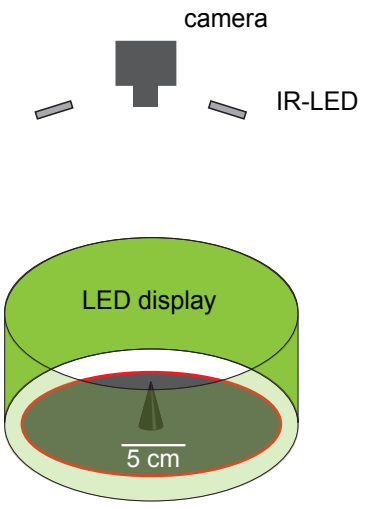

Figure 2.2: Experimental apparatus: Arena with dynamic visual display. A schematic side view of the arena with the visual display composed of modular LED display panels. Thermal barrier is depicted in red. Near-IR LEDs mounted with camera above the arena. A single, central cone was used in these experiments (blue cone in Figure 2.1F). Scale bar = 5 cm.

2.2.3 Arena design

In Arena 1 (Fig. 2.1C), the thermal barrier was 0.64 cm high around the platform. It consisted of a cylindrical aluminum walled chamber heated by 55°C recirculating water. The painted aluminum surface facing the arena was ∼38°C. An array of four CPU fans blowing room air onto the bottom of the acrylic arena floor passively maintained the floor temperature. The surface temperature profile of the arena floor was 24°C at the center and rose gradually to 26°C at a distance of 2 cm from the thermal barrier, beyond which the temperature rose rapidly to 30°C as measured by a thermocouple.

In Arena 2 (Fig. 2.1D), the thermal barrier was flush with the top surface of the arena floor. It consisted of a 0.2 mm thick, 24 mm wide band of galvanized steel wrapped with a thin electric rope heater (OmegaLux, Stamford, CT, USA), powered by a variable AC transformer (Staco, Dayton, OH, USA) in open loop. The arena floor was insulated from the thermal barrier by a thin strip of neoprene. The arena floor was constructed of a 0.6 cm thick aluminum plate with four circular thermoelectric (TE) modules (TE Technology, Inc., Traverse City, MI, USA) bolted to the underside, each with a water-cooled temperature exchanger. A thermistor, mounted at the center of the underside of the floor, provided input to a PID controller driving the four TE modules in parallel with a set point of 25°C. The surface temperature of the arena floor varied by less then 1°C as measured by a non-contact infrared thermometer (OmegaScope, Stamford, CT, USA).

Arena 3 was similar to Arena 2, with the same active cooling system, thermal

barrier, camera and near-IR lighting. However, this arena was slightly smaller, 19 cm in diameter, in order it fit inside the cylinder of LED panels. As a consequence, it was cooled with three equally spaced TE modules rather than the four used in the Arena 2. The visual surround consisted of a cylinder, 21.9 cm in diameter, composed of 60 modular panels emitting green light (Reiser and Dickinson, 2008). These panels were controlled in real-time based on the flies' x–y position determined by the Flytrax tracking program (Straw and Dickinson, 2009).

Flies were introduced into the arena by placing them into a black vial with a neck that fit securely into a 3 mm hole in the arena floor. Each fly was allowed to crawl up the vial and out onto the surface of the arena, thereby avoiding the effects of mechanical agitation caused by aspirating flies with a mouth pipette. After the fly entered the arena, the hole was plugged with a stopper that was flush with the arena floor. Flies that did not enter the arena within 1 min were discarded. Of the 191 individual trials attempted for this manuscript with this loading method, only 11 flies (6%) failed to enter the arena by crawling up and out of the black vials. Thus, there is no evidence that our data are biased by inadvertently selecting against flies with weak gravitaxis behavior. In trials using flies with antennal manipulations (which exhibited reduced negative-gravitaxic response) we gently tapped the animals into the arena from above. The floor of the arena was washed with detergent and rinsed between each trial.

2.2.4 Fly visualization and tracking

Data were collected using a digital camera mounted 48 cm above the arena floor with a 720 nm high–pass optical filter (R72, Hoya Huntington Beach, CA, USA) (Fig. 1B). The flies were visualized using near-IR light, which reflects well off of the fly's cuticle, and the arena floor was painted matte black to maximize contrast. In Arena 1, we used a camera (Scorpion, Point Grey, Richmond, BC, Canada) with 1600 x 1200 pixel resolution. Image stacks were collected at 10 frames per second (fps) and analyzed in real-time by a custom software program developed in MATLAB (Mathworks, Waltham, MA, USA). In Arena 2, we used a camera with 1280 x 1024 pixel resolution (A622F, Basler, Exton, PA, USA). Using this camera, images were collected at 20 fps and analyzed in real time using Motmot, open source camera software written in Python, using the FlyTrax plug-in (Straw and Dickinson, 2009). Both tracking programs determined the fly's 2-dimensional (2D) position and body orientation with 180 ambiguity based on background subtraction. The images of the flies in our movies are approximately 10 pixels long and 5 pixels wide. For each frame, cropped images of a 100 x 100 pixel region around the fly (used for testing automated algorithms) were saved along with the 2D coordinates of the fly, body axis angle and a time stamp. A single full-resolution image of the arena was also saved. All data were collected in Arena 2 unless otherwise noted.

2.2.5 Experimental design

Empty arena

To examine the role of visual input on basic locomotor activity, 66 individual flies were tracked within an empty arena (i.e., void of the conical objects), surrounded by the random checkerboard panorama. Half the flies were tested under lit conditions (450 lux measured at the center of the arena) and half tested in complete darkness. To achieve these conditions, we replaced the translucent cylinder with an opaque black cylinder and all ambient light was eliminated from the room (measured illuminance $<<$ 1 lux). Example trajectories and speed profiles are shown in Figure 2.3A,B. We present examples that are representative of the data and have an arena crossing in the fifth minute in order to show the difference in the speed profiles of flies in light versus dark conditions.

Arena with objects

To test the effect of a more complex topology on the flies' exploratory behavior, we placed four right angle cones of equal lateral surface area but of differing heights and slopes in the arena. The geometric dimensions of these cones and the color code that will be used throughout the paper to identify cone type are shown in Figure 2.1F. Under these conditions, we performed 45 trials (20 in Arena 1 and 25 in Arena 2). Each object (painted black to match the floor and allow visualization of the flies while they were on the object) was placed in one of four fixed locations, making a square within the arena, but the relative order was randomized between trials (Fig. 2.1E).

The objects were washed with detergent and rinsed between trials. To test whether the assessment of the objects by the flies was absolute or relative, in one set of experiments we removed the tallest, steepest object and arranged the cones in the same grid leaving one spot empty (Fig. 2.1E) in 24 trials. To test the role of visual input on object exploration we performed another 45 trials in complete darkness (20 in Arena 1 arena and 25 in Arena 2). Example trajectories and speed profiles are shown in Figure 2.3C,D. To test the role of gravitational sensation on object exploration we performed 40 trials with flies whose antennae were immobilized at the joint between the second and third segments. Finally, to test the combined effect of the sensory manipulations, we performed 40 trials using flies with immobilized antenna joints in complete darkness.

Arena with dynamic visual display

To test the simple hypothesis that flies distinguish between the cones during the approach and remember this information in order to control their exploration on the cones, we used Arena 3, which has a dynamic visual display (Fig. 2.2). A single centrally located cone was used in these experiments. It was the tallest, steepest (blue) cone (Fig. 2.1F). The behavior of the flies with immobilized antennae was tested under three conditions: (1) statically displayed random checkerboard pattern (n=25), (2) in the dark (n=19), and (3) statically displayed random checkerboard pattern when the flies were on the floor, but when the flies reached the cone the panels were ramped off (n=22). The cone location was digitized before the trial. When the fly's x–y position was within the area of the cone's footprint, a control

signal was sent to the panels to ramp the LEDs off though eight levels of grayscale. The ramp-off was used to avoid stimulating jumps.

2.2.6 Data analysis

The positional and orientation data were recorded in real time but were post-processed using custom software written in Python (www.python.org) and MATLAB (Mathworks, Waltham, MA, USA). All trials were reviewed by examining the stored video record with the tracking data superimposed. Any trials with gross tracking errors (e.g., fly position was lost) were discarded and not included in the enumeration of trial numbers used for analysis. Of 332 trials recorded for this manuscript, only 8 were discarded for tracking errors.

For each trial with cones present, the locations of the cones were digitized and used to determine the periods of the trial in which a fly was exploring each cone. Because of the cone steepness and the central position of the camera, flies exploring the far side of a cone could have been incorrectly classified as 'off cone' with the use of a simple digitization based on the footprint of the cone. To prevent this, the digitized footprint was expanded such that a fly whose center did not appear to be within the footprint of the cone, but was indeed on the cone was correctly classified as 'on cone.' The assignment of 'on' or 'off' cone was manually checked against the saved video for each trial.

In trials without cones present or 'off' cone, the 2D position of the fly was smoothed with a Kalman smoother (Kevin Murphy's Kalman filter MATLAB toolbox) and used

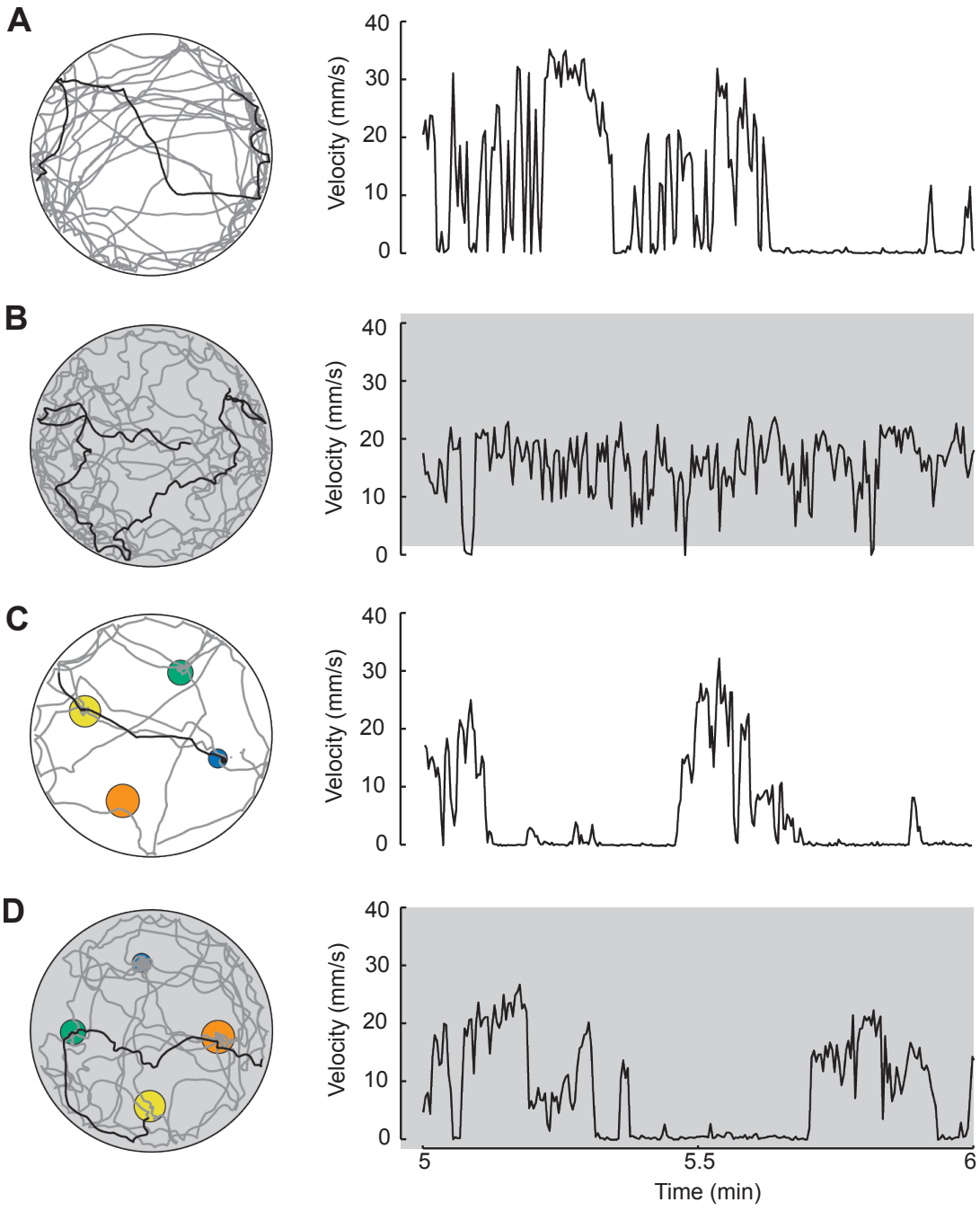

Figure 2.3: Example trajectories and corresponding velocity plots. Each 10 min trajectory is plotted in gray with the fifth minute plotted in black. The speed profile for that same period is plotted to the right. Trials run in darkness are shown with a gray background. In trajectories with cones present, the footprint of each cone is highlighted according the color scheme in Fig. 2.1F. Representative traces where chosen for the following cases: (A) empty arena with lights on, (B) empty arena in darkness, (C) four cones with lights on, and (D) four cones in darkness.

to calculate translational speed and total distance travelled. For trials with cones present, we calculated the 3D position of the fly on the cones using the tracked 2D positions, a model of the 3D structure of the arena, and a standard pinhole camera model. The 3D model of the arena was created from the known geometry of the arena and cones and hand digitization of the cone positions in each trial. The surface of this model was extruded by 1 mm as an approximation for flies' own height above the floor. Through each 2D fly position on the calibrated image plane of the camera, we projected a ray (from the 3D location of the pinhole camera model center) and intersected it with the extruded 3D model of the arena to find the estimated 3D position of the fly. We calculated the 3D positions for a second time with a fly height of 2 mm and used the magnitude of the difference between the two z-position data sets as an estimate of the error in the 3D positions. The 3D position of the fly was smoothed with a Kalman smoother using the error estimate to assign the uncertainty in the observation data. We evaluated the quality of the 3D position estimates on the tallest, steepest cone (and the stop/walk assignment described below) by recording simultaneously with a second camera mounted directly over this cone, and found that both the 3D estimate and stop/walk assignment were accurately determined. An example of the reconstructed 3D trajectory, color coded by velocity in shown in Figure 2.4.

The temporal structure of the flies' locomotor activity can be coarsely modeled as discrete bouts of walking and stopping (Martin, 2004). We manually assigned walks and stops in a subset of data (both 'on' and 'off' cone) based on the small format

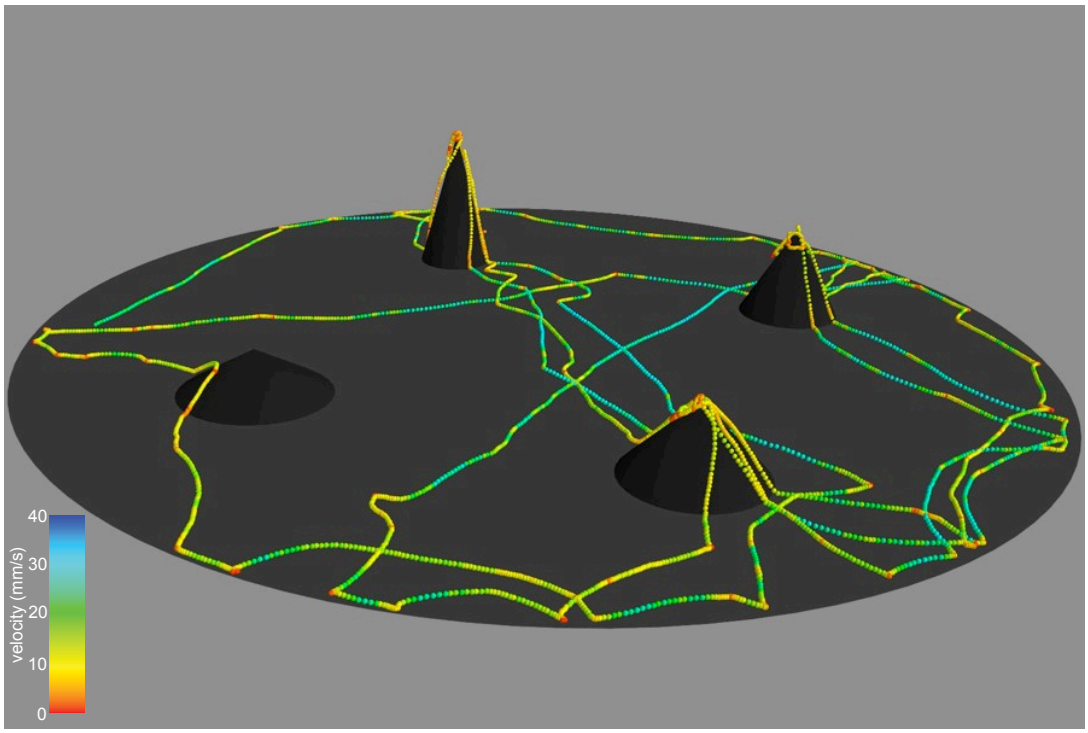

Figure 2.4: An example 3D trajectory color coded by velocity. The reconstructed 3D trajectory of an intact individual fly tracked for ten minutes is shown. It is color coded by velocity: red = low to blue = high.

images. Using these classifications as ground truth, we defined stops and walks based on velocity (3D velocity when 'on' cone) using a dual threshold: When the velocity was above the high threshold (2.5 mm sec^{-1}) the fly was classified as walking and when the velocity was below the low threshold (1 mm sec^{-1}) the fly was classified as stopped. When the velocity was between the two thresholds it maintained its previous classification until the second threshold is crossed. This Schmitt trigger avoids rapid changes in classification caused by a single threshold-based definition. We also defined the minimum walk duration to be 0.1 sec (2 frames at 20 fps) to avoid misclassifying as walks the transient center of mass movements associated with grooming. We defined the minimum stop duration to be 0.1 sec to avoid incorrectly assigning as stops the brief decrease in translational speed associated with sharp turns and pauses. Using these criteria, we determined the percentage of time each fly spent walking or stopped and the duration of each walk and stop bout, as well as the mean and maximum translational speeds during each walk bout. We set a maximum walking speed threshold of 50 mm sec^{-1} to filter out rare events in which the wing-clipped flies jumped within the arena. 'On' cone locomotor activity statistics were only calculated for trials performed in Arena 2, in which we estimated 3D velocity. Additionally, we used the estimated fly z–positions to determine the height at which each stop was performed when the flies were 'on' cone.

The body orientation ambiguity was resolved using a variation of the Viterbi algorithm in which orientation flips and walking rapidly backwards were penalized (Branson et al., 2009), and we then calculated mean angular speed during walking

periods. Using a method for estimating position and orientation error based on trajectory segments of constant velocity described by Branson et al. (2009), we found the orientation tracking error to be 1.5 degrees for the 'off' cone data. As can be seen in Supplementary Movies 2.1 and 2.2, the orientation tracking is highly accurate and it is unlikely an expert human could do better.

2.2.7 Statistics

Much of our data were not normally distributed (nor transformable to normal distribution) therefore, throughout the paper we present the distribution of results using box-and-whisker plots in which the central line (colored magenta when on a colored background) indicates the median, the box outlines the interquartile range of the data, and the whiskers encompass the range from minimum to maximum value, excluding any outliers. Outliers (indicated by a small cross) are values that are more than 1.5 times the interquartile range below or above the 25th or 75th percentiles, respectively.

We used various statistical tests in the analysis of our data; depending upon the assumptions of the tests met by the data, we always used the most powerful test possible (Sokol and Rohlf, 1995). If the data were independent and normal, we used a heteroscedastic t-test. If the data were independent but any of the sets being compared were not normal, then we used a Mann-Whitney U test. In some cases our data were not independent because a fly can only be in one location of the arena at a time. If the data were not independent we used a Wilcoxon signed rank test, and

finally if the data had a large number of tied scores we used a Kolmogorov-Smirnov test. Neither the Wilcoxon nor Kolomogorov-Smirnov tests require that the data be normal. In all cases where data were being compared multiple times we used a Bonferroni correction for multiple comparisons to adjust the p value appropriately. All statistical analysis was performed using SPSS (SPSS Inc, Chicago, IL, USA).

To report the results of our significant tests we use a letter code where the groups labeled with the same letter are not significantly different. A group can have more than one label that indicates that it is not significantly different from any of the groups also labeled with any of those letters. For experiments with multiple cones present, we compared the results of the experiments *within* a trial type, comparing effect of cone type in a given trial condition. Throughout the paper we indicate the results of *within* trial type hypothesis testing with black *lowercase* letters. For example, the results of comparing the encounter rates in Figure 2.7 are indicated with lowercase letters showing that the blue, green and yellow cones are not significantly different, nor are the yellow and orange cones e.g. the blue and green cones are significantly different than the orange cone. When multiple trial conditions were tested (such as different sensory manipulations) we also compared the results *across* trial type, comparing effects of trial conditions on the response to each cone type. We denote the results of *across* trial type hypothesis testing with *uppercase* letters (colored to highlight which cone type is being compared). We only compare the same cone type across different trial conditions. For example, the results of comparing the percentage of time spent on the blue cone across trials with different sensory manipulations in

Figure 2.11 are indicated with uppercase blue letters showing panels A, B, and D are significantly different, but panel C is not significantly different from panel A or B.

2.3 Results

2.3.1 Visual input modulates locomotor behavior

To test how visual input or the lack thereof affects locomotor behavior, we tracked individual starved flies as they explored the large free-walking arena for 10 min (n=66). Half the trials were performed in complete darkness (except for near-IR light). Sample trajectories and translation speed profiles are shown in Figure 2.3A,B. Using the tracked x–y position and body orientation of the fly, we calculated basic statistics of walking behavior (Fig. 2.5). Without visual cues (i.e. in the dark) flies traveled a longer total distance, not because they traveled at a higher mean speed, but because they spent more of their time walking (Fig. 2.5A, B, D). In lit arenas, flies reached higher maximal speeds but spent less time walking (Fig. 2.5C, D). The trajectories of flies in lit arenas appeared straighter than the trajectories of flies in the dark arena (Fig. 2.3), an observation that was confirmed by comparing the mean angular speed of the flies under the two conditions (Fig. 2.5E).

The differences in basic locomotor behaviors due to visual input were for the most part conserved in flies (n=90) exploring the floor of an arena with 3D objects present (Fig. 2.5B–E). In the presence of cones, flies spent more of their time walking while on the arena floor (Fig. 2.5D), and walked at a higher mean speed (Fig. 2.5B) than they

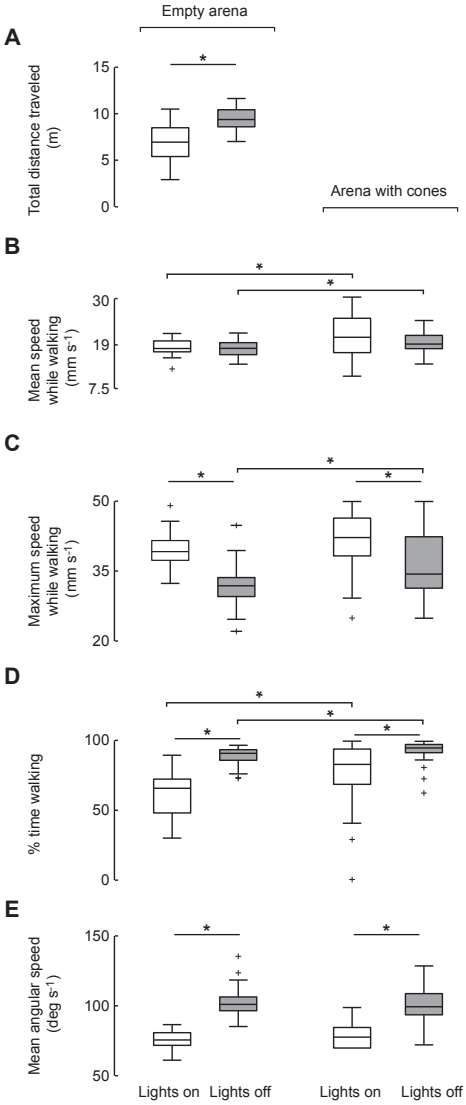

Figure 2.5: Visual information influences the basic statistics of walking. The two leftmost box plots in each panel show data for flies exploring an empty arena in the light (white, N=33) and in the dark (gray, N=33). The two rightmost box plots show data from flies exploring the floor of the arena with cones present in the light (white, N=45) and in darkness (gray, N=45). (A) The total distance traveled by individual flies during 10 min trial. (B) The mean speed calculated while the flies were walking. (C) The maximum speed calculated while the flies were walking. (D) The percentage of time the flies spent in the walking state, normalized for the total time spent on the floor of the arena when cones were present. (E) The mean angular speed calculated while the flies were walking. Statistically comparisons were made using heteroscedastic two-sample t-tests unless the data were not normally distributed in which case the Mann-Whitney U test was used. Asterisks indicate significantly different distributions (P<0.05 with Bonferroni correction).

did when the cones were absent. Curiously, this cone-dependent change in behavior was present even in conditions of darkness when the flies could not see the cones. This result suggests that some mechanical effect of encountering a cone stimulates general locomotor activity with a time constant that last longer than a fly's immediate interaction with the object.

2.3.2 Flies spend more time on tallest, steepest cone

To determine how a topologically complex environment influences the exploratory behavior of flies, we tracked individual flies for 10 min in an arena with four cones of equal lateral surface area but differing height and slope (Fig. 2.1F). As illustrated by the trajectory in Figure 2.4 and Supplementary Movie 2.1, the presence of the cones qualitatively altered the overall exploratory behavior in the arena. Flies appear to orient towards cones from a distance and, once encountered, climb on top of them. To test if particular cones were more attractive than others, we measured the percentage of the 10 min trial that the flies spent on each cone, as well as the arena floor (Fig. 2.6). For simplicity, we will often refer to the cones throughout the paper by the color codes indicated in Figure 2.1F. Thus, the blue cone is the tallest, steepest cone; the green cone is the next tallest, steepest cone, etc. It is important to note, however, that these colors are simply a code for cone shape; the actual color of the cones was black in all experiments. From visual inspection of Figure 2.6A, it is clear that the flies spent much more time on the tallest, steepest cone (blue). As shown in Figure 2.6D, the time spent on the tallest, steepest cone was significantly larger than all other cones

and even larger than the time spent on the arena floor when it is normalized for area. This strong, differential response to the tallest, steepest cone is not consistent with what would be expected from a random walk exploration of the arena surface as the cones all had identical surface area.

2.3.3 Flies make absolute judgment of cone geometry

Flies might spend more time on the tallest, steepest cone because of some absolute sensory cue they perceive about this object or, alternatively, they might make a relative assessment by comparing it with other objects in the arena. To test whether the flies' preference for the tallest, steepest cone was absolute or relative, we removed the blue cone (Fig. 2.1E) and repeated the experiments. When the blue cone was absent, the flies did not spend significantly more time on the green cone than they did when the blue was present (Fig. 2.6B,E). These results suggest that the flies' response to the slope and height of each cone is absolute, and is not made by relative comparison. However, when the blue cone was absent, flies did spend slightly more time on the remaining cones, as evidenced by expanded interquartile ranges for the green and yellow cones in Fig. 2.6E . Such a bias is expected because, without the blue cone present, the flies had more time to encounter and explore the other three cones in the arena. To take this effect into account we created 'pseudo removal' data from the results of the original four-cone experiments by excluding all segments spent on the blue cone and scaling the remaining time to be 100% (Fig. 2.6C,F). The results of the pseudo removal experiment were not significantly different from those in the real

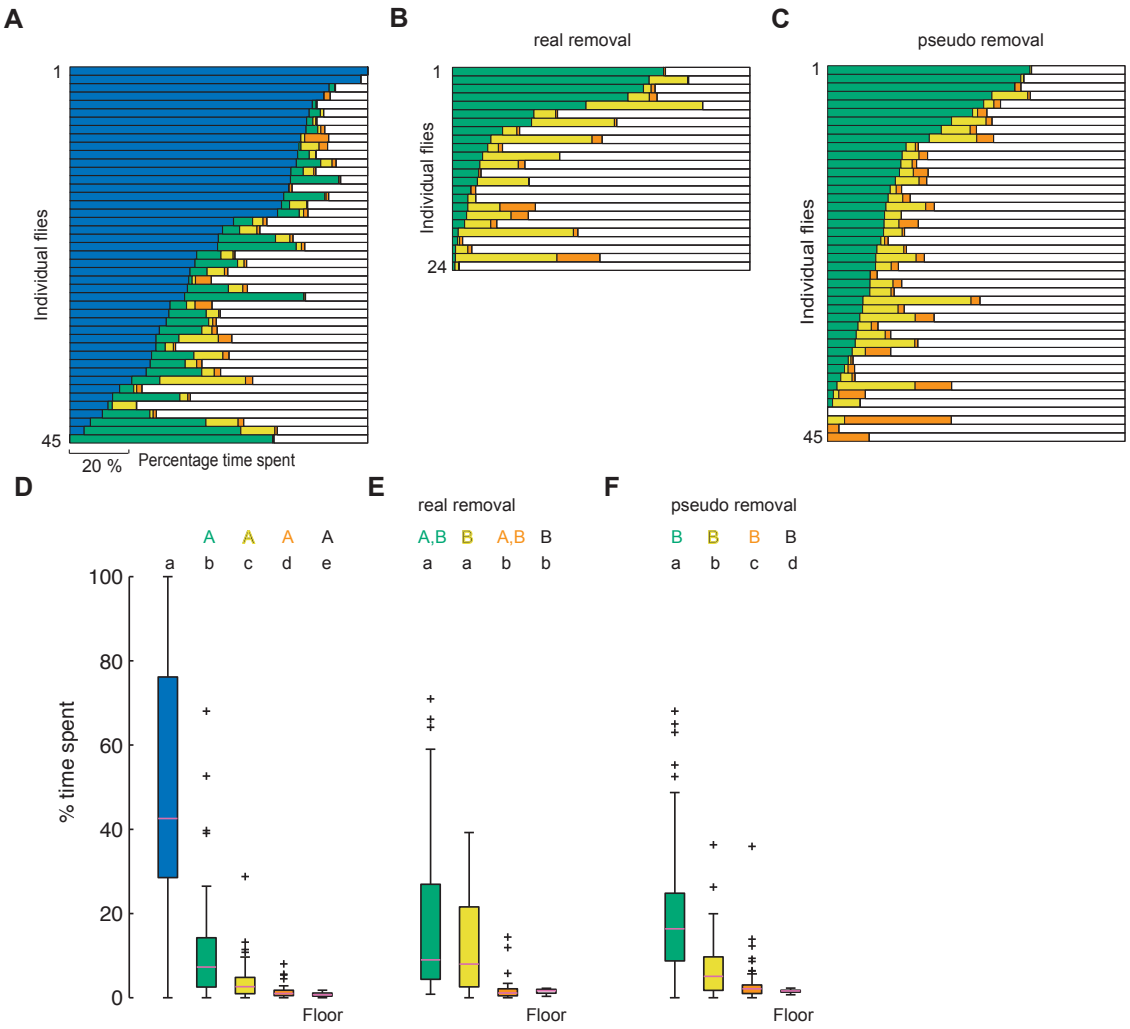

Figure 2.6: Flies spend more time on tallest, steepest cone. Color coded (see Fig. 2.1) horizontal bar graphs show the percentage of the 10 min trial that each fly spent on the four cones and the floor of the arena (white). The data are ranked by the time spent on the blue (A) or green (B and C) cone. (A) Data for trials with all four cones present (N=45). (B) Data from trials in which the tallest, steepest (blue cone) was removed from the arena (N=24). (C) 'Pseudo removal' data created by scaling the data from (A) after excluding visits to the blue cone (see text for details) (N=45). (D, E, F) The distributions of the data in A, B, and C are shown after normalizing for area of the surfaces being explored. The results of statistical tests are indicated with a letter code; groups labeled with the same letter are not statistically different and a group can have more than one label indicating group(s) with any of the same letter are not significantly different (for more details see methods). *Across* trial statistical tests compare a given cone type across experimental conditions and the results are denoted with uppercase letters of the color indicating the cone type being compared (color code from Figure 1F and uppercase black letter = arena floor). Comparisons were made using a Mann-Whitney U test with Bonferroni correction, $P<.05$. *Within* trial statistical tests compare the different cone types in a given experimental condition and homogenous groups are denoted with lowercase black letters. Comparisons were made using Wilcoxons signed ranks test with Bonferroni correction, $P<.05$.

removal experiment (Fig. 2.6E,F), supporting our conclusion that flies' preference is mediated by an absolute measurement of cone geometry.

2.3.4 Flies encounter cones with equal frequency

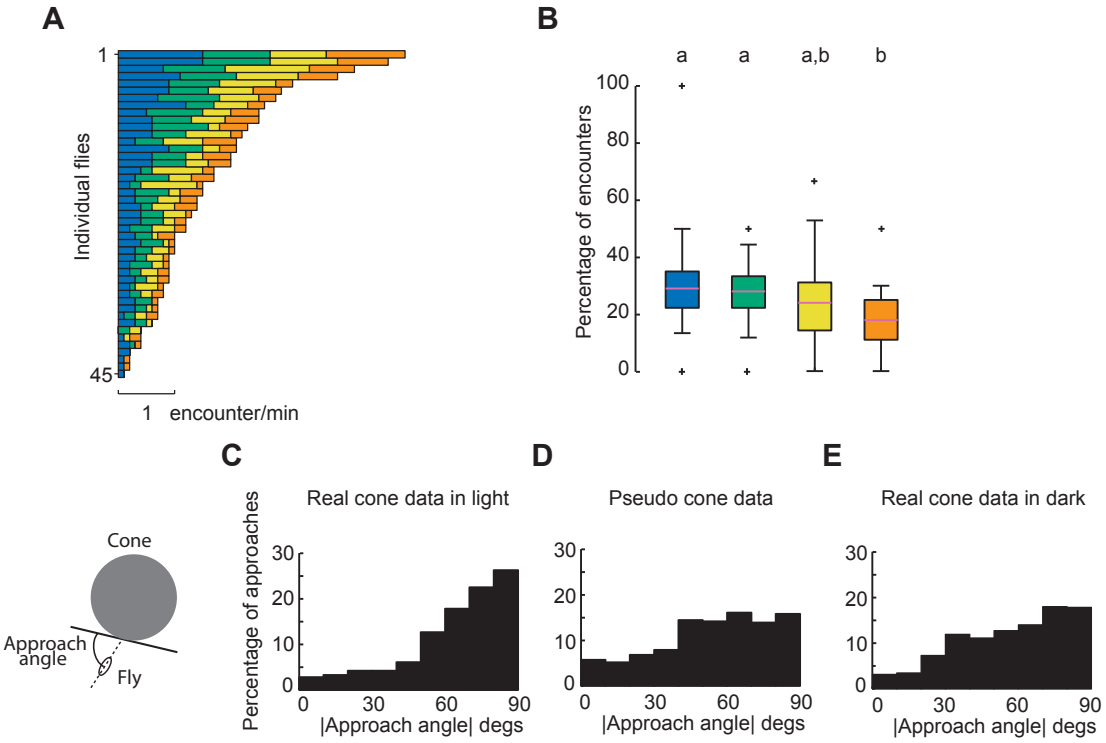

Figure 2.7: Flies exhibit similar encounter rates to objects of differing geometry. (A) Horizontal bar plots indicate the encounter rates of each cone type for each fly, ranked according to total encounter rate. (B) Box plots show the percentage of encounters for each cone type ($N = 45$). See Fig. 2.1F for color code. The Wilcoxon signed rank test for non-independent, non-normal data was used to compare groups ($P<0.05$ with Bonferroni correction for multiple comparisons). See Fig. 2.6 for explanation of letter codes for homogeneous groups. (C) The frequency distribution of approach angles to all cone types in the light. (D) The frequency distribution of approach angles to pseudo cones footprints created from data set in which no cones were present. (E) The frequency distribution of approach angles to all cone types in the dark.

The flies may have spent more time on the tallest, steepest cone because they

oriented towards it more frequently (i.e., it was more attractive from afar), or because, once encountered, they tended to spend more time on it before returning to the arena floor. In order to test between these two alternatives, we calculated the flies' rate of encountering each object. Figure 2.7A shows the individual encounter rates for each fly to each cone, ranked by total number of encounters from highest to lowest. Although there was a large range of encounter rates across individuals, when we examine the percentage of encounters for each cone type, it is clear that the population encountered each cone type with equal probability. The one exception was the shortest, broadest cone (orange), which the flies encountered at a slightly lower rate than the blue and green cones (Fig. 2.7B). These results do not indicate whether the flies encountered the cones by chance, as in a random walk. However, as can be seen by examining the locomotor trajectories in the presence and absence of cones (Fig. 2.3) or examining the 3D trajectory (Fig. 2.4), the presence of the objects in the arena strongly structured the flies' exploratory behavior. Subjectively at least, it appeared as if the flies often walked towards the cones. To quantify this effect, we examined the flies' body orientation relative to the tangent of the circumference of the cone footprint in the frame before they encountered each cone. There is a clear peak in the histogram of the absolute value of approach angle near 90° (Fig. 2.7C), suggesting that flies made a directed approach to the cones rather than randomly encountering them. We compared this to 'pseudo cone' data, in which we analyzed fly trajectories from trials with no objects in the arena as if there had been cones present. These control data exhibit no distinct peak in approach angle as in the case

with real cones present (Fig. 2.7D). Furthermore, we examined the distribution of approach angles when there were real cones present, but under dark conditions (Fig. 5E). These approach angle data resemble our pseudo cone condition, supporting the conclusion that the flies orient toward the cones using visual cues. These analyses, together with the results showing that flies exhibit little preference in encounter rate (Fig. 2.7B), suggests that flies actively orient towards objects, but do not demonstrate preference based on the geometry of the objects on their retina. The slightly lower encounter rate to the orange cone suggests, however, that there may be a lower limit for detection of this cone from a distance. Given that the percentage of encounters did not vary across the three taller, steeper cones, any difference in object attractiveness during approach cannot underlie the preference for the tallest, steepest cone.

2.3.5 Increased residency time on tallest, steepest cone

After ruling out encounter rate as the cause of the flies' preference to spend time on the tallest, steepest cone, we next examined how long the flies remained on each object once they had reached it. Figure 2.8 shows time series plots indicating each fly's location throughout the trial and the residency times on each cone type. From visual inspection, it is clear that the flies' visits to the blue cone were much longer than their visits to any of the other cones, and longer even than most periods of exploring the arena floor (Fig. 2.8A). We have plotted the normalized population distributions on each cone type in two ways. First, we plotted the normalized histograms of the log of residency time for all flies on each cone type in Figure 2.8B, which shows that the

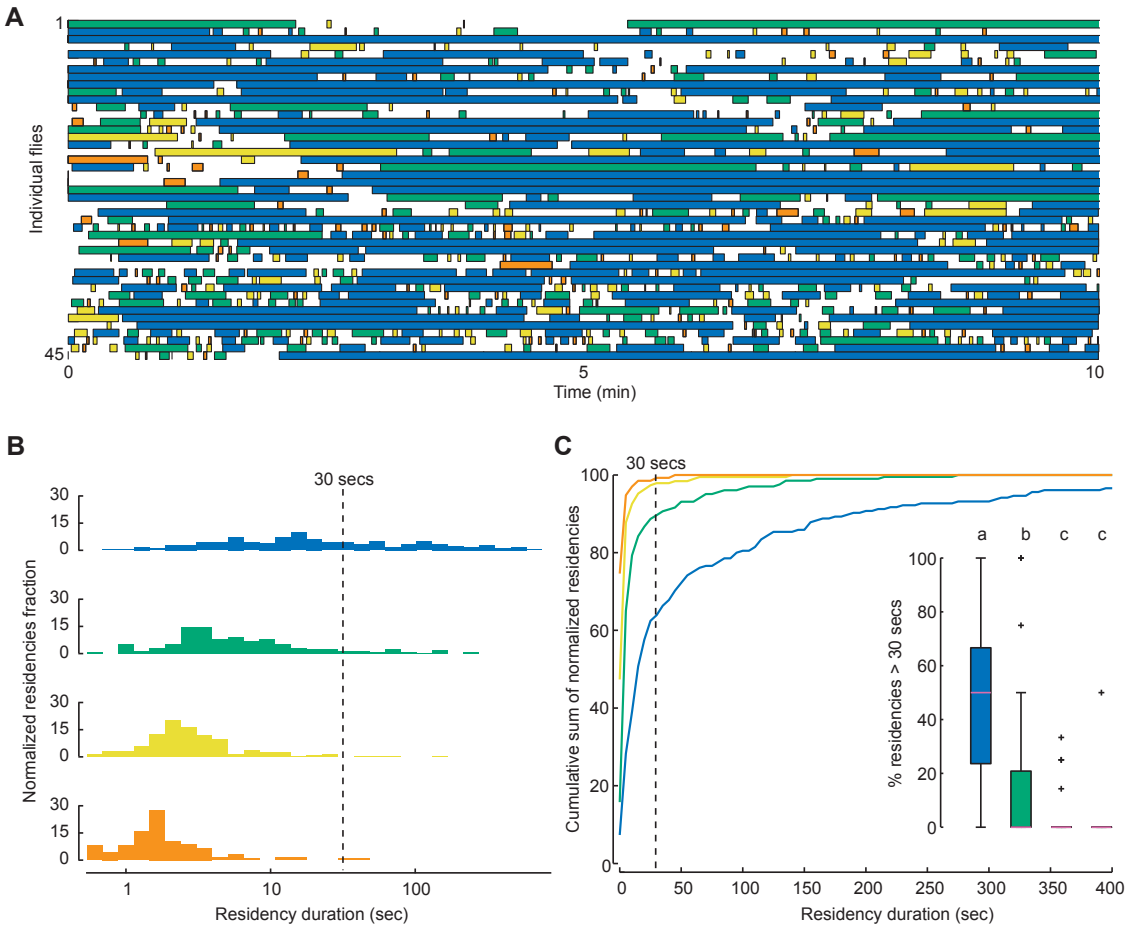

Figure 2.8: Flies exhibit long residency times on tallest, steepest cone. (A) Each row represents the time series data of a single fly (N=45). The color (see Fig. 2.1F) indicates the identity of the cone the fly resides on and white spaces indicate periods spent on the arena floor. (B) Normalized frequency distribution of logged residency durations by all flies on each cone type from data plotted in A. (C) Cumulative sums of the normalized frequency distribution of all residencies durations by all flies. The inset shows the distribution of the percentage of individual flies residency times longer than 30 sec. Statistical comparisons were made using Kolmogorov-Smirnov two-sample test (P<0.05), with Bonferroni correction). See Fig. 2.6 for explanation of letter codes for homogenous groups.

flies' distribution of residencies on the blue cone were shifted towards higher values. Second, we plotted the cumulative sum of the population data for each cone type in Figure 2.8C, which shows a larger portion of long duration residencies on the blue cone than any other cone type. The inset in Figure 2.8C shows the fraction of each individual fly's residencies that were longer than 30 seconds for each cone type. The results show a preponderance of long residency times on the tallest, steepest cone (blue). Although 30 seconds was a somewhat arbitrary choice, the relation holds over a range of thresholds for long residency.

The results of Figure 2.6 suggest the flies perform an absolute rather than comparative measure of cone geometry. To further rule out a role for short-term memory in the assessment of cones, we also examined the residency durations on a given cone type parsed according to the previous cone visited. As shown in Figure 2.9, the type of cone visited immediately before had no effect on the distribution of residency times, indicating that dwell time on a particular cone does not depend on the prior history of cone visits.

2.3.6 Sensory modalities involved in preference for tallest, steepest cone

Together, the results in Figure 2.8 show that the flies, once they reached the tallest, steepest cone, remained on it for longer than the other cones. To investigate what sensory modalities underlie this preference, we repeated the experiments on flies with deficits in their visual and gravitational senses. We impaired vision simply by run-

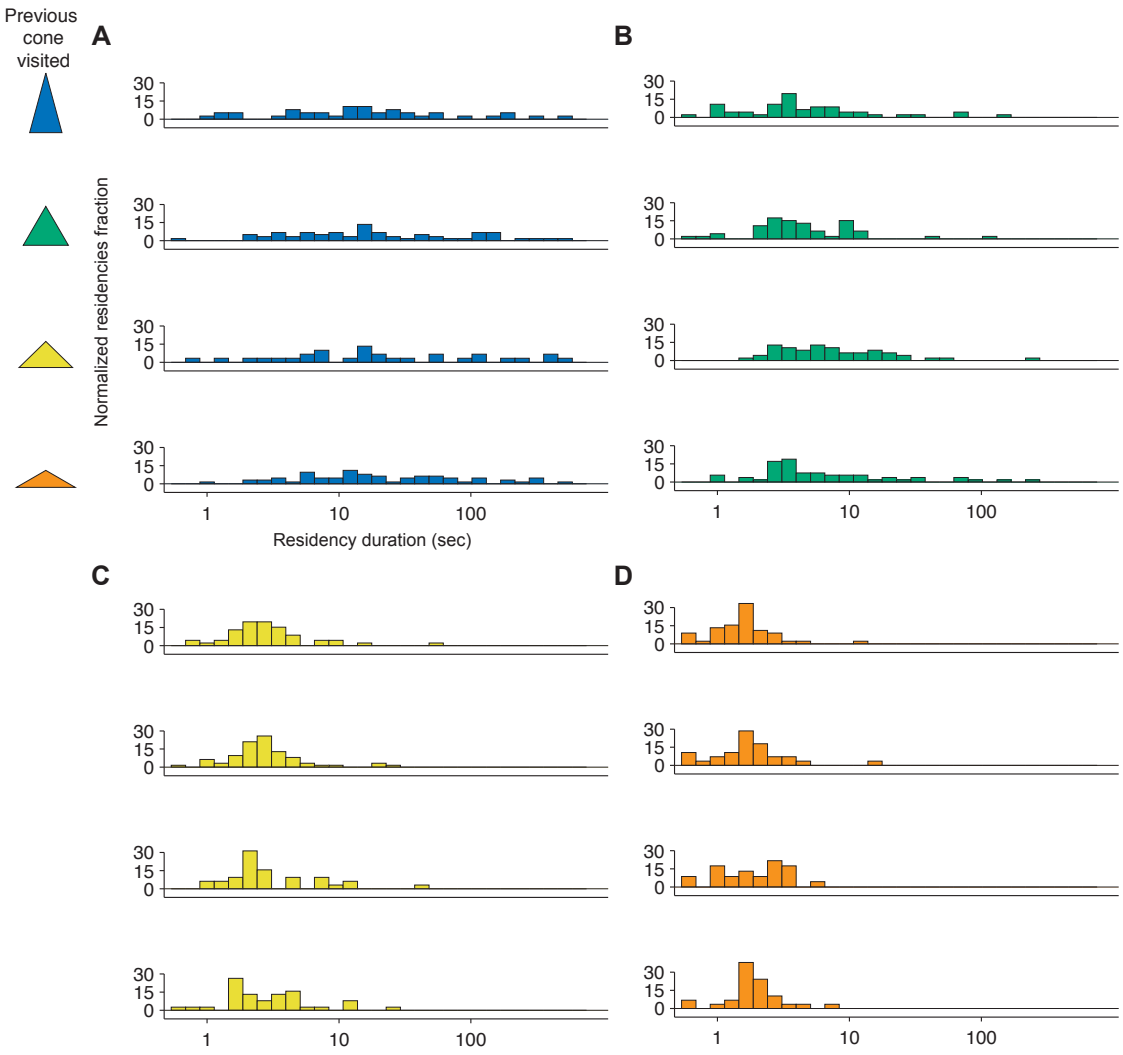

Figure 2.9: Encounter order does not effect residency time durations. Each panel shows the distribution of normalized residency durations for a cone type as shown in Figure 6B, but segregated by the cone visited prior to the current cone (each row of a given panel indicates a different prior cone). Color code as shown in Figure 1F. Axes and row labels are shown in panel A and apply to all panels. We used a Kruskal-Wallis test to test for differences in the distribution of within each panel and found none at $P < 0.01$ (A) Chi-Square .649, df = 3, $N = 190$; (B) Chi-Square 8.639, df = 3, $N = 192$; (C) Chi-Square 0.009, df = 3, $N = 178$; and (D) Chi-Square 2.846, df = 3, $N = 125$.

ning trials in complete darkness (flies could still be visualized by the near–IR sensitive tracking camera because of 850 nm lighting), and we impaired gravitational sense by gluing the joint between the second and third antennal segments, a manipulation that disrupts the function of the Johnston's organ (Budick et al., 2007; Duistermars et al., 2009; Sun et al., 2009). It is important to note that the flies with immobilized antennae exhibit robust locomotor behavior during exploration as measured by our basic statistics (compare Fig. 2.10 to Fig. 2.5). Figure 2.11 shows the percentage of time spent on each cone type arranged according to a Punnett square of the two sensory ablations. Intact flies exhibited the normal behavior, as seen in Figure 2.6. Interestingly, flies with either sensory manipulation (visual, Fig. 2.11B; mechanosensory, Fig. 2.11C) showed fairly typical responses to cone geometry, whereas flies with impairments of both visual and gravitational senses exhibited a greatly diminished preference for the blue cone (Fig. 2.11D and Supplementary Movie 2.2). These results suggest that either visual or antennal mechanosensory modalities alone provide cues sufficient to establish a fly's preference for the tallest, steepest cone. Only with both modalities compromised were the flies unable to assess the properties of the tallest, steepest cone and thus unable to exhibit a preference. Because we could not assume a priori that the same behavioral change (increased residency time) underlies the behavior of flies that had undergone sensory manipulations, we examined the cone residency durations for these flies. Figure 2.12 shows that there were long duration residencies on the blue cone in the flies with either single sensory manipulation. However, the flies with gravitational sensation impairment but intact vision (Fig. 2.12C)

showed significantly stronger responses to the two tallest, steepest cones (blue and green) compared to intact flies (Fig. 2.12A), not distinguishing between them, and exhibited a larger range of responses to all the cones. This may indicate that the visual mechanism used to assess the quality of a cone is less accurate than the mechanisms using the gravitational sense.

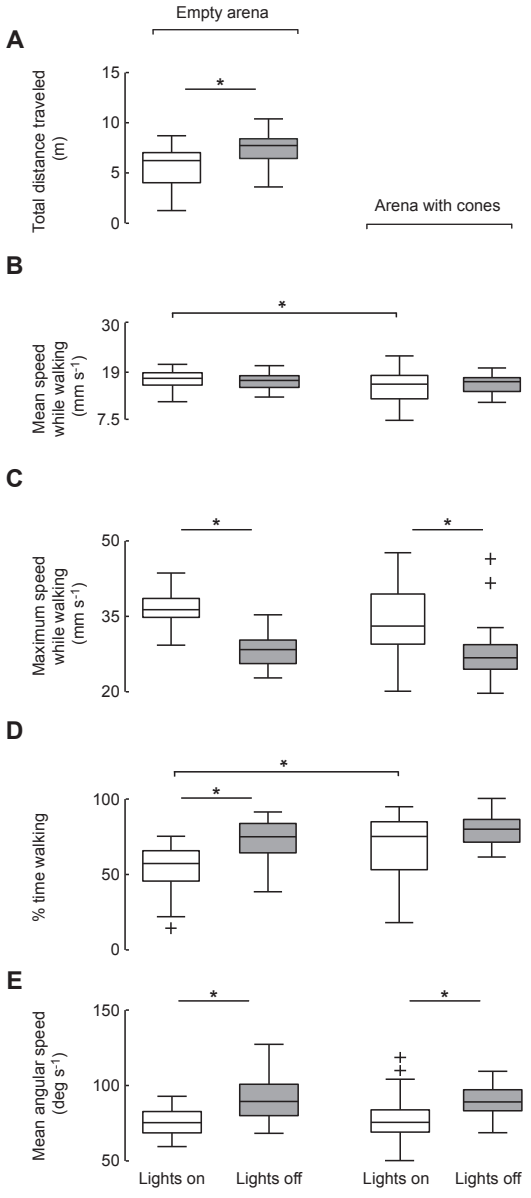

Figure 2.10: Basic statistics of locomotor behavior in flies with antennal immobilization. The two leftmost box plots in each panel show data for flies exploring an empty arena in the light (white, N=34) and in the dark (gray, N=34). The two rightmost box plots show data from flies exploring the floor of the arena with cones present in the light (white, N=40) and in darkness (gray, N=40). (A) The total distance traveled by individual flies during 10 min trial. (B) The mean speed calculated while the flies were walking. (C) The maximum speed calculated while the flies were walking. (D) The percentage of time the flies spent in the walking state, normalized for the total time spent on the floor of the arena when cones were present. (E) The mean angular speed calculated while the flies were walking. Statistically comparisons were made using heteroscedastic two-sample t-tests unless the data were not normally distributed in which case the Mann-Whitney U test was used. Asterisks indicate significantly different distributions (P<0.05) with Bonferroni correction).

Flies might memorize a visual feature of the cone's geometry during approach

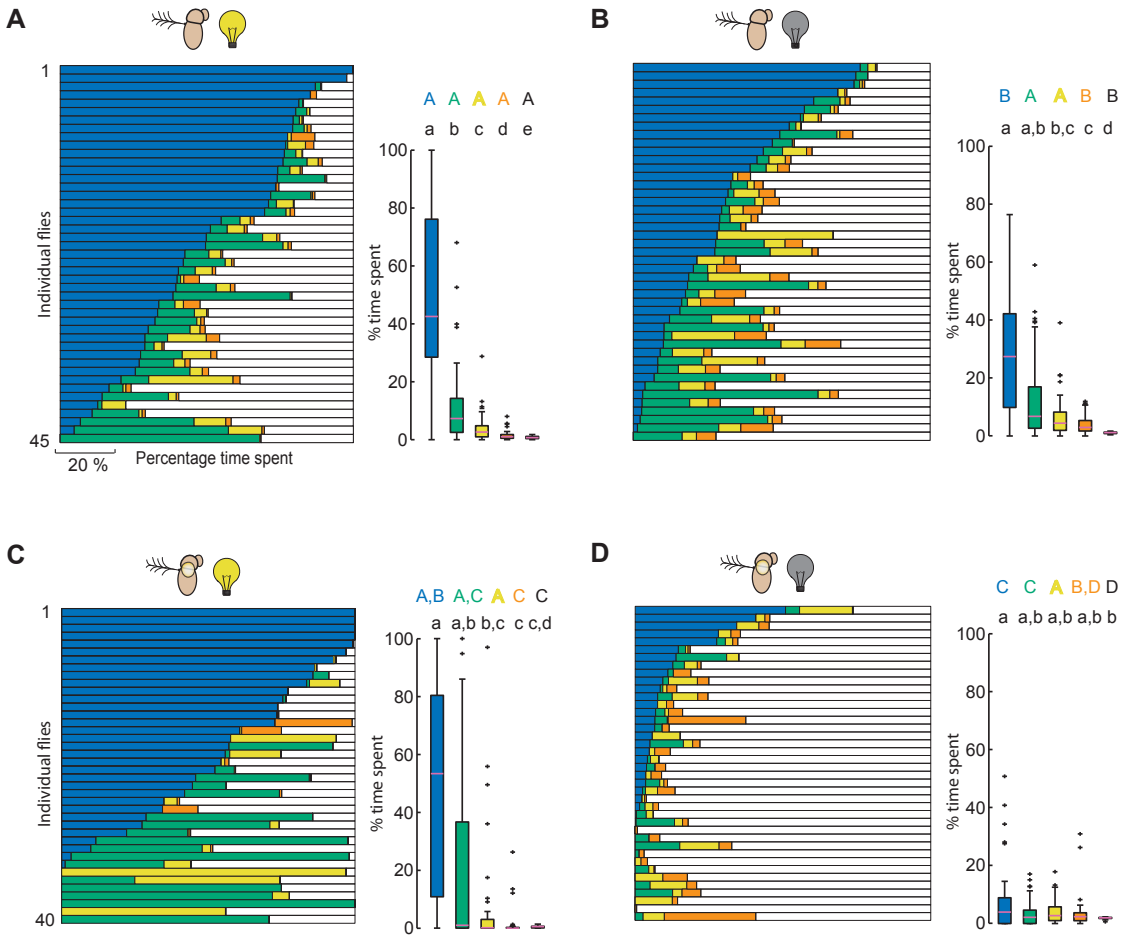

Figure 2.11: Sensory manipulations influence flies' preference for the tallest, steepest cone. The horizontal bar graphs show the percentage of the 10 min trial that each fly spent on each of the four cones and the arena floor (as in Fig. 2.6). Box plots show distribution of data after correcting for surface area which was identical for each cone. (A) Intact flies (N=45). (B) Flies in complete darkness (N= 45). (C) Flies with antennae immobilized (N=40). (D) Flies with antennae immobilized in complete darkness (N=40). See Figure 2.6 for description of statistical analysis and explanation of letter codes for homogenous groups.

to the cone and use this memory to control their exploration behavior once on the cone. The inability of flies without visual or antennal mechanosensory stimuli to sense cones, as measured by time spent on the cones, allows us to test this hypothesis. We placed a single tall, steep cone (blue) in the center of an arena that has dynamic visual surround, Arena 3 (Fig. 2.2). Then we tested the behavior of flies with immobilized antennae that explored the arena under one of three visual conditions: (1) lights on, (2) lights off, and (3) lights on while the flies are on the floor but turned off when the flies are on the cone. The percentage of time spent by the fly on the floor or cone is plotted in Figure 2.13. As expected from Figure 2.11D, the flies without visual stimuli spent less time on the cone than did flies with visual information available (Fig. 2.13A, B). Flies that had visual information available as they explored the floor but not as they explored the cone demonstrated exploration behavior on the cones like that of the flies that had no visual information available throughout the trial (Fig. 2.13B,C). This indicates that the flies are not using memory of the cone's geometry from the approach to control their exploration behavior on the cone.

2.3.7 Alteration of locomotor pattern during object exploration

After having demonstrated that flies can use either visual or mechanosensory cues to assess the geometry of the objects they are exploring, we next wanted to determine how this information alters the structure of their locomotor behavior. The flies' exploratory behavior in the arena can be modeled as periods of walking and stopping.

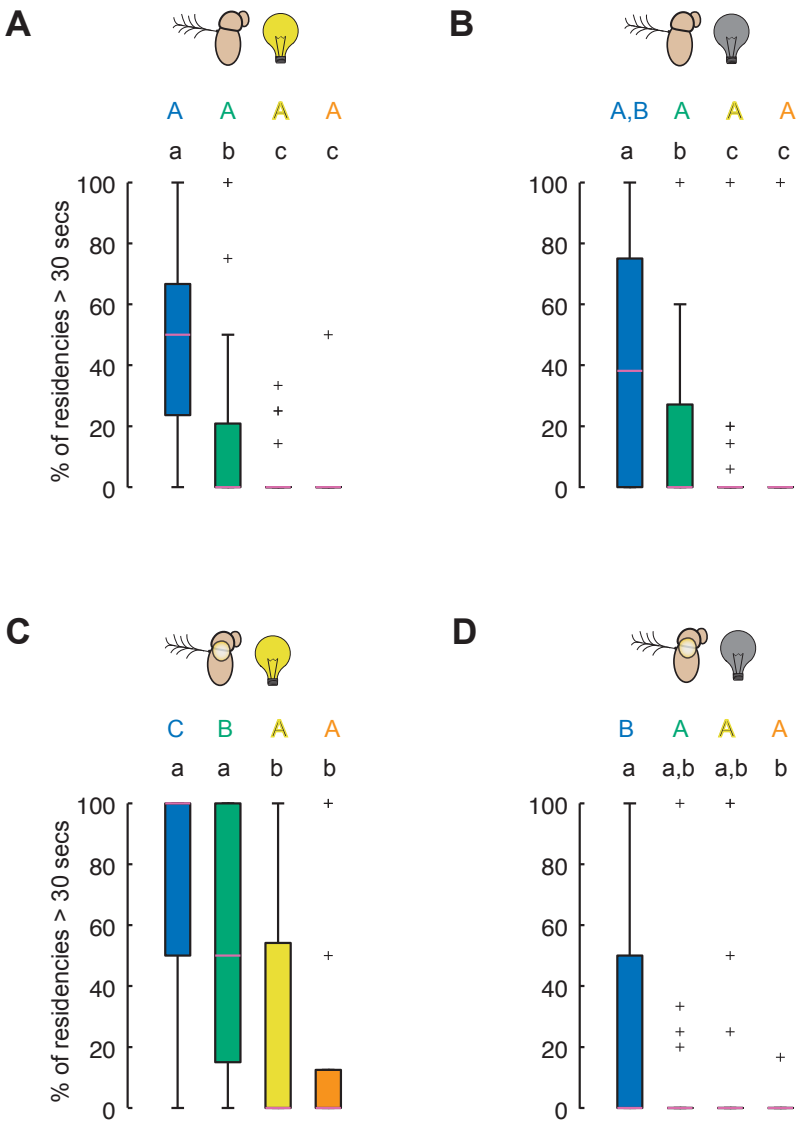

Figure 2.12: Sensory manipulations influence residency times. The percentage of residency durations that were longer than 30 seconds under the four experimental conditions. See Fig. 1F for color code. (A) Intact flies (N=45). (B) Flies in complete darkness (N=45). (C) Flies with antennae immobilized (N=40). (D) Flies with antennae immobilized in complete darkness (N=40). Statistically significant differences *within* and *across* trials were determined using the Kolmogorov-Smirnov two-sample test (P<0.05), with Bonferroni correction). See Fig. 2.6 for explanation of letter codes for homogenous groups.

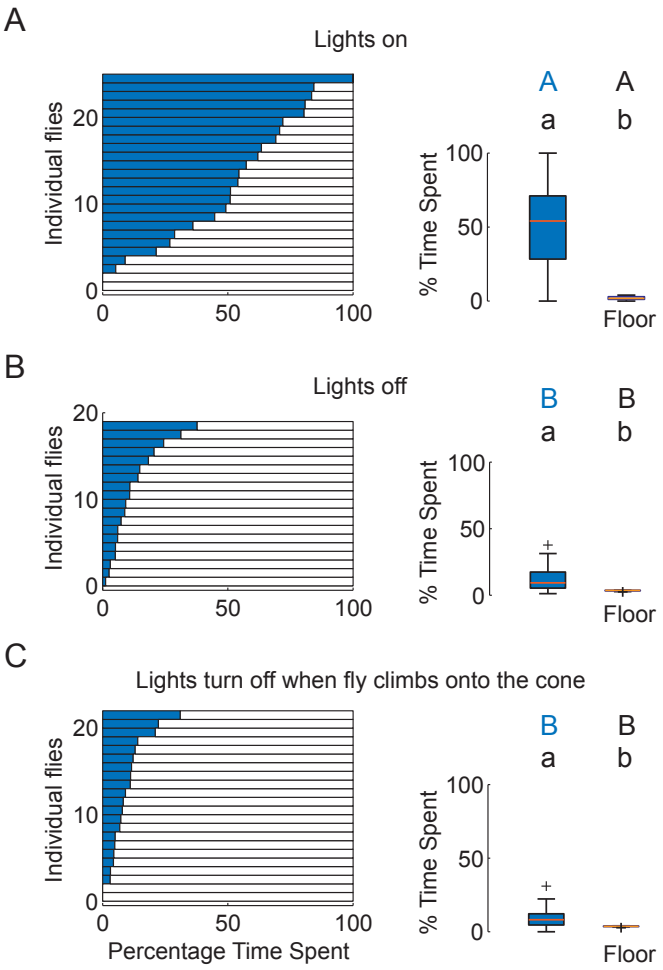

Figure 2.13: Flies do not use memorization of cone geometry during the approach to control exploration behavior. Flies with immobilized antennae explored the arena with a dynamic visual display and a single cone (Fig. 2.2. Horizontal bar graphs show the percentage of the 10 min trial that each fly spent on the single blue cones or the floor of the arena (white). The data are ranked by the time spent on the blue. The box-plots show the distribution of the time spent in each location after normalizing for the area of the surface being explored. The visual conditions were (A) statically displayed random checkerboard pattern (lights on) (N=25), (B) lights off (N=19), and (C) the lights are on while the fly is on the floor, but turn off when the fly climbs onto the cone (N=22). See Fig. 2.6 for explanation of statistically testing and of letter codes for homogeneous groups.

We applied our behavioral definition of walks and stops to the flies' trajectories (see Methods) and quantified the percentage of time stopped on each surface of the arena (all four cones and the floor, Fig. 2.14). Because we assigned all frames of each trajectory as either walks or stops, the percentage of time walking is the inverse of the stop data and is not shown. The flies with unimpaired vision and intact gravity sensation (Fig. 2.14A) were stopped for the majority of the time they were on the blue cone. This was also true of the flies with single sensory impairments, (visual, Fig. 2.14B; gravitational, Fig. 2.14C). Conversely, flies with both visual and antennal mechanosensory impairments (Fig. 2.14D) spent significantly less of their time on the blue cone in a stopped state. Whereas both the intact flies and the visually impaired flies spent significantly less time stopped on the green cone than the blue cone, the flies with impaired gravitation sense (but with vision) did not distinguish between the blue and green cones. Intact flies and the single sensory ablation flies all spent less time stopped on the yellow and orange cones than the blue or green cones. In contrast, the flies with both visual and gravitational sense impairments could not distinguish among any of the cone types as measured by their time stopped. Flies of all types consistently spent the majority of their time on arena floor walking rather than stopped. The intact flies' locomotor pattern shifted to a higher percentage of time stopped when residing on the cones, with the largest shift on the blue cone. Thus, this increase in percentage of time stopped is responsible for the large percentage of time spent on the tallest, steepest cone.

The frequency of stops did not change in a systematic way according to cone type

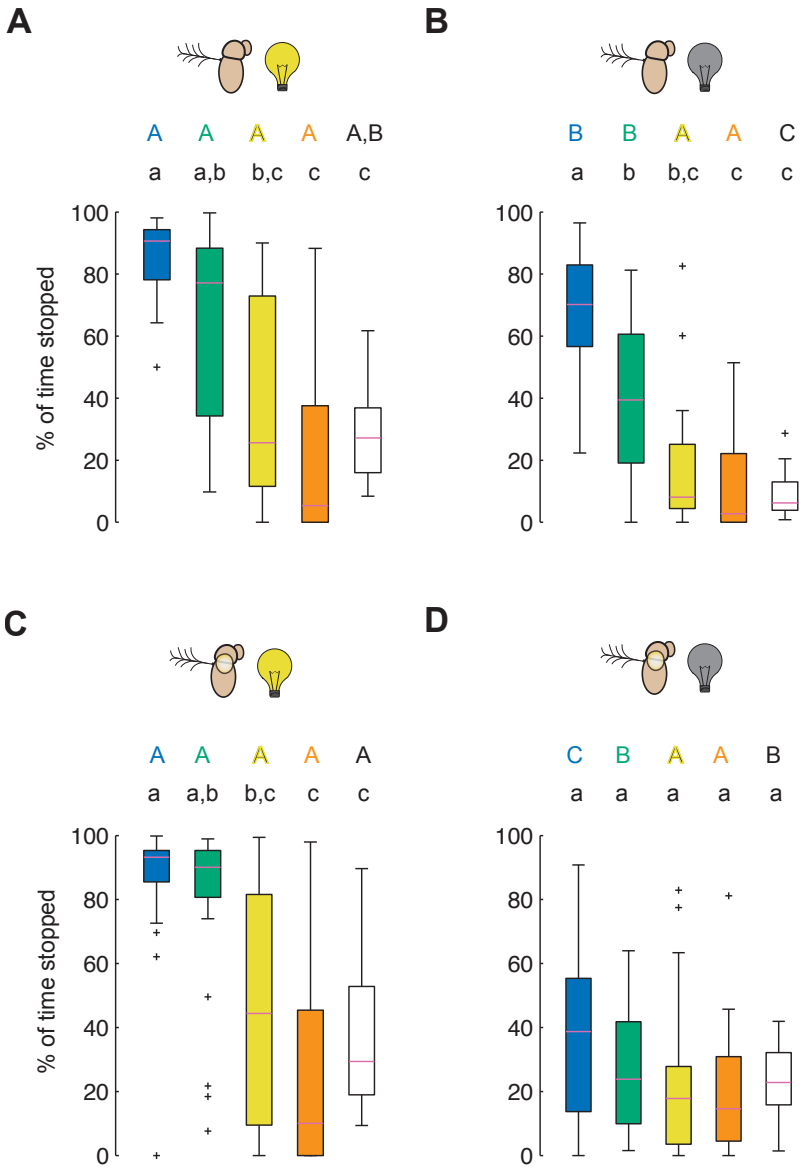

Figure 2.14: Sensory manipulations effect percentage of time spent stopped on cones. Color-coded (see Fig. 2.1F) box plots indicate the percentage of time stopped on each surface of the arena, with white indicating the arena floor. (A) Intact flies (N=25). (B) Flies in complete darkness (N=25). (C) Flies with antennae immobilized (N=40). (D) Flies with antennae immobilized in complete darkness (N=40). Statistically significant differences *within* and *across* trials were determined using the Mann-Whitney U test (P<0.05, with Bonferroni correction). See Fig. 2.6 for explanation of letter codes for homogenous groups.

(Fig. 2.15), however the duration of stops did vary according to the type of cone the fly was exploring. The cumulative sums of the percentage of stop durations for all stops by all flies are presented in Figure 2.16, with the portion of each individual fly's distribution of stop durations that was longer than 10 sec shown in the inset. Figure 2.16A shows that intact flies on the tallest, steepest cone performed a larger percentage of long stops than they did on the yellow and orange cone types. Flies with single sensory impairments, visual (Fig. 2.16B) and antennal mechanosensory (Fig. 2.16C), still exhibited significantly more long stops while exploring the blue cone than the yellow and orange cones. Their responses to the cones were not significantly different than those of the intact flies. In contrast, flies with impairments in both their visual and gravitational senses (Fig. 2.16D) performed few long stops on any of the cone types, indicating their inability to sense cues that would allow them to assess a cones geometry.

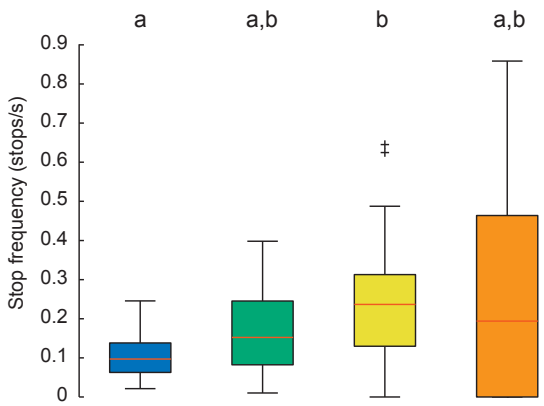

Figure 2.15: Frequency of stops does not underlie the increase in time spent on the tallest, steeper cones. The distribution of the stop frequency (stops/s) of flies exploring each of the cones is shown. See Figure 2.1F for color code. The Wilcoxon signed rank test for non-independent, non-normal data was used to compare groups ($P<0.05$ with Bonferroni correction for multiple comparisons). See Fig. 2.6 for explanation of letter codes for homogenous groups.)

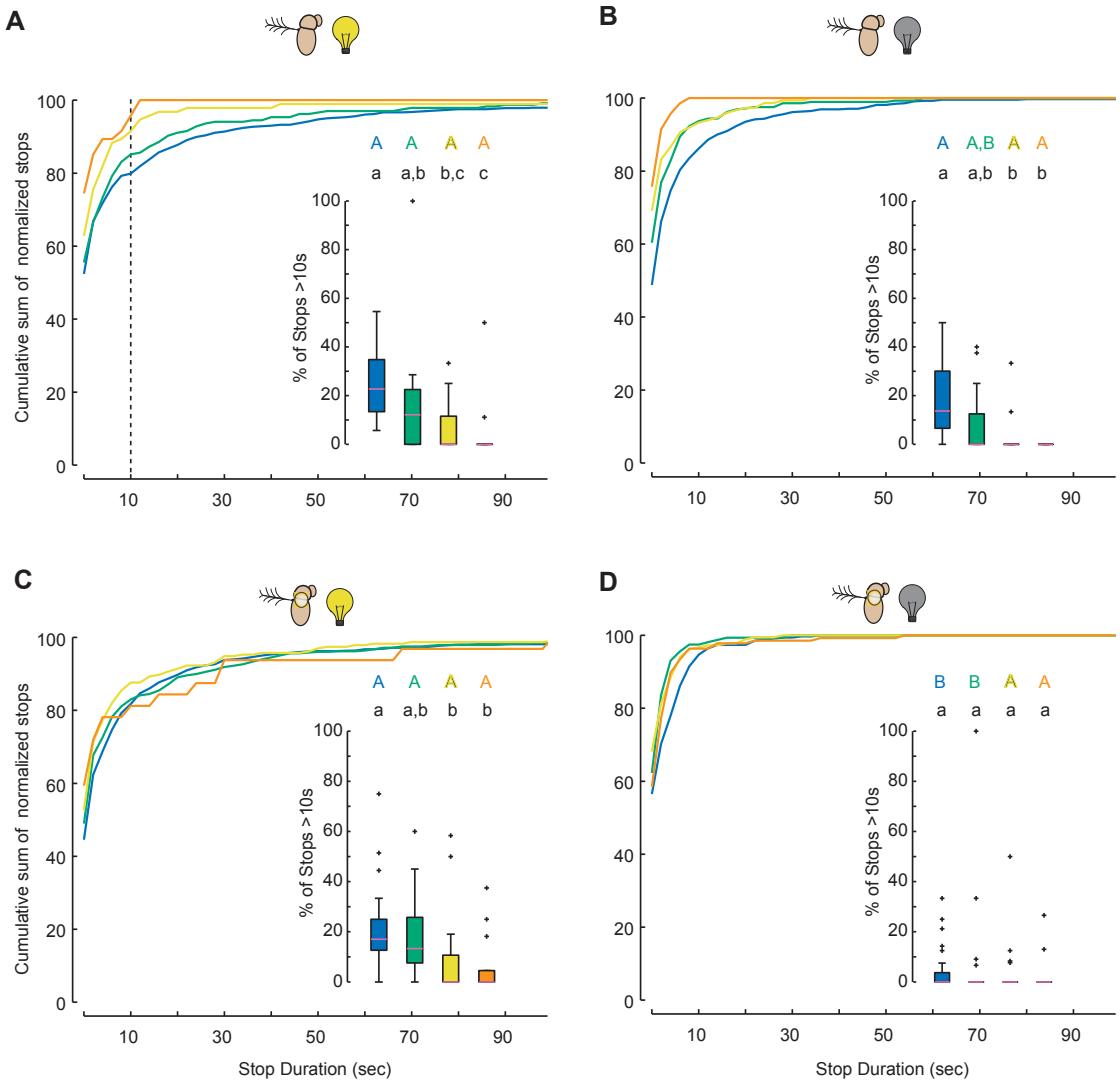

Figure 2.16: Sensory manipulations influence distributions of stop durations. Each panel shows cumulative sums of the normalized distribution of stop durations, with insets indicating the percentage of stop durations that were longer than 10 sec (see Fig. 2.8C). See Fig. 2.1F for color code. (A) Intact flies (N=25). (B) Flies in complete darkness (N=25). (C) Flies with antennae immobilized (N=40). (D) Flies with antennae immobilized in complete darkness (N=40). Statistically significant differences *within* and *across* trials were determined using the Kolmogorov-Smirnov two-sample test (P<0.05, with Bonferroni correction). See Fig. 2.6 for explanation of letter codes for homogenous groups.

2.3.8 Flies perform stops at the top of tallest, steepest cone

Having determined that the assessment of cone geometry plays a role in structuring locomotor behavior, we were interested in where the flies stopped on the cones. The colored histograms in Figure 2.17 show the fraction of stops performed by the flies on each cone at a given elevation, and the elevations of long stops (defined in Fig. 2.16), are shown by the superimposed black histograms. The intact flies clearly show a preference for stopping at the top of the tallest, steepest (blue) cone, and the long stops are also primarily at the top of the cone (Fig. 2.17A). These flies also perform the majority of their stops at the top of the green and yellow cones but not the orange cone. Flies with single sensory manipulations (visual Fig. 2.17B and mechanosensory Fig. 2.17C) also perform the majority of their stops at the top of the blue, green and yellow cones, but not the orange cone. This indicates that flies using either visual or antennal mechanosensory information can still localize the top of the cones. The flies lacking both visual or antennal mechanosensory information show a less pronounced preference for stopping at high elevations.

2.4 Discussion

We developed a large arena to study the locomotor behavior of walking *Drosophila* in both simple and topologically more complex environments. The role of vision in structuring locomotor behavior was apparent even when 3D objects were absent from the arena (but a surrounding visual panorama was present). Flies exploring an empty, dark arena spent more time walking, traveled a greater distance, and fol-

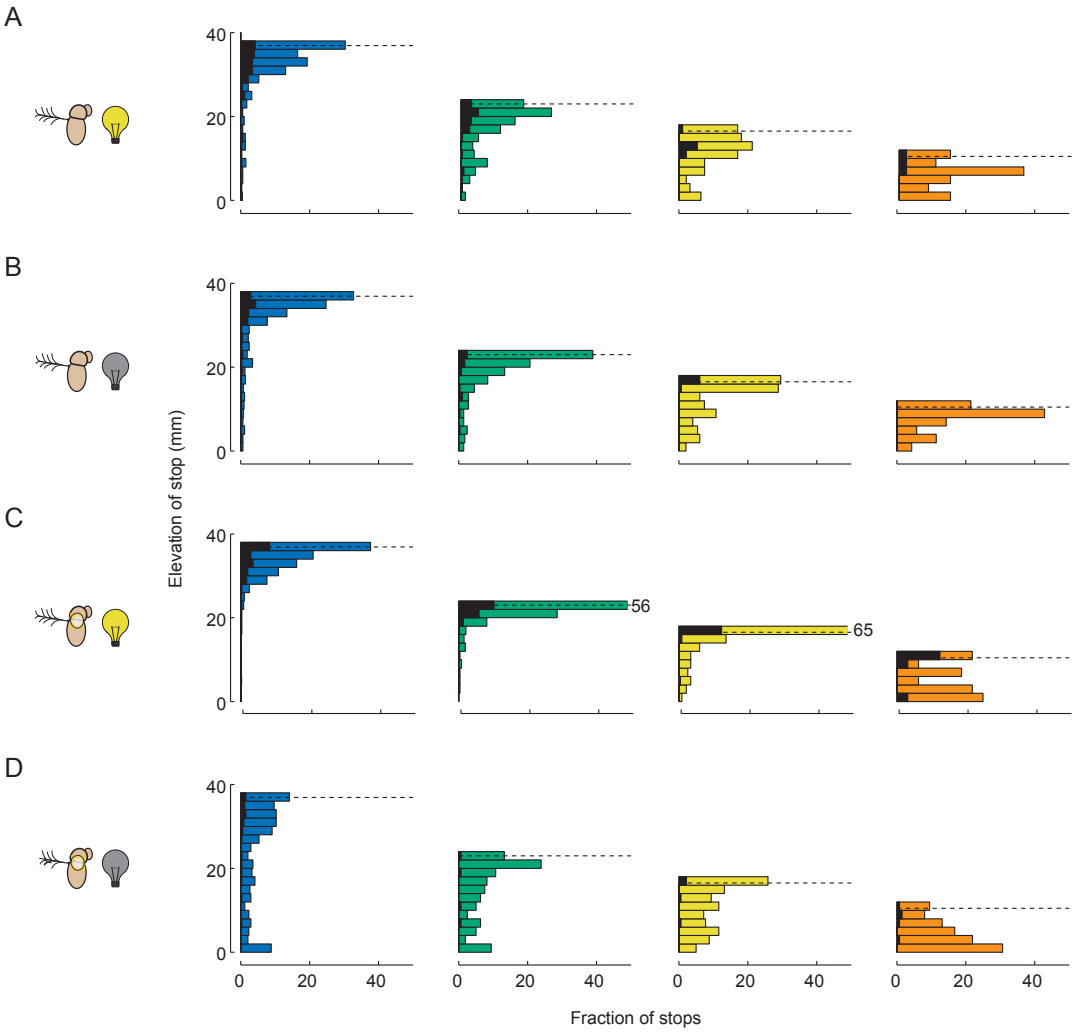

Figure 2.17: Flies tend to stop at the top of the cones. Horizontal bar graphs show the fraction of all stops (colored) and long stops (black) that are performed at a given elevation. Each column represents the stops on a given cone type, color code as in Fig. 1F. The dashed black line in each column is the height of the top of that cone; stop elevations can be taller than the height of the cone because we included the flies' body height (1 mm) in our 3D model. Each row is a different sensory condition: (A) intact flies (N= 25), (B) flies in complete darkness (N= 25), (C) flies with antennae immobilized (N=40) and (D) flies with antennae immobilized in complete darkness (N=40). In C, the top bin of the green and yellow histograms is truncated at 50% for presentation purposes; the real values are 56% (green) and 65% (yellow).

lowed more convoluted paths than flies exploring a lit arena (Figs 2.3, 2.5). While exploring an environment containing a set of cones, flies spent substantially more time on the tallest, steepest cone even though all cones had the same surface area (Fig. 2.6). Cone removal experiments suggest that the flies assess object geometry via some absolute measure and not by comparison with other objects (Figs 2.6, 2.9) or memory (Fig. 2.13). The increased time spent on the tallest, steepest cone is due to longer residency times once encountering the object (Fig. 2.8) and not a greater attractiveness during approaches (Fig. 2.7). The increased residency times are in turn explained by a shift in the distribution of stop durations towards long stopping intervals (Fig. 2.16). These long stops occur at the top of the cone (Fig. 2.17). Experiments conducted in complete darkness and with flies whose antennal mechanosensory function was impaired indicated that flies can use either visual or mechanosensory cues to assess cone geometry (Figs. 2.11–2.16). Only if both modalities are impaired do the flies demonstrate no preference for tall, steep objects (Figs. 2.11–2.16).

We deliberately designed these experiments using objects that control for lateral surface area, and as a consequence two potentially salient features of geometry, slope and height, were positively correlated. Thus, in none of our experiments could we distinguish between the flies' response to slope and height. It is clearly of interest to determine which of these two features of object geometry are encoded by the visual-mediated and mechanosensory-mediated mechanisms. We report results of experiments that decorrelate object slope and height in Chapter 3.

2.4.1 Visual stimuli influence the statistics of locomotor behavior

This work corroborates earlier studies showing that salient visual information can structure the locomotor behavior of walking fruit flies (Figs 2.3–2.5) (Bulthoff et al., 1982; Götz, 1980, 1994; Götz and Wenking, 1973; Horn, 1978; Neuser et al., 2008; Schuster et al., 2002; Strauss and Pichler, 1998; Strauss et al., 1997). Further, we have shown that the presence or absence of visual stimuli can change fundamental characteristics of walking behavior such as maximal translational speed, walking bout duration, and mean angular speed (Fig. 2.5). The observed changes in the statistics of walking behavior are likely due to visual reflexes, such as object fixation and both rotatory and translatory optomotor responses (Götz, 1975, 1980; Götz and Wenking, 1973; Kalmus, 1964; Katsov and Clandinin, 2008; Zhu et al., 2009). Indeed, all animals depend on external cues in order to maintain a straight course over a significant time or distance (Dusenbery, 1992), and even humans depend on visual and auditory cues to walk straight (Schaeffer, 1928).

2.4.2 Object fixation

Whereas the visual environment we used in our experiments was much more complicated than those used in earlier experiments of object fixation in walking flies, our results confirm certain components of those earlier studies. Walking flies used vision to orient towards 3D objects (Fig. 2.7), as observed in earlier experiments with virtual or unreachable visual objects (Götz, 1980; Horn, 1978; Horn and Wehher, 1975).

Götz and colleagues also described a curious behavioral phenomenon when a fly is presented with two equally attractive, but unreachable, objects on opposite sides of an arena – an experiment known as 'Buridan's paradigm'. Under such conditions, flies tend to walk back and forth between the two objects indefinitely even if the objects are of different size and shape (Bulthoff et al., 1982; Götz, 1980; Strauss and Pichler, 1998). This has been explained as an alteration between fixation and anti-fixation of objects and may facilitate efficient search among multiple visual targets (Götz, 1989, 1994). Whereas we did observe a similar indifference to object geometry during the approach phase of exploratory behavior (Fig. 2.7), we did not observe a regular and sustained alteration of approach to different objects, perhaps because in our arena the flies could actually reach the objects and explore them, thereby breaking the cycle of fixation and anti-fixation that is required for Buridan's paradigm.

2.4.3 Preference for tall, steep objects

Our experiments demonstrate that hungry *Drosophila* exhibit a preference for tall, steep objects and that they assess object geometry using either visual cues, mechansensory cues or a combination of the two. However, we discovered this preference in a laboratory setting using hungry flies whose wings had been clipped, and it is therefore not immediately clear what selective pressure in a natural environment would lead to this innate and robust behavior. We speculate that the strongest drive on these hungry flies would be to find food and that the preference for tall, steep objects is somehow related to a food search strategy. Our experimental arena contained no

source of attractive odor, which hungry flies would otherwise use to search for food (Bell, 1991). One possible ethological interpretation of our results is that hungry flies prefer high perches because by moving above the ground-air boundary layer they increase the likelihood of encountering an odor plume from a distant food source. In this scenario, the long stop periods represent pauses in which the flies are waiting for the chance encounter of an attractive odor. Another possibility, which is not mutually exclusive, is that the long stop periods on a steep slope represent a predator avoidance strategy. Flies might be avoiding the open field of the arena floor because they would be more vulnerable when walking or stopping on open ground rather then when perched on a vertical object. Yet another possibility is that steep surfaces or high elevations may represent good take-off locations, and anecdotally we have observed that flies appear much more likely to jump from the surface of a steep cone than from the arena floor. Although it is tempting to interpret such jumps as attempted flight initiations, it is very likely that wing clipping – a manipulation that was necessary for our experiments – alters the behavioral state of the flies. It is noteworthy that for the most part the wing-clipped flies did not persistently try to escape from the arena by jumping, even though such flies will perform escape jumps in responses to looming stimuli with the same probability as intact flies (Card and Dickinson, 2008).

2.4.4 Sensory modalities involved in cone assessment

Although our results implicate both vision and the mechanosensory function of the antennae in the flies' ability to assess the geometry of 3D objects, such conclusions

must be made with some caution. Several recent studies suggest that the JO is used in gravitational sensing in *Drosophila* (Armstrong et al., 2006; Baker et al., 2007; Kamikouchi et al., 2009; Sun et al., 2009), however, insects are known to have other mechanosensory systems capable of measuring gravity and posture (Beckingham et al., 2005). Thus, we cannot assume that immobilizing the antennal joint removes all cues about the flies' orientation in the gravitational field. Moreover, by immobilizing the joint we have likely compromised the function of the entire JO, which is also known to function in audition (Eberl et al., 2000) and wind detection (Yorozu et al., 2009). Another problem is that by removing all visible light we eliminate sensory input to both the compound eyes and the ocelli.

Despite the caveats with our sensory manipulations, it is nevertheless informative that together these two relatively simple sensory manipulations do appear to be sufficient to eliminate the flies' preference for tall, steep objects (Figs. 2.11–2.16). Our experiments on intact flies in the dark suggest that the flies are able to sense the slope or height of a given cone using the antennal mechanosensory system. Recent work has shown that some JO neurons are responsive to steady-state deflections of the third antennal segment relative the second (Kamikouchi et al., 2009), as well as body rotations designed to simulate gravity (Sun et al., 2009). Further, the increased likelihood of long stops on tall, steep objects is similar to a recently described behavior in which flies cease walking in response to air currents (Yorozu et al., 2009). This behavior is mediated by a subset of mechanoreceptor neurons within the JO, which are also thought to underlie gravity sensing (Kamikouchi et al., 2009). Motivated by

these two recent studies, we attempted to test flies in which this subset of JO neurons were ablated by ectopic expression of ricin A, but the results were confounded by additional effects on locomotor behavior (A. Robie and M. Dickinson, unpublished). We also note that although the JO is well-suited to perform an instantaneous assessment of surface slope, it is also possible that the fly uses its gravitational sense in combination with an idiothetic step counter, such as that proposed for the desert ant *Cataglyphus* (Wittlinger et al., 2006), to perform vertical path integration, thus providing an estimate of object height.

Flies with visual cues available, but with the JO immobilized, also showed a preference for the tallest, steepest cone. There are many mechanisms by which flies might employ visual cues to assess the object geometry. Once atop the cones, flies might estimate height by actively peering to provide motion parallax cues. *Drosophila* do use motion parallax cues to estimate the distance to objects as they approach (Schuster et al., 2002; Pick and Strauss, 2005), and locusts nymphs use active peering to judge the distance to objects before they jump (Wallace, 1959). Another possibility, suggested by the studies showing that bees are able to integrate optic flow to estimate distance flown (Srinivasan et al., 2000), is that flies might also use optic flow to measure the distance traveled up the surface of an object – a form of path integration using visual information rather than ideothetic cues. To accurately measure height, such a behavior would require some JO-independent measure of gravity or body posture. Another possible vision-based mechanism is that flies might use their compound eyes or ocelli to determine body orientation relative to the local horizon

and thus estimate the steepness of the surface they are exploring. Whether the compound eyes or the ocelli are involved, it is interesting to note that the flies with vision intact but their JOs impaired exhibit a decreased ability to distinguish between the blue and green cones in our experiments, suggesting that the vision-based means of assessing cone geometry is less precise than the mechanosensory-based mechanism.

In this work, we have focused on describing flies' preference for tall, steep objects, the underlying change in locomotor statistics responsible for this preference, and the sensory modalities used for the assessment of object geometry. Our research has identified an innate behavior in which sensory information from the visual system and the antennae are used to regulate locomotion in the context of the exploratory behavior of hungry flies. In the future, it will be of interest to determine the functional role of this behavior in the animal's natural history, as well as elucidate the underlying neural mechanisms.

Chapter 3

The antennae can sense object slope

3.1 Introduction

Flies respond to objects of high slope and elevation by shifting their locomotor behavior towards longer duration stops (Chap. 2). The assessment of object geometry can be done using either visual or mechanosensory cues. We examined the role of object height and slope in shaping the exploratory behavior of freely walking fruit flies. The results suggest that the flies' antennal mechanosensory system is able to judge the slope of objects rather than the height. The experiments did not, however, indicate whether their visual system distinguishes among objects by slope or height.

3.2 Methods and materials

3.2.1 Flies

We used mated three-day-old female fruit flies, *Drosophila melanogaster* Meigen, from a laboratory population descended from 200 wild-caught isofemale lines for all experiments. The flies were maintained on a 16:8 light:dark cycle and all experiments were conducted during the evening activity peak. The day before experiments were performed, we anesthetized the flies by cooling them in order to clip the wings between the first and second cross vein. If the antennae were immobilized, it was also done at this time by fixing the joint between the second and third antennal segments with UV-cured glue. Flies were then allowed to recover overnight and were wet starved 12 hours before the midpoint of the experimental session. Thirty minutes before the experimental session the flies were transferred into individual vials with a water source

and allowed to acclimate to the experimental light conditions.

3.2.2 Arena

All experiments were conducted in the large free-walking arena described in Chapter 2 as Arena 2. I will briefly summarize the key aspects of the arena here. This arena consisted of a 24.5 cm diameter metal plate surrounded by a thermal barrier and a backlit static visual pattern. The temperature of the arena floor was actively controlled by feedback from a thermocouple to four TE modules that heat or cool the plate to the temperature set point of 24°C. The arena was illuminated with near-IR LEDs from above so that the fly could be recorded using a camera sensitive in the near-IR (A622f, Basler) operating at 20 fps (Fig. 2.1). The fly's x–y position and body orientation were recorded in real-time using the camera software package Motmot (Straw and Dickinson, 2009) with the FlyTrax plug-in.

3.2.3 Data analysis

The data were analyzed as in Chapter 2 using custom software written in Python (www.python.org) and MATLAB (Mathworks, Waltham, MA, USA). The 2D position data were used together with a model of the arena to estimate the flies' 3D positions in the arena. The position data were smoothed with a Kalman filter and used to calculate the flies' 3D velocity. The flies' locomotor behavior was segmented into periods of walking or stops based on a two threshold velocity behavior classifier. The location of the fly in each frame of the movie ('on' or 'off' cone) was determined by

hand digitization of the objects' position for each trial. For some of the analysis we considered only those stops that occurred at the top of cones. The top of the cone was defined as within 6 mm (∼2 fly body lengths) of the top of a given cone.

3.2.4 Statistics

We present data as box-and-whisker plots because many of the distributions were not normal (for more details on this presentation style see Chap. 2). All statistical analysis was done with SPSS software package (SPSS Inc, Chicago, IL, USA) and is reported as described more extensively in Chapter 2.

3.2.5 Experimental design

Arena with objects of varied geometry

The objects used in Chapter 2 to demonstrate that flies prefer the tallest, steepest object in the arena (as assayed by amount of time spent exploring each object), were designed to have equal lateral surface area and as a consequence confounded slope and height. In order to test which aspect of the objects' geometry the flies sense, we created two new sets of objects that decorrelate slope and height. These objects were based on the geometry of the cones of equal lateral surface area from Chapter 2. The set of objects of equal height but varied slope were all as tall as the blue cone (36 mm) and varied in the same increments of slope. The set of objects of equal slope were as steep as the blue cone (75°) and varied by same increments of height. The three sets of cones are shown in Figure 3.1. We used only three cones in each experiment

instead of four as in the last chapter because there was little difference in the flies' responses to the two shortest, broadest cones (yellow and orange) in Chapter 2. In addition, the footprint of a cone with a height of 36 mm and slope of 30° would fill more than a quarter of the arena area.

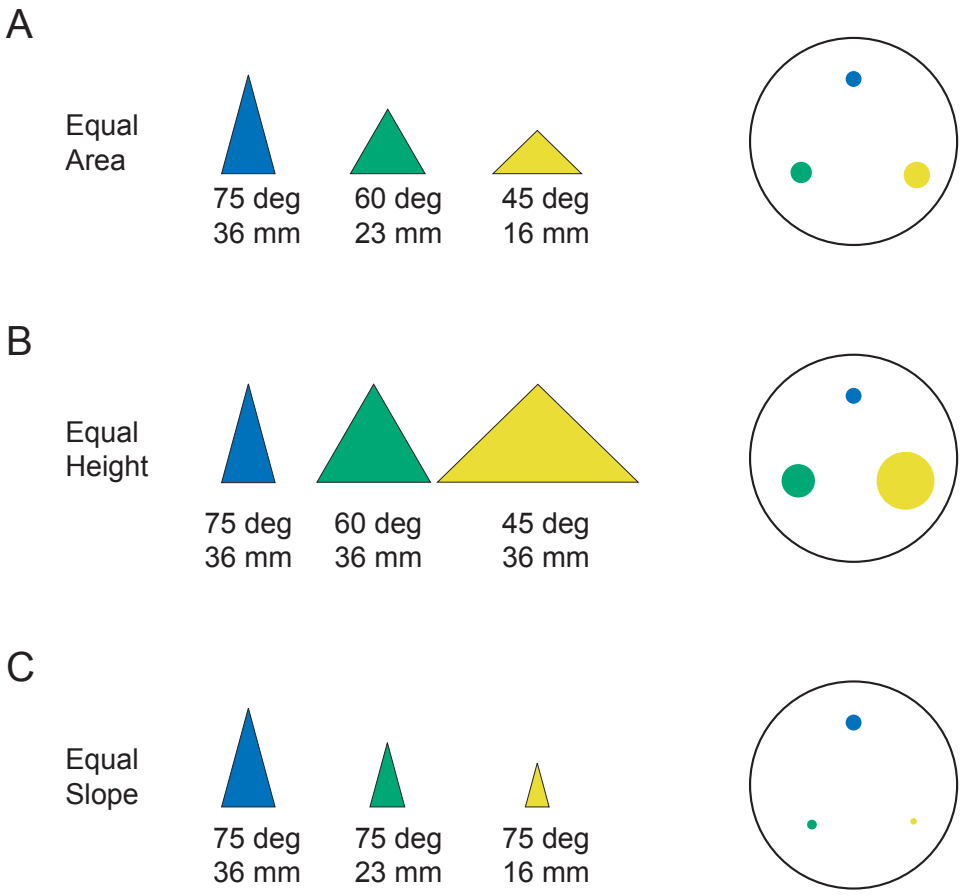

Figure 3.1: The geometry of the equal area, equal height and equal slope object sets. Each row shows the geometry and color code used for a given cone set as well as the footprint of those cones in the arena. (A) Cones of equal lateral surface area, (B) cones of equal height (36 mm) and (C) cones of equal slope (75°).

In these experiments each trial consisted of an individual fly exploring the arena for 20 minutes. We tested flies on three different cone sets: (1) intact flies exploring the arena with equal area cones, (2) equal height cones, or (3) equal slope cones. In

addition, for each cone set, we tested flies in each of the four sensory conditions described in Chapter 2: (1) control (intact) flies, (2) flies without visual information but unmanipulated antennae, (3) flies with visual information available but immobilized antennae, and (4) flies without visual information and immobilized antennae. In each trial the three objects of a given set were place in the arena on a triangular grid with their relative positions systematically cycled. All the flies were loaded into the arena by gently tapping them from the individual starvation chambers into the arena. The arena and objects were washed with detergent and rinsed between each trial.

3.3 Results

3.3.1 Flies show preference for the tallest, steepest object

We changed the experimental conditions from those described in Chapter 2 by reducing the number of cones in the arena from four to three and allowing the individual flies to explore the arena for 20 minutes rather than 10 minutes. We increased the exploration time in order to increase the likelihood the flies would encounter and explore all of the objects in the arena. Due to these changes in the experimental protocol, we first needed to examine whether the results were consistent with those seen in Chapter 2. In Figure 3.2 we summarize the behavior of intact flies that explored the arena with three objects of equal lateral surface area. These objects (Fig. 3.1) were the same geometry as the blue, green and yellow cones from Chapter 2 (Fig. 2.1F). Figure 3.2A shows that the flies spent significantly more time on the tallest, steepest object in the

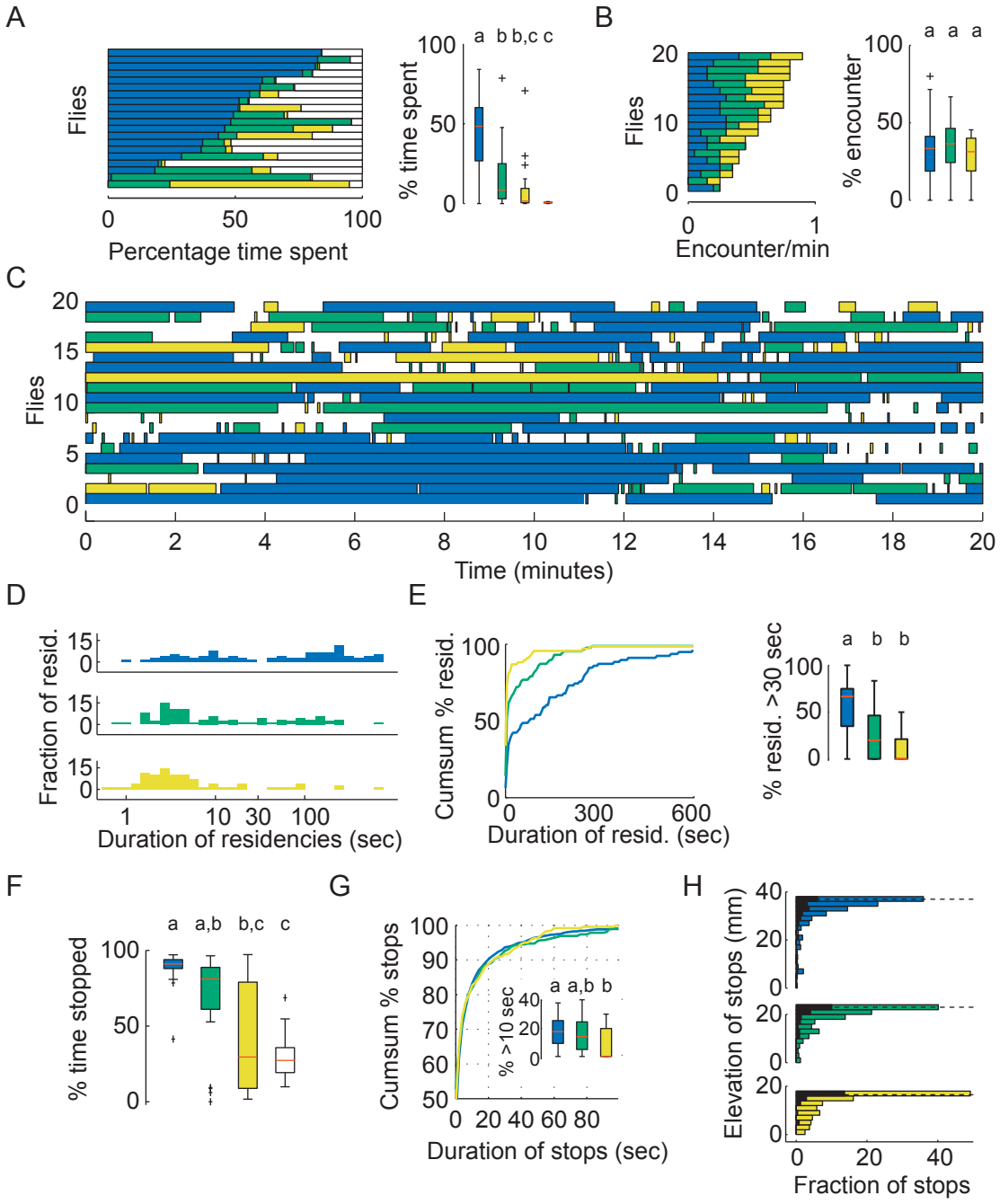

Figure 3.2: Flies behavior exploring arena with objects of equal area. For color code see Fig. 3.1A. (A) Percentage time spent after Fig. 2.6A,D. (B) Encounter rate and percentage of encounters after Fig. 2.7A,B. (C) Ethograms after Fig. 2.8A. (D) Histogram of residency durations after Fig. 2.8B. (E) Cumulative sum of residency durations and percentage of individuals' residencies longer than 30 secs after Fig. 2.8C. (F) Percentage of time stopped in a given location after Fig. 2.14A. (G) Cumulative sum of stop durations and percentage of individuals' stops longer than 10 secs after Fig. 2.16A. (H) Elevation of stops after Fig. 2.17A. (n=20)

arena, which is consistent with the results of Figure 2.6A,D. Figure 3.2B, the percentage of encounters, was also consistent with the four-cone experiments (Fig. 2.7B). Visual inspection of the time history of the flies' exploratory behavior indicates they spent more time on the blue cone once it was encountered (Fig. 3.2C), and the percentage of an individual's residency times that were longer than 30 seconds shows that the flies spent significantly longer on the blue cone once it was reached than the other cone types (Fig. 3.2D,E). This increase in longer duration residencies on the tallest, steepest object is consistent with that observed in the four-cone experiments (Fig. 2.8). However, we did observe a few more long residencies on the broadest, shortest cone than expected from our prior experiments, perhaps due to the longer exploration period. In Chapter 2, we reported that the increased residency time on the blue cone was due to a shift in locomotor behavior towards longer duration stops (Figs 2.14, 2.16). It is also the case in the three-cone experiments that flies spent more time stopped when on the blue than the yellow cone (Fig. 3.2F) and that this difference is due to an increase in the long duration stops (Fig. 3.2G). The flies also tended to stop near the top of the cones (Fig. 3.2H) as we saw in the four-cone trials (Fig. 2.17A).

3.3.2 Flies maybe able to assess height and slope of cones

After having demonstrated that the behavior of the flies in an arena with three cones was comparable to the prior experiments with four cones, we tested the role of object slope and height on the flies' exploratory behavior. We were interested in what

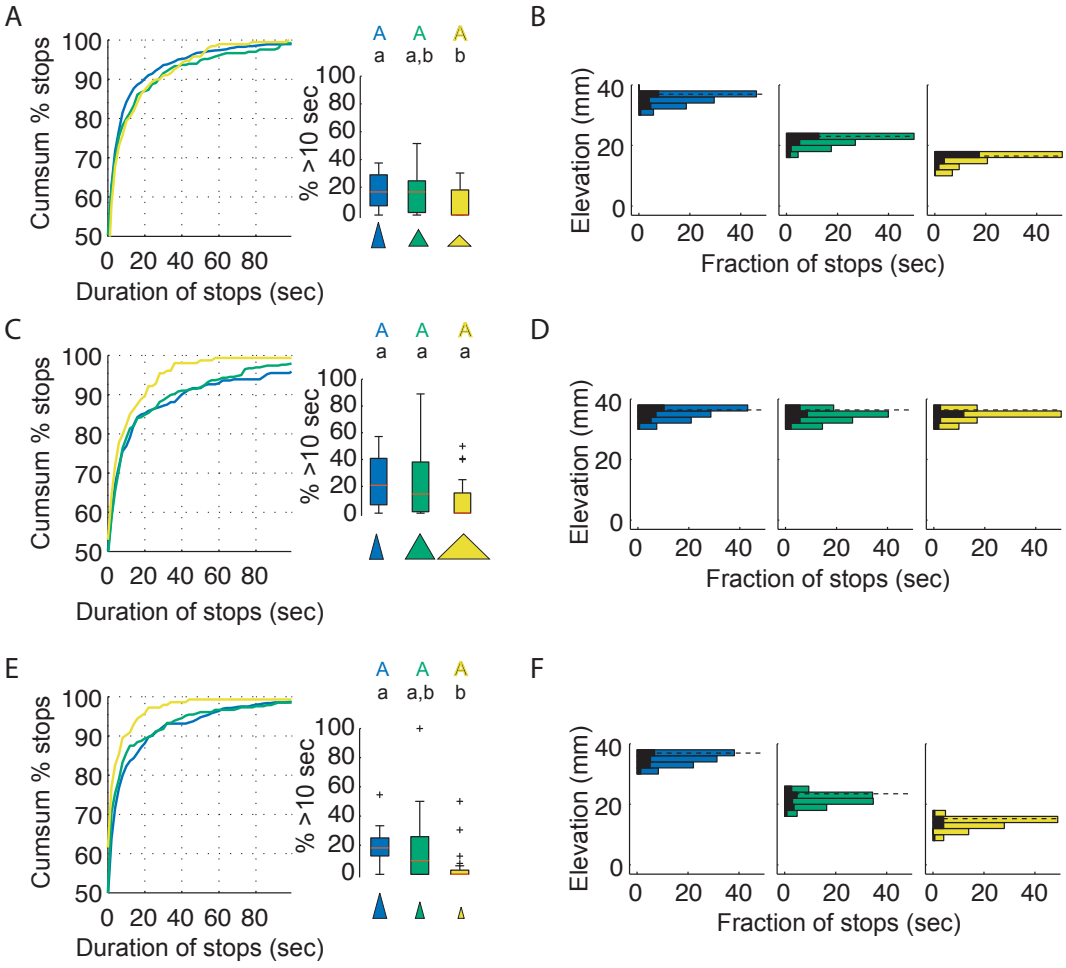

Figure 3.3: Flies can assess height and slope of objects. By selecting for stops that happen at the top of the cones we compare equal height and equal slope objects. For color code see Fig. 3.1. Cumulative sum of stop duration and the percentage of individual flies' stops longer than 10 secs after Fig. 2.16 in arena with objects of (A) equal area (n=20), (C) equal height (n=23), and (E) equal slope (n=24). Horizontal histograms of stop elevations on cones of (B) equal area, (D) equal height and (F) equal slope.

feature (slope or height) of the equal lateral surface area cones the flies were using in their assessment of object geometry. A clearer understanding of the stimuli would be informative as to the neuronal mechanisms underlying the behavioral change. In order to identify the basis of the flies' behavioral responses to these dimensions of geometry we created object sets of equal height but varied slope, and equal slope but varied height (Fig. 3.1). Our ability to control the height at which a fly stops is limited, however, because a fly is free to stop anywhere on a cone. Thus, even though a fly explores an arena with equal height cones, this does not guarantee that all of the stops occur at the same height. For this reason we restricted our analysis to the stops that occurred at the tops of cones. Plots of the normalized cumulative sum of stop duration and the proportion of individual's stops that were longer than 10 secs are shown in Figure 3.3A. Restricting the analysis to stops that occured at the top of cones does not effect the results of differential stop durations on the blue cone compared to the yellow cone, as was seen in the analysis of all stops shown in Figure 3.2G. The horizontal histograms in Figure 3.3B are the distribution of those stops at the 'top' of the cones that were used in the restricted analysis of stop duration.

In the simple case of the flies using only one of the geometric dimensions (i.e., slope or height), we would expect to see a differential response to the blue cone compared to the yellow cone in only the data from flies exploring the cones of equal height or equal slope. In Figure 3.3C, the cumulative sum and stop duration plots are shown for the flies exploring the arena with cones of equal height, which tests the role of slope. Although the cumulative sum data do seem to indicate a differential response to the

blue and yellow cones, this difference was not significant as assessed by a comparison of long duration stops. However, the probability value was .035 (not significant at the .05 level after Bonferroni correction) suggesting that the flies may indeed be able to distinguish slope independent of height. The data for the flies exploring the equal slope cones, which test the role of height, are shown in Figure 3.3E. Here, there is also a difference in the cumulative sum lines, but in this case there was a significant difference between the blue and yellow distributions. Together, these data do not eliminate the possibility that the flies can use both the geometric features (slope and height) independently in their assessment of objects.

3.3.3 Flies may use vision to assess object slope or height

After concluding that there was not sufficient evidence to suggest that the flies used one aspect of geometry exclusively, we tested whether the sensory systems (vision and graviperception) were used to detect specific features of object geometry (Figs 3.5, 3.4). First, we tested the visually based response to cones of equal height and equal slope (Fig. 3.4). Flies without visual information and with immobilized antennae did not distinguish (as measured by stop duration distributions at the 'top' of the cones) between the cones in the equal height condition (Fig. 3.4B) or equal slope condition (Fig. 3.4D). This is consistent with the results in Chapter 2 that show that flies without visual information and with immobilized antennae did not show a preference among the cones of equal lateral surface area. There does, however, seem to be a larger range in the individual behavior than we saw in the four-cone condition

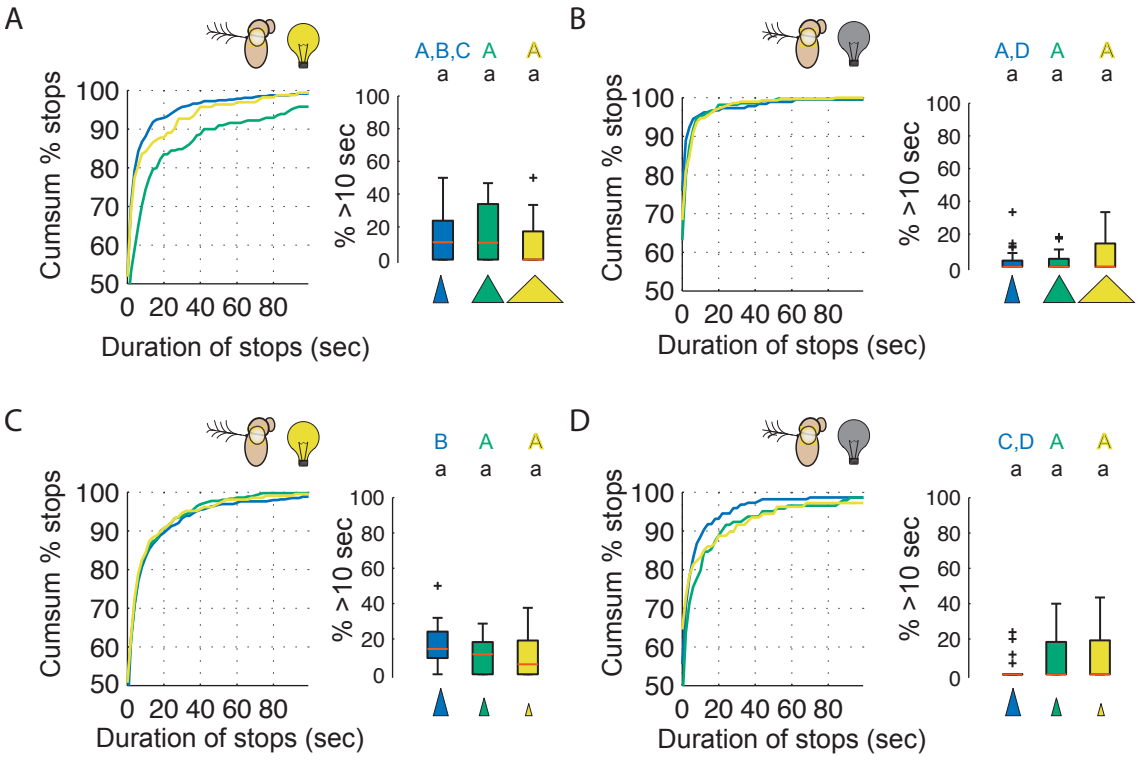

Figure 3.4: Flies may use vision to assess slope or height of objects. Flies with immobilized antennae explored the arena with objects of (A) equal height in the light (n=22), (B) equal height in the dark (n=25), (C) equal slope in the light (n=21) and (D) equal slope in the dark (n=23). Using only stops that occurred at the top of the cones (within 6 mm of top), the cumulative sum of stop durations and the percentage of individual flies' stops longer than 10 secs are shown (after Fig. 2.16). For color code, see Fig. 3.1.

(Fig. 2.16D). The lower n in this data set and small footprint of the equal slope cones may be responsible for this subtle difference in results. For example, only 15 of the 23 flies tested in Figure 3.4D encountered the shortest of the cones. Flies with visual information available but with immobilized antennae did not show a significantly different response to the cones with equal height but variable slope (Fig. 3.4A) or to the cones with equal slope but variable height (Fig. 3.4C). However, in both cases the P values comparing the responses to the blue and yellows cones were low enough to suggest that the flies were able to distinguish these objects and that a repetition of the experiments with a larger sample size might lead to a more definitive results.

3.3.4 Antennal mechanosensation assesses object slope

Second, we tested the graviperception-based response to cones of equal height and equal slope (Fig. 3.5). Figure 3.4B,D are repeated for comparison. Again, these flies did not show a significant shift towards long duration stops at the top of any of the equal height or equal slope cones (Fig. 3.5B,D). In contrast, flies with unmanipulated antennae (in the dark) did show a preference for the steepest (blue) of the equal height cones relative to the flattest cone (yellow) (Fig. 3.5A), indicating the flies can sense the different slopes of the equal height cones using their antennae. The flies with unmanipulated antennae exploring the equal slope cones showed an increase in long duration stops on these cones of variable height (Fig. 3.5C), indicating that the equally steep slope of these cones was sufficient to elicit the shift in locomotor behavior. Together, these results suggest that the slope of the cone is sensed by the

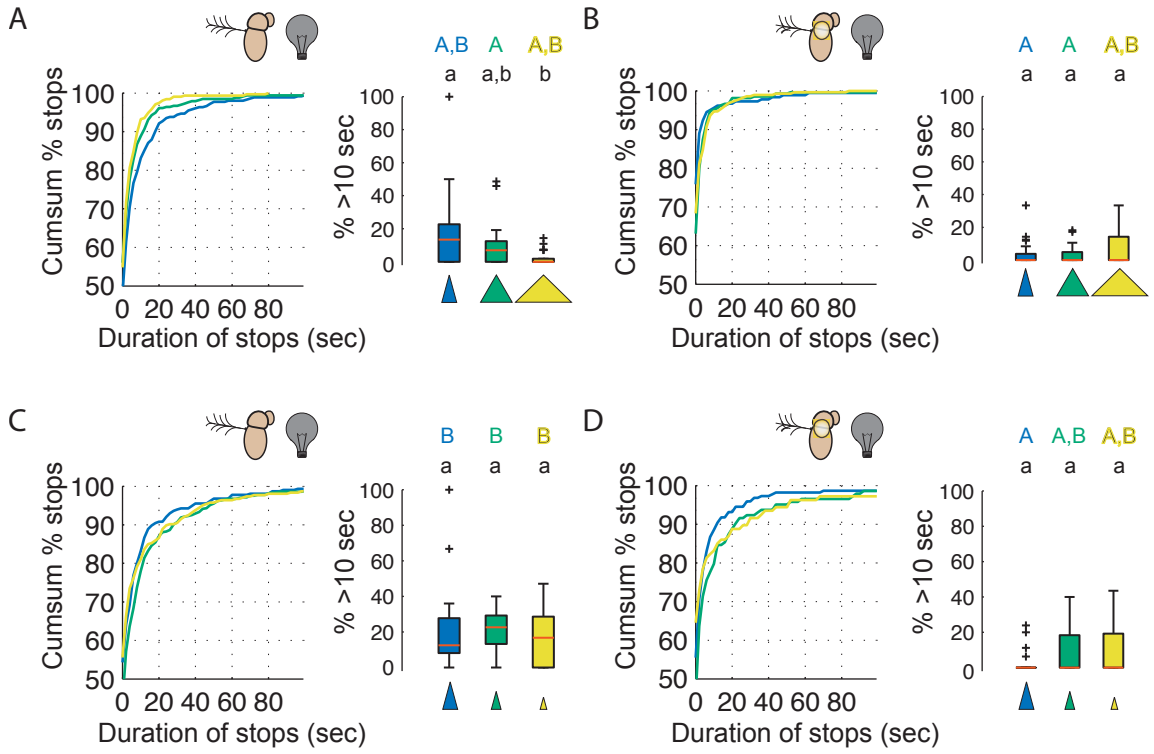

Figure 3.5: Flies use antennal mechanosensory system to assess the slope of objects. Flies in the dark explored the arena with objects of (A) equal height (n=22), (B) equal height with immobilized antennae (n=25), (C) equal slope (n=19), and (D) equal slope with immobilized antennae (n=23). Using only stops that happen at the top of the cones (within 6 mm of top), the cumulative sum of stop durations and the percentage of individual flies' stops longer than 10 secs are shown (after Fig. 2.16). Color code, see Fig. 3.1.

antennae, and that high object slope is a sufficient cue to change the flies' exploration behavior regardless of the height of the object.

3.4 Discussion

As we showed in Chapter 2, while exploring an environment containing a set of cones of equal lateral surface, walking *Drosophila* show a temporal preference for the tallest, steepest cone. The increase in time spent on the tallest, steepest cone is due to a shift in locomotor behavior towards stops of longer duration. In this work, we first recapitulated these results with a slightly different experimental paradigm. We presented only the three taller, steeper cones and doubled the length of trials to 20 minutes (Fig. 3.2). Experiments on intact flies exploring the arena with objects of equal height or equal slope did not strongly indicate that the flies use only one aspect of cone geometry (Fig. 3.3). In contrast, experiments with sensory manipulations do indicate that the flies' use information from their antennae to assess object slope (Fig. 3.5). The results of experiments with sensory manipulations to test whether flies use their visual system to determine slope or height were inconclusive.

In the collection of these data, we doubled the trial length, in order to increase the likelihood that flies would encounter and explore all the cones in the arena. However, there were still many trials in which the flies did not encounter all the cones, and, in the extreme, a third of the flies tested, in a given cone set and sensory condition, did not encounter a given cone type. This further reduced our effective sample size and limited our interpretation. Additionally, the reduction of cone number from

four to three was necessary due to object size considerations, but the similarity in the response to the blue and green cones left us with a comparison between just two sensory conditions (blue to yellow) rather than the four cone types in Chapter 2. This clearly reduces the accuracy of conclusions that can be drawn from such comparisons.

3.4.1 What aspect of object geometry does vision assess?

The results of Chapter 2 indicate that the flies can use visual information to distinguish between the cones of equal lateral surface area, but varied height and slope. Whereas our experiments here with intact flies exploring cones of equal height or of equal slope did not suggest the use of slope in cone assessment (Fig. 3.3E), we nevertheless showed through sensory manipulation experiments that the flies' sense object slope using their antennae (Fig. 3.5). The sensory manipulations focused on the role of vision in cone assessment were not conclusive (Fig. 3.4). The results might be unclear because of low n or stimulus range. Alternatively, the experiments may not have tested the cone quality that the flies use vision to distinguish. For example, the equal area cones also vary in the radius of curvature at the top and in the slant height (the distance along the lateral surface from the base to the apex). We cannot rule out the use of visual information in measuring slope or height by the mechanisms proposed in the discussion of Chapter 2; in fact the results of the intact flies exploring the cones decorrelated in slope and height suggest a role for the height in cone assessment (Fig. 3.3). The flies use antennal mechanosensory information to assess slope but not height, which suggests they use vision, or possibly a different unidentified

sensory system, to assess object height.

3.4.2 The antennal mechanosensory system senses object slope

Despite the caveats mentioned above, and those discussed in Chapter 2 concerning the crudeness of our sensory manipulations, our results strongly suggest that the flies use their antennal mechanosensory system to sense the slope of the object that they are exploring (Fig. 3.5). The flies show a shift towards long duration stops on all cones of differing height, but of equally steep slope when the information from the antennae, but not the visual system, is available. Additionally, the height of stops is not sensed by the antennal mechanosensory system; when visual information is not available, only on the object of steep slope (equal height cones) does the behavior shift toward long duration stops.

Both of these results support the hypothesis that flies are using their antennal mechanosensory system to sense the slope of the object they are exploring. This is consistent with recent reports that flies can use their Johnston's organ (JOs) to sense a static deflection of the third antennal segment relative to the second (Kamikouchi et al., 2009; Yorozu et al., 2009). Behaviorally, a subset of JO neurons have been shown to be important in transducing gravity as measured by the negative gravitaxis seen in the tube climbing assay and vertical choice maze (Kamikouchi et al., 2009; Sun et al., 2009).

If the JOs are the primary mechanosensory organ involved in the detection of gravity, it raises the question of how body orientation complicates the ability to sense

the gravitational field. Do flies respond in a similar manner to the same gravitational vector when their body is at different orientations and therefore different directions of displacement of the third antennal segment relative to the second? The structure of the JO suggests it should be able to respond to displacement of the third antennal segment relative to second for the full range of body orientations relative to the gravitational field (Kamikouchi et al., 2006). Additionally, functional studies recorded neuronal activity in the antennal nerve (recorded at the gap between the first and second antennal segments) in response to rotations about the yaw, pitch and roll axes (Sun et al., 2009). However, static deflections in opposing directions have been shown to activate and inactivate subsets of the JO neurons as measured by calcium imaging in the axons (Yorozu et al., 2009) and cell bodies (Kamikouchi et al., 2009). Such differential signals could provide information about the flies' body orientation in the gravitational field. It would be very informative to be able to resolve the flies' body orientation as they explored the cones. Are the flies performing long stops in a particular orientation? This could indicate that the behavioral response is due to the direct activitation of a specific subset of the gravity sensing JO neurons. In contrast, if long stops were performed in arbitrary orientations, this might indicate the flies' ability to use the magnitude but not directional signal of the stretch receptors of a particular subset of JO mechanosensory neurons. In fact, the subsets of JO neurons (C and E) implicated in graviperception are organized in a ring around the center of rotation. These subsets were defined based on morphology and further refined into seven subgroups. However, the functional exploration of these subgroups has been

limited by the specificity of the driver lines expressing in these neurons.

In this work, we have shown that the fly is able to use the movement of the distal antennal segment due to gravity to sense the slope of an object that it is exploring. This is likely transduced by the JOs. The behavioral response to slope provides another useful tool in the determination of the underlying neural mechanisms of graviperception. However, the visual stimuli resulting in the change in locomotor exploration behavior on objects of high slope and height is still unclear. In the future, it will be of interest to determine what aspect of cone exploration provides stimuli to the visual systems.

Chapter 4

High-throughput ethomics in large groups of *Drosophila*

4.1 Introduction

We propose a general-purpose, automated, quantitative and high-throughput system for measuring the behavior of interacting fruit flies. Our system uses machine vision techniques to automatically track large groups of unmarked flies while maintaining their distinct identities. We thus obtained trajectories: The position and orientation of each fly in each frame of a recorded video. Our system also includes automatic behavior detectors based on machine learning, which condense these trajectories into ethograms: meaningful, quantitative statistics of social and individual behavior. Because our system can be used to quickly measure many detailed statistics of fly behavior, it can be used to discover and quantify subtle behavioral differences between populations of flies and between individuals within a population. We have designed our tracker to be adaptable to other laboratory setups, and our machine learning software can be used to specify new, automatic behavior detectors without programming. We therefore envision it will foster a more effective exploitation of genetic tools in behavioral neuroscience.

4.2 Results

4.2.1 System overview

The behavioral arena used initially to test and develop our system consisted of a 24.5 cm diameter platform with an overhead Fire-Wire camera and infrared radiation (IR) lighting (Fig. 4.1). The arena design is described in greater detail in Chapter 2 (Arena

2). The software component consisted of a tracker for computing fly trajectories from captured digital video (Fig. 4.2) and a behavior detector, which may be trained from examples (Fig. 4.3). The system was accurate: The x–y position of a fly was estimated with a median error of 0.03 mm (2% of body length) and orientation with a median error of 4° (Figs. 4.2E, A.1 and A.2). Identity errors were absent with minimal user supervision and occurred every 1.5 h per fly in fully automatic mode. Details of the tracking algorithm, behavior detector and system evaluation are provided in Appendix A.

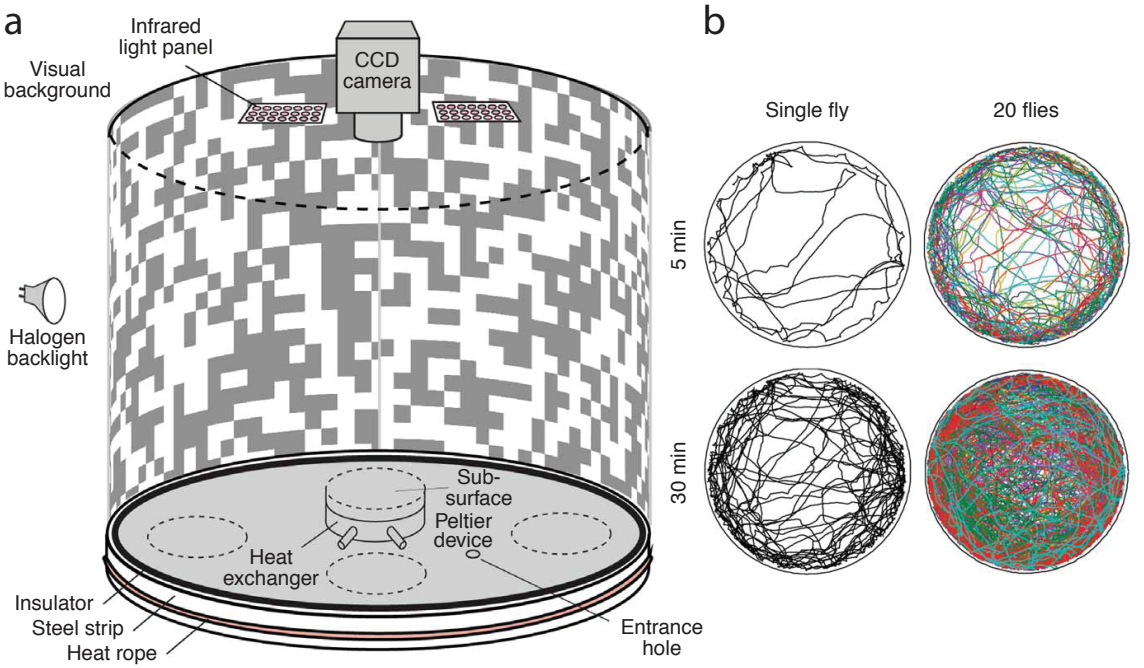

Figure 4.1: Walking arena with sample trajectories. (A) Schematic diagram of the walking arena. A 24.5 cm tall printed paper cylinder is backlit by an array of 8 halogen lights (only one is shown). At the top is a 1,280 x 1,024 pixel charge-coupled device (CCD) camera with an eight mm lens and IR pass filter, and two arrays of 850 nm LEDs. The circular, 24.5 cm diameter, 6 mm thick aluminum base is thermally controlled by four Peltier devices and heat exchangers mounted on the underside (only one is shown) and is surrounded by a heat barrier composed of an insulating strip and a galvanized steel ring heated by thermal tape. Flies are loaded into the chamber through a hole in the floor with replaceable stopper. (B) The x–y position of a single fly or of 20 flies within the arena for 5 and 30 min of a trial.

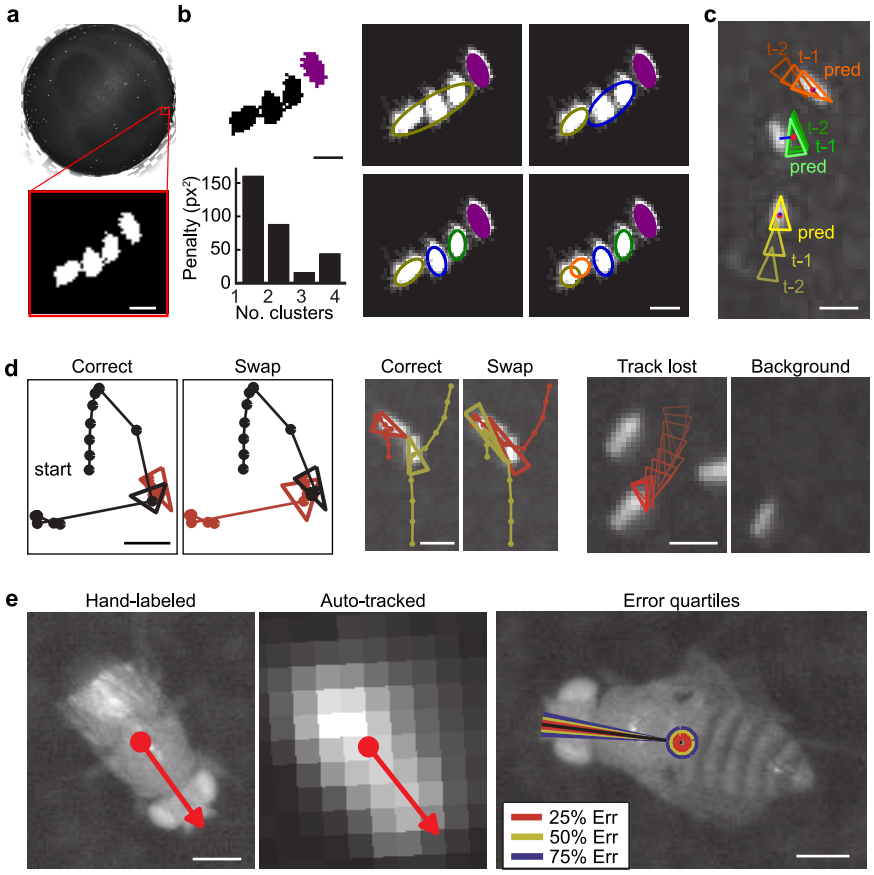

Figure 4.2: Tracking algorithm and evaluation. (A) Example frame of entire arena with the foreground/background classification for pixels in the inset. (B) Detection of individual flies involves grouping foreground pixels. The purple component corresponds to one fly; the large black component corresponds to three. The tracker splits this large component into 1–4 clusters. The penalty based on cluster size is shown for each choice. (C) Identity matching involves pairing predicted and detected positions. Red dots indicate the detected fly positions in frame t; triangles indicate the tracked positions at frames $t-2$ and $t-1$ and the predicted position (pred.) at frame t. Blue lines indicate the lowest-cost match between predicted and detected positions. (D) Identity errors consist of swaps and lost identities. In the first example, the fly (black) jumps near a stationary fly (red), and identities are swapped. Plotted are the correct and automatically computed trajectories (left). Triangles indicate the positions of the flies at the frame of the swap; circles indicate their trajectories. In the second example, a large connected component is split incorrectly (middle); the trajectories are superimposed on the frame in which the swap occurred. In the third example, the lower left fly is still during the majority of the trial, becoming part of the background model (right); shown is the frame in which the fly's trajectory is lost as well as the background model at that instant. (E) A comparison of the center and orientation of a fly manually labeled on a HR image (60 pixels mm^{-1}) to those automatically computed from a LR image (4 pixels mm^{-1}). Quartiles of the sampled center position and orientation errors plotted on an example HR image. The median error was 0.0292 mm (0.117 pixels) for the center and 3.141 for the orientation. Scale bars, 2.5 mm (A–D) and 0.5 mm (E).

To test the potential of using multiple fly trajectories for automated behavior analysis, we carried out three proof-of-concept experiments. First, we defined automatic detectors for several individual and social behaviors exhibited by flies walking in a circular arena. Then, we used these detectors to produce ethograms for flies in different gender groupings. To determine whether these ethograms are useful descriptions of the flies' behavior, we used them to classify flies according to gender (male versus female), genotype (wild type versus *fruitless*), and sensory environment (lights on versus lights off). The Fruitless protein is a transcription factor that plays a role in the sex determination pathway in flies. Male *fruitless* mutants exhibit several behavioral abnormalities, including inter-male courtship chains (Hall, 1978). Second, we quantified differences in the behavior of individuals within a population and found that those differences were stable throughout each trial. Third, we examined the spatial distributions of the relative positions of flies during social interactions. We compared the distributions for pairs of flies of the same and different sex as well as for male *fruitless* mutants. All analyses described below were derived from 21 30-minute trials, each comprising 20 flies, a total of 210 fly-hours. In eight trials we used only females; in six, only males; in five, half male and half female; and in two trials, we used male flies homozygous for the fru^1 allele of *fruitless* ($fru^1/\ fru^1$). In four of the female-only trials we provided no visual stimuli by running the trial in complete darkness except for the IR lighting used by the tracking system. Examples of each of the trial types (all female, all male, female and male, male and *fruitless* male, all female with lights on, and all females with lights off) are available in Supplementary

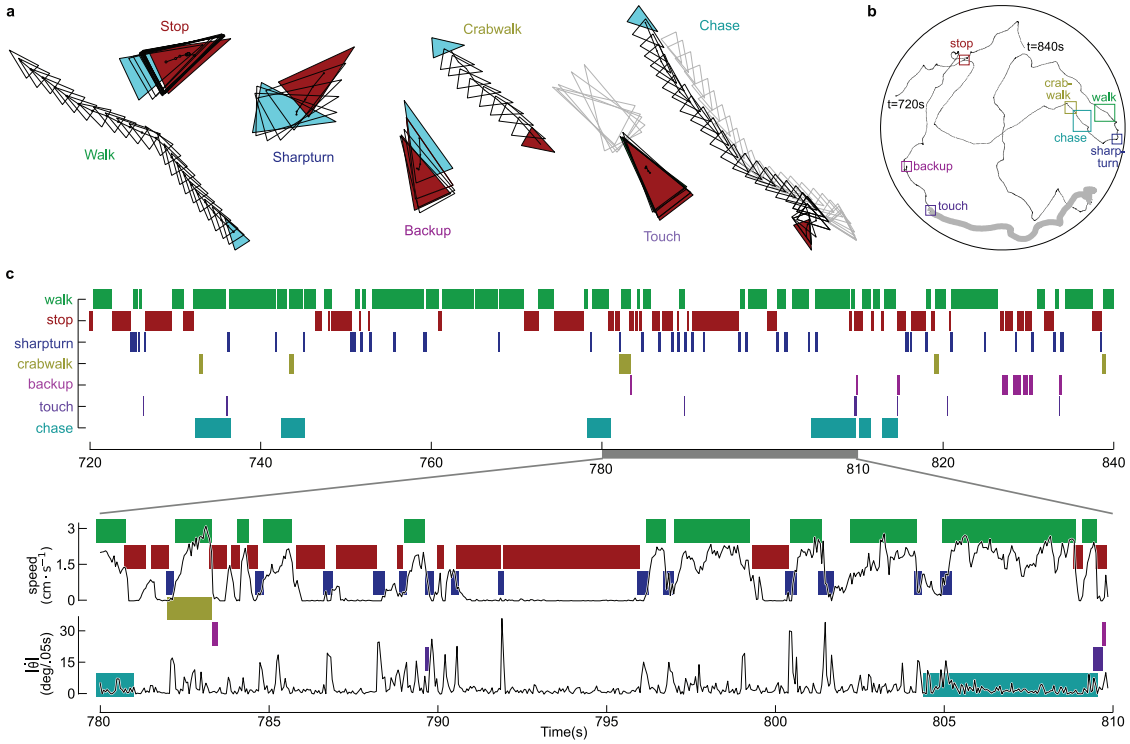

Figure 4.3: Ethograms of eight automatically-detected behaviors. (A) Examples of behaviors detected (from the trajectory shown in B). Triangles indicate the fly's positions in every frame. Cyan and red triangles are plotted at the start and end of each behavior example, respectively; only the start of the walk example is shown. For touching and chasing, we plotted in gray the position of the other fly. (B) Sample 2 min trajectory for a male fly in a mixed-sex arena. The colored boxes indicate trajectory segments in A. (C) Behavior classifications for the 2 min trajectory (top). A mark at $t = 780$ for the 'chase' row indicates that the fly was chasing at that time. Plots of translational and angular speed for a 30 s span of the trajectory ($t = 780$–810 s), superimposed over the behavior classifications (bottom).

Movies 4.1–6.

4.2.2 Automatic ethograms

We created automatic detectors for eight behaviors with a wide range of sequence durations, velocities and accelerations (Fig. 4.3A, Supplementary Movie 4.7 and Table A.3). These behaviors represented the majority of the flies' actions in our circular

arena. We trained most detectors from a few manually segmented trajectories (Appendix A.2). The software is user-friendly, and detectors for new behaviors can be created without additional programming. Six of the behaviors involve basic locomotor actions, and two of the behaviors relate to social interactions between flies. Most of the time the flies either walked at a relatively constant velocity ('walk') or stopped in place ('stop'). The next-most common behavior was 'sharp turn', in which a fly made a large, rapid change in orientation. Other locomotor classifications included 'crabwalks', in which the fly walked with a substantial sideways component, and 'backups', in which the fly's translational velocity was negative. 'Jumps' consisted of rapid translations within the arena. A 'touch' occurred when the head of one fly came in contact with another fly. 'Chases' were cases in which one fly (always a male) followed another across the arena. An automatic detector for a given behavior (for example, the walk detector) input the trajectory for an individual fly (Fig. 4.3B) (or for a pair of flies, for social behaviors), derived per-frame statistics such as the translational speed, angular speed or distance to the second fly (for social behaviors), then segmented the trajectory into bouts in which the fly was and was not performing the given behavior (Fig. 4.3C).

By collecting the statistics of these eight behaviors into a vector, we created ethograms: rich, quantitative descriptions of each individual fly's behavior. For each fly, we computed three types of such description, consisting of the frequency with which each individual fly performed each behavior, the fraction of time a fly performed a behavior and mean behavior duration. To visualize differences among

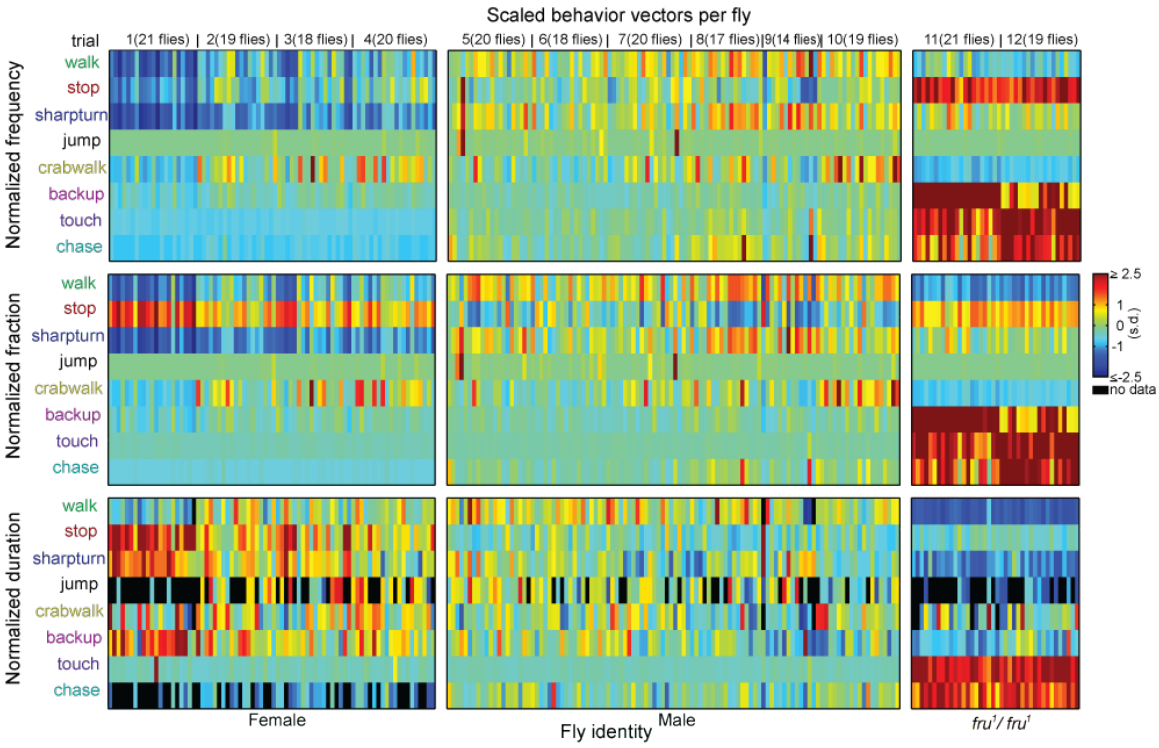

Figure 4.4: Example behavioral vectors for female, male and male $fru^1/\,fru^1$ flies in single-sex trials. Each column corresponds to a fly and each row within a vector type to a behavior (n =78 (female), 108 (male) and 40 ($fru^1/\,fru^1$). Each panel shows the frequency (top), fraction of time (middle), and mean duration (bottom) with which each fly performed a behavior. Color indicates the s.d. from the mean frequency (top), the mean fraction of time (middle), and mean bout duration (bottom) for each behavior.

female, male and male fru^1/fru^1 flies, we grouped the flies by type and displayed the behavior frequency in pseudocolor (Fig. 4.4). Inspection of this 'behavioral microarray' suggested that the behavioral vectors of female, male and fru^1/fru^1 male flies differed consistently. We quantified these differences by computing the mean and standard error behavior vectors for each type of fly (Fig. 4.5).

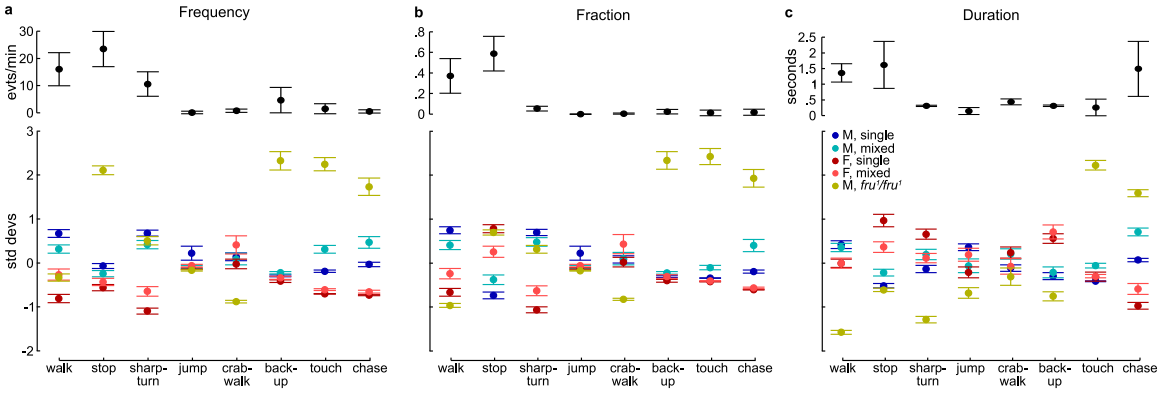

Figure 4.5: Summary statistics of behavior. For each fly and behavior, we computed (a) the frequency of onsets of the behavior (Fig. 4.4, top), (b) fraction of time the fly performed the behavior (Fig. 4.4, middle), and (c) mean duration of sequences of the behavior (Fig. 4.4, bottom). The mean and standard deviation of these statistics over the entire fly population is shown in the top row (black). In the bottom row (colored), we show the normalized (z-scored) mean and standard error for each of the five fly and trial types (male/wild type/single-sex, ..., female/wild type/mixed-sex, fru^1/fru^1. These plots show that many of these behavioral statistics are significantly different for different fly types.

To determine whether these ethograms are powerful descriptors of behavior, we tested whether we could predict the sex of a fly (male versus female), its genotype (wild type males versus fru^1/fru^1 male), or its sensory environment (lights on versus lights off) based solely on components of the automatically generated behavioral vector (Fig. 4.6). We found that predictors based on the statistics of each of the eight behaviors independently distinguished sex with accuracies all better than chance, with touch frequency performing best (96.8% accuracy) and sharp turn frequency

performing best of the locomotor behaviors (83.9% accuracy). A predictor based on the combination of all behaviors had an accuracy of 96.9%. Even a predictor based solely on locomotor behaviors (excluding touches and chases) predicted sex with an accuracy of 95.5%. We are not advocating using behavioral statistics for sexing flies. Our mixed-sex trials (Figs. 4.7 and 4.8) used a fly's median image area for determining sex, a technique that achieves 96.2% accuracy. Instead, these behavior prediction accuracies are evidence that the ethograms were strongly correlated with gender.

Predictors of genotype (wild type versus fru^1/fru^1 males) were even more robust (Fig. 4.6B). Frequency of backups achieved the best performance (99.3% accuracy). Using all behaviors or all locomotor behaviors, *fruitless* males could be classified with 100% accuracy. Predictors of sensory environment using only locomotor behaviors were also very accurate at 98.1% (Fig. 4.6C). Of the locomotor behaviors, 'stops' best predicted whether a fly had visual information available or not (87.7%). This technique of behavioral profiling could easily be extended to include more behaviors or more features of each behavior (Appendix A.2).

4.2.3 Behavioral variation between and within individuals

We observed that the trajectories of individual flies looked qualitatively different (Fig. 4.7A). For example, some flies traveled more than others and some spent a larger fraction of time near the arena wall. Because our algorithm kept track of each fly's trajectory, we could easily gather data on a large number of flies and explore

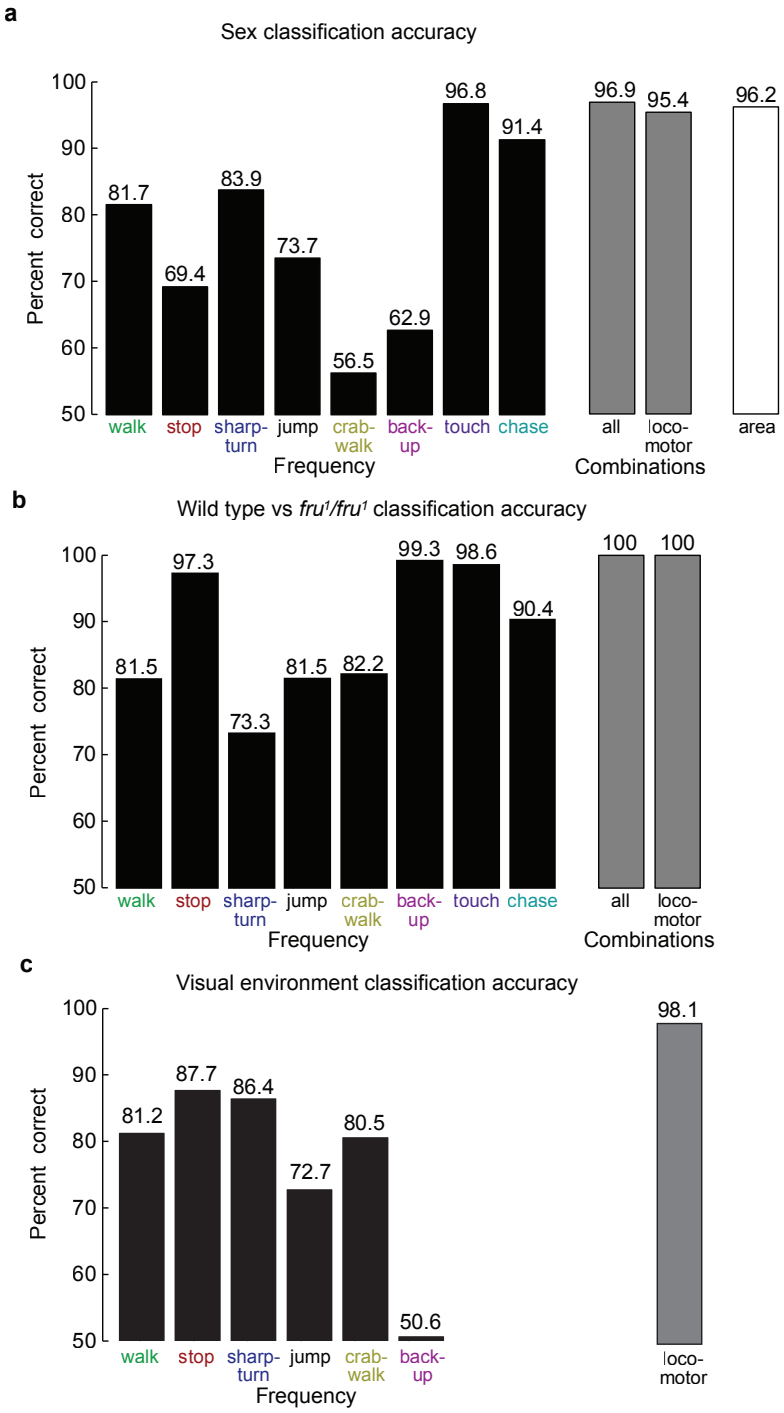

Figure 4.6: Accuracy from automatically detected behaviors. Black bars, cross-validation error of single-threshold classifiers based on frequency. Gray bars, logistic regression classifiers from all eight and the six locomotor behaviors. White bar, accuracy of classifying sex based on the image area of the fly (Appendix A.1.5.6). Accuracy of (A) sex prediction, (B) genotype prediction (wild type versus fru^1/fru^1) and (C) sensory environment.

statistical differences in behavior across individuals. To this end, we computed behavioral statistics separately for the first 15 minutes and the second 15 minutes of each 30-minute trial and calculated the correlation between the two halves. We considered three statistics of locomotor behavior: the mean speed during walking episodes, the fraction of frames the fly was classified as walking and the mean duration of walking episodes (Fig. 4.7B). The correlation between the first- and second-half statistics was significant ($P < 2.2 \text{ x } 10^{-16}$) and positive for all three walking metrics, indicating that individuals maintained behavioral tendencies throughout the 30-minute trials. Thus, although within the tested strain of wild type flies we found substantial differences in walking behavior, each individual fly walked consistently over time.

We also investigated whether there were consistent differences in chasing behavior across individual flies during a 30-min trial. For the first and second half of each trial, we computed the frequency with which a fly begins chasing another fly, the frequency with which other flies begin chasing a given fly and the mean time duration of chase sequences initiated by a given fly (Fig. 4.7c). As with the walking experiments, we computed the correlation between behavioral statistics gathered during the first and second half of each trial. We found small, but significant, positive correlations for frequency of chasing ($P = 3.89 \text{ x } 10^{-16}$) and frequency of being chased ($P = 1.54 \text{ x } 10^{-3}$) but no significant correlation for duration of chase sequences ($P = 0.261$).

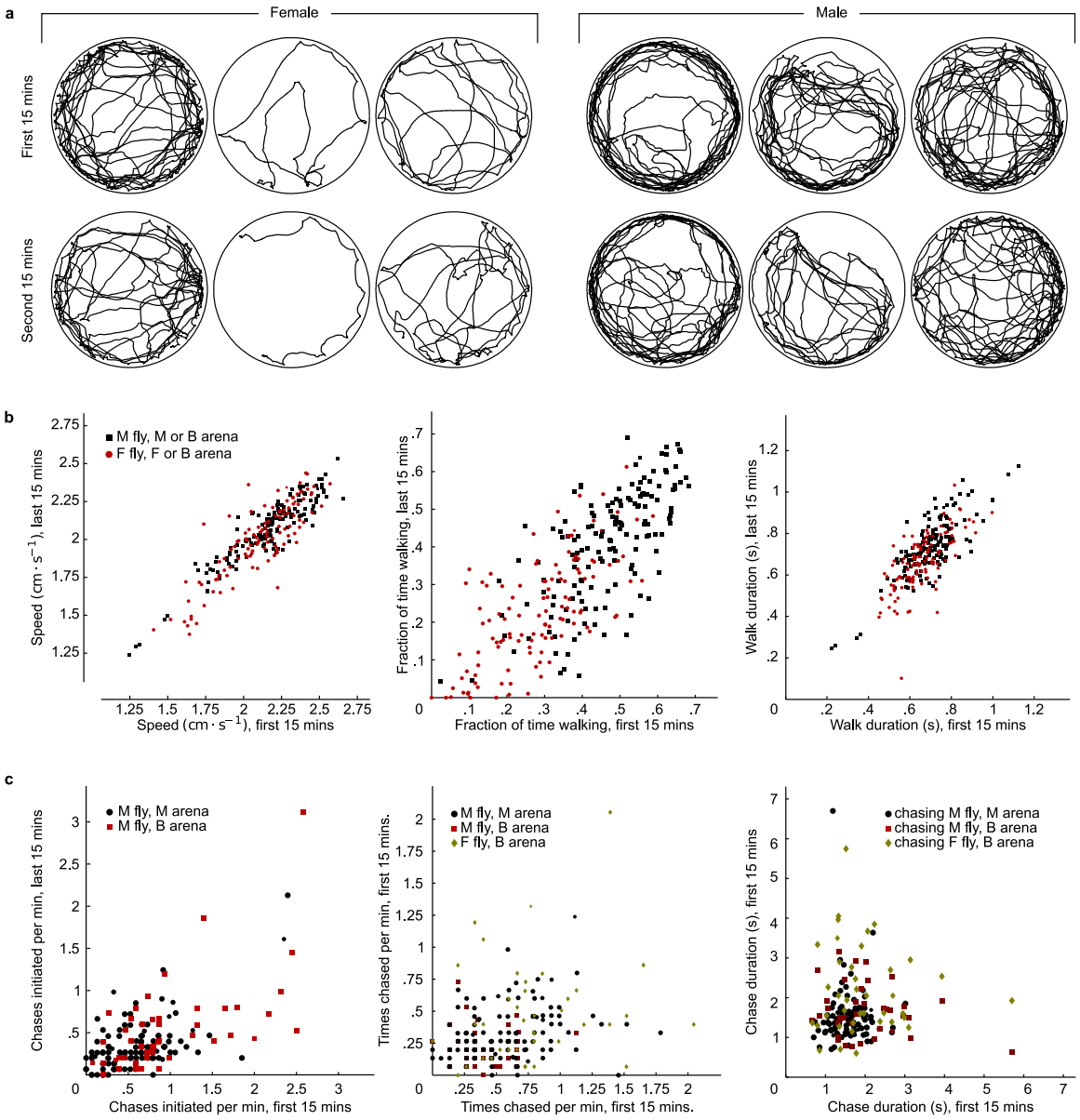

Figure 4.7: Differences within and among individual flies. (A) The first and second halves of trajectories for three male and three female flies from the same trial. (B) Scatter plots of walking statistics from each individual fly in the first 15 minutes of its trajectory against the same statistics from the last 15 minutes of its trajectory for flies in all trial types (female, n = 132 and male, n = 159). Walking statistics examined were: (i) mean speed in frames in which fly was classified as walking: $r = 0.889$, $p < 2.2\text{e}{-16}$ (r indicates Pearson's correlation coefficient and p the probability that the null hypothesis of r non-positive is correct), (ii) fraction of frames fly is classified as walking: $r = 0.689$, $p < 2.2\text{e}{-16}$ (iii) mean duration of sequences of consecutive walking frames: $r = 0.765$, $p < 2.2\text{e}{-16}$. (C) Chasing behavior differences. We repeated the above procedure for chasing behavioral statistics: (i) frequency with which the fly begins chasing another fly: $r = 0.592$, $p = 3.89\text{e}{-16}$, (ii) frequency with which a fly is chased by another fly: $r = 0.213$, $p = 1.54\text{e}{-03}$, and (iii) mean duration of chases: $r = 0.054$, $p = 0.261$. Thus, only the first two correlations are significantly different from zero.

4.2.4 Gender differences and fly-fly interactions

Because our data consisted of the location and orientation of all individuals at all times, we could examine the spatial distributions of the relative positions of flies during social interactions. We compared the distributions of inter-fly distances for different gender pairings in single-sex and mixed-sex trials (for example, male-to-male distance in mixed-sex trial) (Fig. 4.8a). As a control, we created a semi-synthetic dataset by artificially staggering in time all 20 trajectories relative to one another. We left the first fly's trajectory unchanged but shifted the second fly's trajectory in time so that it started at $t = 1.5$ min, with the last 1.5 min of its original trajectory wrapped around to fill the time from $t = 0$ to $t = 1.5$ min; we shifted the third fly's trajectory by 3 min, the fourth by 4.5 min and so forth. These data approximated trajectories in which the flies do not interact.

The peaks in the male-to-male and male-to-female distributions compared to the synthetic data indicated that males actively approach other flies to a distance of 2.5–3.5 mm. In addition, the relatively low frequency of close interactions (< 4 mm) between females suggested that they maintained a larger buffer between themselves. These findings were robust across trial type (for example, males approached other males as closely in mixed-sex arenas as in single-sex arenas). We also observed that the flies' centroids never moved within 1.5 mm of each other, which is expected given this distance roughly corresponds to a fly's body width.

To explore spatial differences during social interactions, we created a new behavioral classification termed 'encounter' describing those trajectory intervals in which

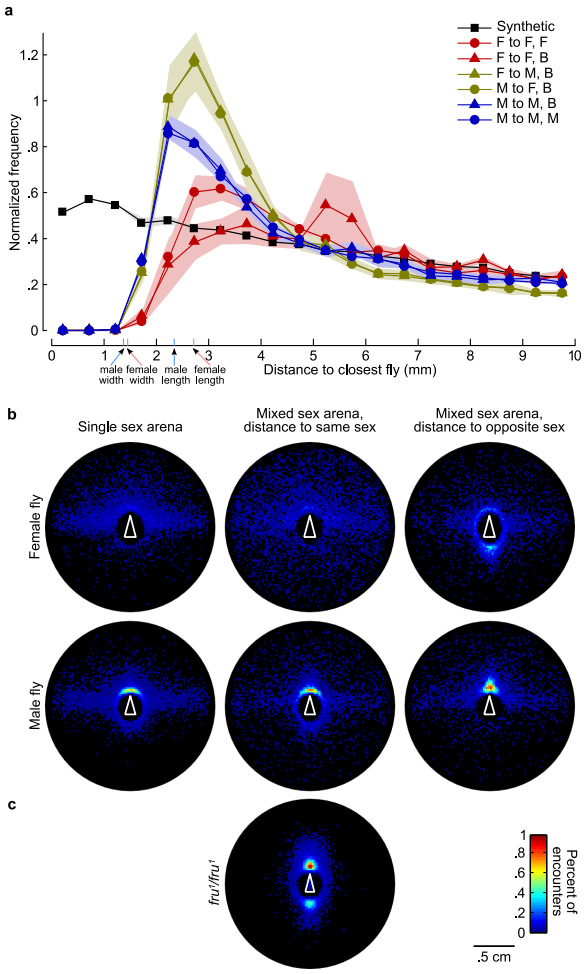

Figure 4.8: Spatial analysis of social interactions. (A) Normalized histogram of inter-fly distances to the nearest fly for each fly in each frame. The frequency was normalized both by the total number of counts and by the area of the bin. Each encounter was counted only once by ignoring all but the first frame in which both flies were stopped. The 'synthetic' condition shows a control in which we decorrelated fly positions by staggering the trajectories in time and collapsed data from all conditions. The lightly shaded regions indicate 1 s.d. in normalized frequency, approximated by randomly splitting the flies into five groups. For comparison, the pink and blue tick marks indicate the mean fly widths and heights for female and male flies, respectively. (B) Histogram of the x–y relative position of one fly in the coordinate system of another at the closest point of an encounter. Each plot corresponds to a different social condition, as indicated. The white triangle in each plot shows the fixed position of the given fly. The pixel color indicates the frequency with which the closest fly is in the corresponding location bin. (C) Histogram of the x–y mutual position between fru^1/fru^1 males. Scale bar, 0.5 cm.

the distance between a pair of flies was less than 10 mm. For each encounter, we computed the relative location of one fly in the coordinate system of the other at the time when the distance between them was minimal. We computed histograms of these relative locations over all encounters of each gender pairing and trial type (Fig. 4.8B). These histograms were consistent with our qualitative knowledge of courtship behavior. For interactions involving males, the majority of the encounters occurred very near the other fly, when the flies were almost in direct contact. In contrast, the relative locations of the female-female encounters were more diffuse. It is apparent from the hot spot near the head of the flies in Figure 4.8B that males often took a position so that another fly was right in front of them, an orientation that is consistent with their chasing behavior. Conversely, a hot spot is visible directly behind females in mixed-sex trials, indicating that they are being chased by males. Notably, two hot spots are apparent in the encounter histograms of fru^1/fru^1 males (Fig. 4.8C), indicating a social phenotype that is intermediate between that of males and females. The data in this figure represent a quantitative and reproducible measure of the chaining phenotype that is characteristic of many male *fruitless* mutants (Hall, 1978).

4.3 Discussion

We developed software that allowed us to automatically track and analyze up to 50 individual flies (a density of 0.1 fly cm^2 in our arena) simultaneously for long periods of time. We estimate that the behavioral analyses shown in Figure 4.3 would have taken a human operator between 3,000 and 5,000 hours to produce manually.

The observations on individual behavior would have taken much longer. The software (http://www.dickinson.caltech.edu/ ctrax) is open-source and was developed to function in a wide array of experimental contexts. Furthermore, it is easy for a biologist to train the system to detect new behaviors by providing a few examples using a graphical user interface designed for this purpose.

The open arena used for most of our analysis required clipping the flies' wings, a manipulation that may affect aspects of their behavior, for example, the production of courtship song. In addition, although the open arena apparatus allowed us to perform the rigorous groundtruthing presented, it is custom-built and would not be instantly available to the research community. However, we analyzed data that were collected in a much simpler and easy-to-replicate chamber, consisting of a backlit plastic chamber with a glass top (Simon and Dickinson, 2010). This analysis demonstrated that our software works on data collected from intact flies in an inexpensive and easily reproduced device.

Our method benefits from insight gained from previous approaches to the study of behavior in Drosophila. The first, inspired by a classic 'countercurrent' apparatus (Benzer, 1967), involves crafting a simple mechanical contraption that isolates behavioral outliers in a large population. This method is easy to perform and thus amenable to high-throughput screens but does not provide detailed measurements on individual flies. In addition, complex behaviors (for example, courtship and aggression) are not easily screened by these techniques. The second, exemplified by tethered flight arenas (Götz, 1968) and 'Buridan's paradigm' (Bulthoff et al., 1982), involves

developing a sophisticated apparatus that provides detailed, time-resolved measurements of individual flies. This approach offers a rich view of behavior but does not allow for high-throughput screens. In addition, behavioral analyses that depend on elaborate, custom-made instruments do not easily proliferate throughout the scientific community. The third approach, exemplified by the use of 'courtship wheels' (Siegel and Hall, 1979), provides detailed information on the complex behaviors of individual flies but relies on manual scoring by human observers and is labor-intensive and subjective.

Our system combines the key features of prior behavior analysis methods and is thus a complementary tool to genetic manipulation for the study of the neural bases of behavior. Because each fly is tracked and measured individually, it is possible to quantify the behavior of individual flies as well as fly-fly interactions. The system's flexibility allows many different individual and social behaviors to be defined and automatically detected. The definitions for these behaviors are interpretable and quantitative, allowing researchers to easily reproduce experiments. Finally, the system supports high-throughput screening, facilitating its use with genetic manipulations.

4.4 Materials and methods

4.4.1 Flies

Unless noted, all experiments were carried out on adult *Drosophila melanogaster* selected from a laboratory population that was derived from 200 wild-caught isofemale

lines. fru^1/fru^1 flies were derived from a fru^1/ TM3 stock (a gift from M. Arbietman). Flies were maintained on 16:8 light:dark cycle and all experiments were conducted during the evening activity peak. Approximately 24 hours prior to each experimental trial, we collected between 20 and 50 flies (two-day-old) from culture bottles and anesthetized them using a cold plate cooled to 2°C. While they were anesthetized we clipped both wings of each fly to approximately hlaf their normal length so that they could not fly out of the arena. After cold anesthetization the flies are allowed to recover overnight in food vials and 6 hours prior to experiments were transferred to vials with damp paper for wet starvation. All experiments were performed during the evening peak in circadian activity.

4.4.2 Algorithms

See Appendix A for details of the tracking algorithm and the behavior classifier.

Chapter 5

Concluding remarks

I have developed a new arena for studying the behavior of walking fruit flies in a relatively large, but controlled sensory landscape. Tracking the body position and orientation of an individual continuously over the course of the experiment allowed quantitative behavioral analysis of hungry flies exploring complex topologies. These analyses showed a shift in locomotor behavior toward longer duration stops on the surface of tall, steep objects. The flies assessed object geometry with either visual or mechanosensory cues. Development of a multiple fly tracker increased the throughput of behavioral experiments in this arena without compromising temporal or spatial resolution. The tracker maintains the identity of individual flies, allowing for automated behavioral analysis of individual flies and their social context.

5.1 Significant scientific contributions

5.1.1 Chapter 2: Object preference is mediated by vision and graviperception

- I developed a walking arena in which flies are confined to the surface via a heat barrier and wing clipping. The sensory landscape is carefully controlled and tracking in the near-IR allows for manipulation of the visual stimuli without compromising tracking performance. The position and body orientation of an individual fly are tracked over the course of the experiment. Real-time tracking of an individual fly's position allows for feedback control of a dynamic visual display.

- When exploring the arena with objects present, flies demonstrate a temporal preference for the tallest, steepest object in the arena. This temporal preference is due to increased residency on these objects rather than increased attraction during approach.

- The temporal preference is mediated by an absolute assessment of the objects' geometry rather than comparison or memory.

- The temporal preference is due to a shift in locomotor behavior towards longer duration stops rather than an increase in stop frequency. These long stops occur primarily at the top of the objects.

- The flies' assessment of the object can be mediated by either vision or graviperception whereas removal of stimuli to both sensory systems abolishes the preference (as measured by stop duration distributions).

5.1.2 Chapter 3: The antennae can sense object slope

- The antennal mechanosensory system mediates the assessment of object slope, as opposed to the height, as measured by the behavioral shift toward longer duration stops at the top of the objects.

5.1.3 Chapter 4: High-throughput ethomics in large groups of flies

- We developed an automated fly tracker that maintains individual identity in large groups of flies and requires minimal post-processing supervision.
- We developed automated behavioral detectors for a set of six locomotor behaviors and two social behaviors.
- 'Behavioral microarrays,' which consist of the statistical analysis of the frequency with which the defined behaviors were performed, duration of instances of the behavior, and fraction of time spent performing the behavior, are sufficient to distinguish between flies based on the flies' sex (male vs. female), genotype (male vs. *fruitless* male) or sensory condition (light vs. no light).
- There is a large range in the population behavior; however, an individual's behavior profile is consistent over the time period of the trial (30 minutes).
- Males approach closer to other flies (male or female) than do females, and spatial analysis of encounters show that males are most often located behind the other fly during encounters.

5.2 Emerging understanding of multimodal control of walking behavior

Returning to the hierarchy of behavioral analysis (Fig. 1.1), the work reported in this thesis is largely concerned with exploratory behavior for resource localization. The function of the newly described behavior is unknown; hungry, walking fruit flies spend more time on the tallest, steepest object in an arena (Chap. 2). The function likely relates to the localization of resources, such as food or refugia, as discussed in Chapter 2. However, I did make progress in understanding the mechanisms underlying this behavior through quantitative analysis of locomotor behavior. Additionally, I assisted in the development of a new automated system for studying the locomotor and social behaviors of large groups of walking flies (Chap. 4). This represents a large step forward in the quantitative analysis of fly behavior. It will allow further studies into the mechanisms of resource localization and the neural control of behavior, in combination with the powerful genetic techniques available in the fruit fly.

The change in flies' behavior during exploration of tall, steep objects is due to a shift in the locomotor pattern towards longer duration stops. These long duration stops can be mediated by either the visual or antennal mechanosensory systems. Therefore, vision and graviperception provide information about the objects that is used by the nervous system to control the motor circuits of limb movement. What are the neural circuits involved in this behavior? To begin to answer this question, I can consider this behavior in the context of what is known about the circuitry and

the processing of information in the fly's nervous system.

Although the feature of cone geometry that the visual system senses was not determined, my results do suggest that the object slope is sensed by the antennal mechanosensory system. It is likely that the Johnston's organs (JOs) of the antennae play a primary role in the transduction of antennal joint displacement due to gravity into neural information. The JOs mediate other behaviors in walking flies that also have a locomotor mechanism. In courtship, auditory signals from the song of males cause a receptive female to slow her locomotion (Tompkins et al., 1982). In wind sensation, walking flies cease locomotion in response to low-velocity airflow (Yorozu et al., 2009). These common mechanisms of behavioral response suggest that the information from the JOs is used to control the activity of motor circuits. This information is integrated with information from other sensory systems as well as internal state. For example, in contrast to Tompkins et al. (1982), Yorozu et al. (2009) did not report an effect of courtship song on locomotion; this is probably due to the use of group-housed males and females in the testing assay. Mated females are not receptive (an internal state) to courtship. It is unlikely that information is integrated at the level of the JOs, as Kamikouchi et al. (2006) showed that morphological and projection target segregation of subpopulations of JO neurons. The anatomically defined subpopulations align with functional segregation of different subpopulations transducing different qualities of antennal movement. (Kamikouchi et al., 2009; Yorozu et al., 2009). However, this does not eliminate the possibility of feedback onto the processes of the JO neurons in the output neuropil.

In the antennal mechanosensory and motor center (AMMC), the targets of the subpopulations of the JOs neurons are functional segregated into zones. Some of these AMMC zones also receive information from other antennal mechanosensory receptors not in the JOs. Additionally, the AMMC contains the motor neurons that innervate the antennal muscles (Nation, 2008). This localization of the circuit elements is suggestive that local circuits within the AMMC mediate the antennal positioning reflex (Horn and Kessler, 1975), thus necessitating integration at the level of the AMMC. It is reasonable to suggest that the integration of antennal mechanosensory information involved in the control of locomotion is also integrated in the AMMC, but this is not necessarily the case.

Changes in limb movement underlie the behavior of object preference. Walking circuits, in the ventral nerve cord, generate the motor commands to the limbs. Whereas the walking circuits have not been dissected in fruit flies, they have been extensively studied in cockroaches and stick insects (reviewed by Ritzmann and Büschges (2007)). Circuits in each of the three segmental ganglia of the thorax control the limb movement of the respective pair of legs. Each side of the bilaterally symmetrical ganglia contains a neural circuit controlling limb motor output to the ipsilateral limb. This circuit contains sensory inputs from the limb, interneurons, central pattern generators (CPGs) and motor neurons. The CPGs are thought to provide patterning of activity to each of the leg joints, but sensory reflexes are important for the function of these motor circuits, and may provide timing coordination between the CPGs for a given leg.

How are walking behaviors coordinated between the limbs? Lesion experiments implicate information from the brain; walking behaviors are deficient in preparations with neck connective lesions (summarized by Ritzmann and Büschges (2007)). Experiments in cockroaches showed that, without descending from the brain, the coordination of activity between the segments was deregulated and walking activity was reduced (Ridgel and Ritzmann, 2005).

Where does this input come from in the brain? Genetic lesion experiments, performed in *Drosophila*, suggest the central complex (CX) is involved (Martin et al., 1999; Strauss, 2002; Strauss and Heisenberg, 1993, 1991). The CX is composed of four unpaired midline ganglia in the brain. The CX is highly structured and interconnected with a basic architecture of repeated columnar units (Homberg, 1989; Young and Armstrong, 2010). The CX receives input from a large portion of the brain, in particular the optic glomeruli (or foci) and the antennal areas, but not from primary sensory neurons (Homberg, 1989). Mutants with gross anatomical deficits restricted to the CX show uncorrected asymmetries in behavioral output, uncoordinated limb motion during turning behavior, and reduced locomotor drive (Strauss, 2002). The genetic screen of gravitaxic maze behavior by Armstrong et al. (2006), which first identified the AMMCs involvement in the gravitation response in fruit flies, also implicated the CX. Further studies with spatially and temporally controlled neuronal silencing confirmed the role of the AMMC and CX in the flies' gravitaxic maze performance (Baker et al., 2007). Taken together, these studies suggest that the CX may mediate the transfer of information from the sensory systems to the motor centers.

More specifically, the CX may mediate the change in locomotor behavior we described in flies' exploration of objects. Additionally, in my experiments removing all visual input, flies displayed an inability to stabilize straight walking (Chaps. 2 and 4). The CX may use visual information as a spatial reference frame in its coordination of locomotion output.

However, the inputs and outputs of the CX are not well described, and whether the sensory information is integrated pre-, in, or post-CX is not known. A recent genetic dissection of the CX structure, described presynaptic markers in processes of CX neurons in the lateral triangle, as well as the ventral bodies, both regions of the protocerebrum (Young and Armstrong, 2010). There are also postsynaptic markers in the processes of CX neurons localized to the ventral bodies. This suggests information flow from the lateral triangle and ventral body, processing in the CX and output back to the ventral bodies. Homberg reports that CX projection neurons do not connect directly to descending neurons (Homberg, 1989), which are mainly localized to the lateral protocerebrum. This suggests that there are multiple layers of neurons between the sensory inputs and motor outputs in the CX pathway. The CX is not the only pathway for sensory-motor information, many of the descending neurons are responsive to sensory stimuli. Thus, there are likely multiple pathways of information flow to the thorax that may mediate behaviors of different speed and complexity.

Sensory information from multiple modalities is often correlated because they are sensing the same system, the external environment. In my experiments, I showed

that the visual system and the antennal mechanosensory system, while they measure very different physical cues, are both able to mediate the behavioral response of object preference. However, the behavior responses are not identical; the visual response may involve a less accurate assessment of object geometry than the gravitational response. There are other examples of complementary sensory systems. For instance, in flight stability the ocelli and visual system, as discussed in Chapter 1.5, are both able to measure intensity differences caused by body roll and pitch, but the occellar pathway is faster. The halteres, a mechanosensory system, also measure body angular velocity and respond maximally to faster rotations than does the visual system (Sherman and Dickinson, 2003). Together, these systems increase the range of body rotations the fly can sense without loss of sensitivity. Complementary sensory modalities may be adaptive because they sense different dimensions of stimuli from the environment. Thus, they enable integration across modalities that reduces noise in the output and increases the robustness of behavior.

5.3 Future experiments

The new tracking and behavioral analysis described in Chapter 4, allows for much higher throughput of behavioral experiments. This will be useful for any number of experiments studying the behavioral and sensory ecology of flies. Although my arena requires wing clipping, which limits throughput and perhaps precludes the study of wing involved behaviors such as courtship and aggression, the tracking system was designed to be able to generalize to other experimental apparatus. An arena

developed in the laboratory in response to the Ctrax system allows intact flies to be tracked on a planar surface via a lid and a clever design tweak: The arena floor slopes up around the edge (Simon and Dickinson, 2010). This arena was also designed with backlighting through the floor, which increases the quality of images.

However, future studies of the mechanism underlying the flies behavioral response to slope require a different direction of arena development. In order to definitively show that the antennae sense the slope of an object's surface rather than any other co-varying geometric feature, such as radius of curvature, experiments need to be done on a flat plate that is tilted to various angles. In preliminary experiments tilting my arena, I found that many of the flies escaped the arena by jumping during the course of the trials. However, the flies that remained in the arena did seem to be performing long stops. To test this quantitatively would require developing an arena that confines the flies to a flat plate, has a lid, and can be tilted co-axially with the camera and lighting systems. The use of the Ctrax system would enhance the throughput of such experiments.

Additionally, the ability to determine the fly's body orientation while it is on an inclined plane (or a cone) would allow more detailed analysis of exploratory behavior. For example, it could be determined whether the flies are performing oriented responses to gravity or if long duration stops are more likely to occur in a particular orientation relative to the gravity vector. In order to increase the throughput of such an experiment by tracking multiple flies some modification to the apparatus and experimental design would be necessary. Preliminary experiments using the four-

cone experimental conditions required significant amounts of post-processing identity error correction. A multi-camera tracking system would improve the tracking and would enable more accurate determination of the flies' z–position as well as body orientation. However, the behavior of groups of female flies at the top of the cone many not recapitulate the individual fly behavior because of social interactions. From Chapter 2, we know that the flies prefer to stop near the top of the cones, but from the experiments in Chapter 4 we also know that females maintain a spatial distance from other females. The interactions of these competing drives occur when groups of female flies try to occupy the top region of the cone at the same time; females tend to 'jostle' one another, often pushing each other off the cone (Supplementary Movie 5.1).

The putative involvement of the Johnston's organ (JO) in the behavioral response to slope provides a new assay for genetic circuit-breaking techniques to elucidate circuit structure and function. Future experiments could use the locomotor response of flies to slope to identify central brain cells involved in graviperception. Additionally, the known involvement of the visual system in cone assessment provides an opportunity to study the integration of these two sensory modalities on motor output.

The work of this thesis did not identify the feature of cone geometry that the visual system uses in cone assessment, nor did it distinguish between contributions from the ocelli and the compound eye. Occlusion or genetic manipulation experiments may be informative as to the role of either or both light-processing pathways. The arena developed with real-time feedback to a dynamic visual display allows for future

experiments that dissect the visually based cone assessment. For example, the horizon could be manipulated as the fly climbed the cone. These types of psychophysical experiments with quantitative behavioral readouts should help determine the role of vision in object preference.

Appendix A

Ctrax algorithm

A.1 Tracking algorithm

Our purpose in developing both the algorithm and the apparatus was to create a reliable system for obtaining interesting behavioral statistics for use by behavioral geneticists. Our tracking algorithm combined techniques from the computer vision literature to achieve this goal. The tracking algorithm input a stored video sequence and computed the trajectory of each fly (center position and orientation in each frame). Tracking was achieved by alternating two steps: fly detection and identity assignment. At each new frame, flies were first detected and their positions and orientations were computed. Next, each detected fly in frame t was associated with a fly detected in the previous frame $t-1$. Example tracked trajectories are shown in Figure 4.1b. Our tracking algorithm is described below. First, we describe the pre-processing steps, in which the tracker learns what the arena image looks like without flies in it (Appendix A.1.1.1), what regions of the image flies are in (Appendix A.1.1.2), and what shapes a fly can take (Appendix A.1.1.3). Then, we provide details of how the positions of flies in the current video frame are estimated (Appendix A.1.2). Next, we describe how the observed fly positions are assigned identities by matching them with the positions predicted from the previous frames (Appendix A.1.3). We then describe how tracks are modified in hindsight so that track births and deaths are avoided (Appendix A.1.4.1). Finally, we describe the post-processing step to resolve the head-tail orientation ambiguity (Appendix A.1.4.2).

A.1.1 Pre-processing

A.1.1.1 Background modeling

Detection was based on background subtraction (Piccardi, 2004). In our laboratory setting, we ensured that the camera was still and the IR lighting was constant, thus the only objects moving in the video are flies. The appearance and variability of the arena without flies (the background) was estimated before tracking as the pixelwise median of a set of frames sampled from the entire video sequence. The variability was estimated as the pixelwise median absolute deviation from the background image. We modeled the background pixel intensities at each location in the image as independent Gaussian distributions. Instead of fitting each Gaussian using the maximum likelihood estimates (the sample mean and standard deviation), we used the more robust median and median absolute deviation. That is, the tracker estimated the center of the Gaussian $\mu(\mathbf{p})$ at a given pixel location $\mathbf{p}$ as the median pixel intensity of the sampled frames at that location:

$$\mu(\mathbf{p}) = \underset{\{t=0,\Delta,2\Delta,\ldots,T)\}}{\text{median}} I_t(\mathbf{p}),$$

where I_t was the video frame at time t, T was the number of frames in the video, and Δ was the interval between sampled frames.[1] At each frame, the tracker also computed the absolute difference between the observed pixel value $I_t(\mathbf{p})$ and the median $\mu(\mathbf{p})$. The tracker estimated the standard deviation from the median such

[1] We chose $\Delta = \lfloor T/200 \rfloor$ in all our experiments.

absolute difference:

$$\sigma(\mathbf{p}) = c \underset{\{t=0,\Delta,2\Delta,\ldots,T)\}}{\text{median}} |I_t(\mathbf{p}) - \mu(\mathbf{p})|$$

where the constant c ensured that the correct fraction of the data was within one standard deviation:

$$c = 1/(\sqrt{2}\text{erf}^{-1}(.5)) \approx 1.4826.$$

Using the median made our algorithm tolerant to flies that do not move for long periods of time (Branson and Belongie, 2005). Note that it is good practice to estimate the background model from video taken after the flies have been introduced because the arena may be inadvertently jostled in the process of introducing flies. Movement of the arena or camera of just one pixel can cause large errors in background subtraction.

A.1.1.2 Region of interest

The tracker automatically detected the circular arena floor by fitting a large circle to edges in the background image using the Hough circle transform (Kimme et al., 1975). All pixels outside of the arena floor were labeled as background. This step was necessary because the wall of the arena was extremely reflective. As the flies were restricted from walking on the wall by the heat barrier, most foreground pixels on the wall were due to reflections of flies on the arena floor. In addition, in future experiments we plan to use dynamic LED panels to affect the flies' behavior, as in Reiser and Dickinson (2008). Thus, we would like to ignore all foreground detections not on the floor of the arena. Additionally, we plan to extend the tracker interface to allow arena shapes other than the circle.

A.1.1.3 Shape modeling

As discussed below in detail in Appendix A.1.2.3, the tracker decided whether to merge, split, or delete connected components based on the expected image area of a fly. The shape parameters were computed automatically. To compute the female shape parameters, in 50 frames evenly spaced through each all-female video, the tracker detected all connected components and computed the mean and standard deviation of their areas. The maximum and minimum area bounds were set to the mean plus and minus three standard deviations. The same computation was performed for the male parameters using the all-male videos. The mixed arena parameters were set as the extrema of the single-sex parameters (since females are larger than males, the minimum area was set to the minimum area for males and the maximum area was set to the maximum area for females).[2] Currently, we only used the fly's area to model its shape, but in future work we plan to use the length of the major and minor axes and the eccentricities of the ellipses as well.

A.1.2 Observation detection

In our setup, the flies appeared bright and the background dark (the tracker will also work with dark flies on a light background). Foreground pixels, that is, pixels belonging to flies, were detected when the difference between the pixel and background intensity exceeded a multiple of the background variability (Fig. 4.2a). This step

[2] In all our experiments, we used the same fly area parameters. The minimum area was 16.77 px^2 = 1.0488 mm^2 for all-male arenas, 21.445 px^2 = 1.3155 mm^2 for all-female arenas, and 16.78 px^2 = 1.0488 mm^2 for mixed arenas. The maximum area was 63.19 px^2 = 3.9494 mm^2 for all-male arenas, 76.945 px^2 = 4.8091 mm^2 for all-female arenas, and 76.945 px^2 = 4.8091 mm^2 for mixed arenas. The mean area was the average of these extreme values.

relies on the flies (and only the flies) looking significantly different from the background; poor camera quality and excessive video compression can compromise this step. Next, foreground pixels were grouped together into single fly detections. Ideally, each connected component (Gonzalez and Woods, 2007) of foreground pixels would correspond to exactly one fly. We thus initially fit an ellipse to each connected component by fitting a Gaussian to the locations of the corresponding foreground pixels. Owing to flies sometimes coming into contact and inevitable errors in pixel labeling, some connected components might have corresponded to many, part of one, or no flies. These errors were corrected automatically by detecting connected components that are too large or small and considering multiple splitting or merging hypotheses (Fig. 4.2b).

Below, we overview the steps involved in estimating the positions of flies in the current frame. To understand the choices made, it is beneficial to view observation detection in terms of probabilistic modeling and inference. The general goal in detection is to find the positions of the flies that best explains the current video frame. More formally, we would like to find the positions of the flies of maximum density given the current video frame. Let $\mathbf{x}_i = (x, y, \theta, a, b)^\top$ be the ellipse position for the ith fly detected (the x- and y-coordinates of the centroid, the orientation, the semi-major axis length, and the semi-minor axis length), $\mathcal{X} = \{\mathbf{x}_1, ..., \mathbf{x}_N\}$ be a set of N fly positions, and I be the current video frame. We would like to find $\mathcal{X}$ that maximizes

$$p(\mathcal{X}|I) \propto p(\mathcal{X})p(I|\mathcal{X}).$$

We assumed that the prior density on fly positions was independent for each fly:

$$p(\mathcal{X}) = \prod_{i=1}^{N} p(\mathbf{x}_i).$$

Our prior on the position of a single fly $p(\mathbf{x}_i)$ was the model of the fly's area:

$$p(\mathbf{x}_i) \propto \exp[-|\pi a_i b_i - \mu_{area}|/\sigma_{area}].$$

To compute the likelihood of the video frame I given the fly positions $\mathcal{X}$, $p(I|\mathcal{X})$, we constructed the foreground/background labels predicted for each pixel location given $\mathcal{X}$. The label $L_{ij}(\mathcal{X})$ predicted at pixel location (i, j) was labeled foreground if it was part of a fly, that is, if it was inside the ellipse for some fly in $\mathcal{X}$, and background if it was not. We assumed that the intensity of each pixel in the video frame was independent given its label, thus the likelihood factors as

$$p(I|\mathcal{X}) = \prod_{(i,j)} p(I_{ij}|L_{ij}(\mathcal{X})),$$

where $p(I_{ij}|background)$ was the Gaussian background model described in Appendix A.1.1.1 and $p(I_{ij}]|foreground)$ was uniform.

Finding the optimal fly positions was difficult because $p(\mathcal{X}|I)$ has many local maxima and was non-smooth, and $\mathcal{X}$ has a discrete component (the number of flies). We therefore used a sequence of heuristics to try to optimize the criterion efficiently. First, each pixel was classified as foreground or background (Appendix A.1.2.1). Each con-

nected component of foreground pixels usually corresponded to exactly one fly. Thus, initially one ellipse was fit to each of these connected components (Appendix A.1.2.2). To identify connected components that did not correspond to exactly one fly, the tracker found ellipse fits that had a low density according to the prior $p(\mathbf{x}_i)$. For these connected components, the number of ellipses fit to the connected component was iteratively increased or decreased to optimize the criterion (Appendix A.1.2.3).

A.1.2.1 Background subtraction

Classifying a pixel location as foreground (belonging to a fly) or background (not belonging to any fly) is referred to as background subtraction (Piccardi, 2004). To do this classification, the tracker thresholded the likelihood of the observed pixel intensities in the current frame given the background model described in Appendix A.1.1.1. Pixels with high likelihood were labeled background and pixels with low likelihood were labeled foreground. As we used a Gaussian model, it was equivalent to threshold the absolute difference from the mean normalized by the standard deviation:

$$l(\mathbf{p}) = \left\{ \begin{array}{ll} \text{foreground} & |I(\mathbf{p}) - \mu(\mathbf{p})|/\sigma(\mathbf{p}) > threshold \\ \text{background} & \text{otherwise} \end{array} \right\}.$$

The tracking software allowed us to specify the special case that flies were always brighter than the background (or vice-versa). In this case, the signed difference $(I(\mathbf{p}) - \mu(\mathbf{p}))/\sigma(\mathbf{p})$ was thresholded.

To improve robustness to noise, when thresholding foreground from background

pixels, we used a hysteresis approach. The tracker thresholded the difference at a low threshold $thresh_{small}$. If no pixel in the connected component had a difference larger than a larger threshold $thresh_{large}$, then all labels in this connected component were flipped to background.[3]

A.1.2.2 Ellipse fitting

To fit an ellipse to a connected component of foreground pixels, the tracker fitted a 2D Gaussian to the locations of the foreground pixels in the connected component. Given the parameters of the best-fitting Gaussian, the parameters of the ellipse could be computed. Consider all the pixel locations within an ellipse with semi-major axis length a, semi-minor axis length b, and orientation θ. The sample mean of the pixel locations will be close to the ellipse center. The sample covariance of the pixel locations within this ellipse will be close to

$$\Sigma = R^\top \begin{pmatrix} a/2 & 0 \\ 0 & b/2 \end{pmatrix}^2 R,$$

where

$$R = \begin{pmatrix} \cos\theta & \sin\theta \\ -\sin\theta & \cos\theta \end{pmatrix}.$$

Thus, given the covariance matrix Σ, the semi-major and semi-minor axis lengths and orientation could be computed by finding the Eigen decomposition of $\Sigma = U^\top DU$. The axis lengths were twice the square root of the eigenvalues, and the orientation

[3] In all our experiments, we set $thresh_{small} = 10$ and $thresh_{large} = 20$.

could be computed as the arctangent of two of the entries of U:

$$a = 2\sqrt{D_{11}}, \qquad b = 2\sqrt{D_{22}}, \qquad \theta = atan(U_{12}, U_{11}).$$

Instead of just computing the sample mean and covariance of all the pixels in the connected component, the tracker computed a weighted mean and covariance, where the weight of a pixel was proportional to its distance from the background model. Let $\{\mathbf{p}_1, ..., \mathbf{p}_n\}$ be the locations of the pixels in a given connected component. Let the weight of pixel i be the normalized distance of the pixel intensity from the background image:

$$w_i = |I(\mathbf{p}_i) - \mu(\mathbf{p}_i)|/\sigma(\mathbf{p}_i).$$

Then the sample mean and covariance were computed as

$$\begin{aligned} Z &= \sum_i w_i, \\ \mu &= \frac{1}{Z} \sum_i w_i \mathbf{p}_i, \\ \Sigma &= \frac{1}{Z} \sum_i w_i (\mathbf{p}_i - \mu)(\mathbf{p}_i - \mu)^\top. \end{aligned}$$

Using the weighted mean and variance improved our accuracy in two ways. First, it improved robustness to less than perfect threshold parameters, and allowed us to use a single threshold throughout the image, despite lighting differences in different regions. In dimmer parts of the arena, low threshold is needed. In brighter parts, using this low threshold resulted in pixels at the edge of the fly being classified as

foreground. These pixels were actually background, but contain some foreground light from blurring effects. While they were classified as foreground, they had a relatively small weight in the estimate of the ellipse. Second, using the weighted mean and variance improved the subpixel accuracy of our estimates.

A.1.2.3 Splitting and merging connected components

If the prior density $p(\mathbf{x}_i)$ of an ellipse fit $\mathbf{x}_i$ for a given connected component was small, then this connected component may actually have corresponded to multiple flies, part of a fly, or a spurious detection. Recall that the prior density was based only on the area of the ellipse. If the prior density was small because the area of the ellipse was too large, then the tracker determined if fitting multiple flies to the connected component would increase the score $p(\mathcal{X}|I)$. If the prior density was small because the area of the ellipse was too small, then the tracker determined if any of the following would increase the score: (1) lowering the foreground threshold to increase the area, (2) merging the ellipse with nearby ellipses, or (3) deleting the ellipse.

Splitting large components. Because of image blur and the legs of the flies, the pixels surrounding the fly would actually be a blur of foreground and background. Often, these pixels would be classified as foreground but have a higher background likelihood than pixels in the interior of the fly. We observed that relabeling these pixels as background often resulted in large connected components consisting of multiple flies being split into multiple connected components. Thus, the tracker first determined whether raising the foreground threshold for the connected component resulted in multiple,

reasonably sized components.[4] If it did not, then the Expectation-Maximization algorithm was used to fit a mixture of K Gaussians to the weighted pixel locations in the large connected component (Hastie et al., 2001). This approximation found a fit of K ellipses (that do not overlap too much) to the weighted pixel locations in the large connected component. More specifically, a mixture of K Gaussians was the distribution

$$p(\mathbf{p}) = \sum_{k=1}^{K} \pi_k \mathrm{G}(\mathbf{p}; \mu_k, \Sigma_k),$$

where π_k was the relative weight of component k, μ_k and Σ_k were the parameters of the k^{th} Gaussian, and $\mathrm{G}(\mathbf{p}; \mu, \Sigma)$ was the density of the Gaussian with parameters μ and Σ at pixel location $\mathbf{p}$.

The tracker determined the number of components K to split the large component into based on the shape prior $\prod_{k=1}^{K} p(\mathbf{x}_k)$ of the ellipses fit. We empirically observed that this prior did not usually have multiple maxima, thus the tracker greedily choose the number of components. It iteratively increased the number of components it split the large component into, stopping when there was a decrease in the prior.

Fixing small connected components. If a connected component had a small area, the tracker first determined if the ellipse fit was small because the foreground threshold was too high in that region of the image. Note that, in our setup, the ideal threshold varied with location in the image, as the lighting varied with location in the arena. The tracker decreased the foreground threshold for pixels near the connected com-

[4]The tracker iteratively tried increasing the threshold from $thresh_{small}$ to the maximum normalized distance in the connected component for 20 iterations, stopping if it had successfully split the large connected component.

ponent and refit the ellipse.[5] If this did not sufficiently increase the component's area, then the tracker determined whether the connected component corresponded to part of a fly. For each nearby component, the tracker determined whether merging the small component with this nearby component resulted in a small decrease in the image likelihood $p(I|\mathcal{X})$[6] and a large increase in the prior $p(\mathcal{X})$. If the area could not be increased sufficiently in either of these two ways, and the area was smaller than a given threshold[7], then the connected component was deleted.

A.1.3 Identity assignment

Each fly detected in frame t was associated with a trajectory from frame $t-1$. In the first frame, a unique trajectory label was assigned arbitrarily to each detection. In subsequent frames, assuming that each trajectory has been computed up to frame $t-1$, it was extended to frame t by assigning each fly detection in t to the trajectory that best predicted its position and orientation (Fig. 4.2c), where predictions were computed by a constant-velocity model. This was a multiple-assignment problem because trajectories and flies have to be in one-to-one correspondence: two flies could not be associated to the same trajectory and vice-versa (Perera et al., 2006). Thus, the optimal solution needed to be computed simultaneously for all flies. Occasionally, a fly may have escaped or entered the arena, or the detection stage may have made an error. For this reason, our software algorithm allowed a trajectory or a detection to be unmatched when the distance was too large, and pay a constant penalty. The best

[5] The threshold was decreased to 1 standard deviation.
[6] Corresponding to at most 40 px^2 = 2.5 mm^2 increase in normalized distance^2
[7] 5 px^2 = .3125 mm^2

overall assignment was computed using the Hungarian method for minimum-weight perfect bipartite matching (Papadimitriou and Steiglitz, 1998). The assignment step required that the frame rate be sufficiently high relative to the speed of the flies so that the optimal matching between observations and trajectories was easy for a human observer.

A.1.3.1 Constant velocity prediction

In a constant-velocity model, we assumed that the velocity of the fly from frame $t-1$ to the current frame t was the same as the previous velocity from frame $t-2$ to $t-1$. If $\mathbf{x}_{t-1}$ was the position of the fly in frame $t-1$ and $\mathbf{x}_{t-2}$ was the position of the fly in frame $t-2$, then the constant-velocity prediction was that the fly would be at

$$\mathbf{x}^{pred} = \mathbf{x}_{t-1} + (\mathbf{x}_{t-1} - \mathbf{x}_{t-2})$$

in frame t. We used a constant-velocity model for the center of the fly, and a dampened-velocity model for the orientation of the fly, as we observed that the orientation velocity was somewhat noisy. In this dampened-velocity model, we predicted the current orientation velocity to be some fraction of the previous orientation velocity:

$$\theta^{pred} = \theta_{t-1} + \lambda_{dampen}(\theta_{t-1} - \theta_{t-2})_{(-\pi/2,\pi/2]}$$

where λ_{dampen} is a constant between 0 and 1 and the angle difference wraps around at $-\pi/2$ and $\pi/2$.[8]

[8] We used $\lambda_{dampen} = 0.5$.

The penalty for matching the predicted fly position $\mathbf{x}^{pred} = (x^{pred}, y^{pred}, \theta^{pred})$ and the observed fly position $\mathbf{x}^{obs} = (x^{obs}, y^{obs}, \theta^{obs})$ was computed as

$$err(\mathbf{x}^{pred}, \mathbf{x}^{obs}) = (x^{pred} - x^{obs})^2 + (y^{pred} - y^{obs})^2 + w_{orient}(\theta^{pred} - \theta^{obs})^2_{(-\pi/2,\pi/2]}$$

where w_{orient} was the weight of the orientation error relative to the position error, and the angle difference was computed on the interval $(-\pi/2, \pi/2]$.[9] In future work, we plan to explore more complex, accurate models of fly motion.

A.1.3.2 Finding the optimal matching

The error function $err(\mathbf{x}_u^{pred}, \mathbf{x}_v^{obs})$ defined the cost of assigning identity u to the v^{th} detection. If we simply assigned to the v^{th} detection the identity u with the minimum error, then we might have ended up with multiple flies in the current frame with the same identity, and no flies with other identities. Here, we describe the algorithm for computing the best one-to-one matching of identity to observation. By one-to-one matching, we mean that every fly identity was assigned to exactly one observation, and every observation was assigned to exactly one identity.

In fact, the situation was a little more complicated than this, as there was the potential that a fly might escape the arena, a new fly might enter the arena, or there might be an error in detection. For simplicity, let us ignore these possibilities for now; we will return to them later.

In this simplified setup, let N be the number of flies observed in the current frame

[9] We used $w_{orient} = 100px^2/rad^2 = 6.25mm^2/rad^2 = 0.044mm/deg$.

(and therefore the number of identities to assign). We could represent a matching as a set of pairings of identities and observations: $A = \{(i_1, o_1), ..., (i_N, o_N)\}$, where $i_i \in \{1, ..., N\}$ was the identity assigned to observation $o_i \in \{1, ..., N\}$. The penalty for a matching was the sum of the penalties of each individual assignment, as described in the previous section:

$$err(A) = \sum_{j=1}^{N} err(\mathbf{x}_{i_j}^{pred}, \mathbf{x}_{o_j}^{obs}).$$

We required that no identity be assigned to multiple observations: $i_j \neq i_k \forall j \neq k$, and that no observation be assigned multiple identities: $o_j \neq o_k \forall j \neq k$. We also required that every identity and every observation be in some assignment. Our goal was to find the lowest error legal matching.

Let us now expand the definition of a matching and its error to allow some detections or observations not to be matched. In general, we would have preferred an observation to be assigned an existing identity, as we were assuming that track deaths and births were unlikely. However, if forcing an assignment required that the fly accelerated a huge amount, then we preferred to assign a new identity to the fly. Similarly, if the error for assigning an identity to some observation was too large, we preferred to let this fly track die.

As the number of identities to assign might be different than the number of observations, let M be the number of identities to assign. We represented observation o being assigned a new identity as an assignment (i, o) to a dummy identity $i \in \{M + 1, ..., M + N\}$. We represented an identity i not being assigned to any observation as an assignment (i, o) for a dummy observation $o \in \{N+1, ..., N+M\}$. We

then represented a matching as the set of $M+N$ pairs $A = \{(i_1, o_1), ...(i_{M+N}, o_{M+N})\}$ where $i_j \in \{1, ..., M+N\}$ and $o_j \in \{1, ..., M+N\}$. Pairs (i, j) where both the identity and observation were dummy variables ($i > M$ and $j > N$) do not symbolize anything.

Let max_{err} be the maximum amount we expected a fly could accelerate from one frame to the next. We used the fairly large value 100 (corresponds to the fly jumping 25 mm if there was no change in orientation) for this threshold, as flies occasionally jumped and it was rarer that a fly left or entered the arena. We modified the definition of a matching error to include assignment of an observation to a new identity and assignment of an identity to no observation:

$$err(i, o) = \left\{ \begin{array}{ll} err(\mathbf{x}_i^{pred}, \mathbf{x}_o^{obs}) & i \leq M, o \leq N \\ max_{err} & i > M, o \leq N \\ max_{err} & i \leq M, o > N \\ 0 & i > M, o > N \end{array} \right\}.$$

Finding the minimum error perfect matching A was an instance of the square assignment problem, a.k.a. the minimum weight perfect bipartite matching problem (Papadimitriou and Steiglitz, 1998). It could be solved quickly using a number of algorithms. We used the Hungarian method (Papadimitriou and Steiglitz, 1998) to solve this problem (`http://mit.edu/harold/Public/hungarian.tgz`).

A.1.4 Hindsight

A.1.4.1 Detection hindsight

The 'observation detection' step was performed using information from only the current frame, and the 'identity assignment' step assumed that these detections were correct, both without incorporating all available information. First, the observed fly positions in the current frame were fixed without considering the positions of the flies in previous and future frames. Second, our computation of the error of matching an identity with an observation only incorporated information from the previous frames, not the future frames. Third, the error of an assignment was the sum of the errors for each pair of matches independently. In the 'hindsight' step, the tracker determined if a track death or birth in the current frame could be avoided by fixing potential errors in the previous ΔT frames[10]. The tracker determined if tracks were previously merged, split, lost, or the result of spurious detections, resulting in the birth or death of a track in the current frame, this step operated on the assumption that flies rarely enter or leave the arena.

In a merged detection, two flies were tracked as a single fly for a short sequence of frames[11]. A merged detection would exhibit itself as the death of track i_1 in frame t_1 (i.e., identity i_1 would not be assigned to any observations in frame t_1) and the birth of track i_2 in frame $t_2 > t_1$ (the corresponding observation in frame t_2 would not be assigned an existing identity). In addition, there would be some track i_3 that

[10] In our experiments, $\Delta T = 50$ frames = 2.5 seconds.

[11] $\leq$ 50 frames = 2.5 s

could be split into two tracks from frames t_1 to $t_2 - 1$ with low penalty[12]. Finally, the errors of matching the split track to i_1 in frame t_1 and i_2 in frame t_2 would be small[13]. Given the birth of a track i_2 in frame t_2, the tracker therefore first searched the recent history for such tracks i_1 and i_3. The tracker then split i_3 in frames t_1 to $t_2 - 1$ and connected the split tracks to i_1 and i_2.

In a split detection, a single fly was split into two detections for a short sequence of frames[14]. A split detection would exhibit itself as the birth of track i_1 in frame t_1 and the death of i_1 soon after in frame t_2. In addition, there would be another track i_2 that i_1 could be merged with in frames t_1 through $t_2 - 1$ with low penalty[15]. Given the death of a track i_1 in frame t_2, the tracker therefore first searched the recent history for such a track i_2. The tracker then merged track i_1 with i_2 in frames t_1 to $t_2 - 1$, and replaced identity i_2 with i_1.

In a lost detection, a fly was not detected for a short sequence of frames[16]. A lost detection would exhibit itself as the death of track i_1 in frame t_1 followed by the birth of track i_2 in frame t_2 soon after. In addition, the predicted position of fly i_1 in frame t_2 would be close to the observed position of i_2 in frame t_2[17]. Given the birth of fly track i_2 in frame t_2, if the tracker cannot connect i_2 to previous tracks by splitting, it would then search for such a track i_1. It then connected these two tracks. It replaced identity i_2 with i_1, and set the positions of i_1 in frames $t_1 + 1$ through $t_2 - 1$ by linear interpolation.

---

[12] $\leq$ 40 px^2 = 2.5 mm^2
[13] $\leq$ 20 $\approx$ 5 mm^2
[14] $\leq$ 50 frames = 2.5 s
[15] $\leq$ 40 px^2 = 2.5 mm^2
[16] $\leq$ 50 frames = 2.5 s
[17] within 100 px $\approx$ 25 mm

In a spurious detection, the tracker detected a fly for a short sequence of frames where there was no fly[18]. In this case, a fly i would be born in frame t_1 and die soon after in frame t_2. Given the death of fly track i in frame t_2, if it could not connect it to other tracks by merging, it deleted this track if its lifespan was short enough.

A.1.4.2 Orientation ambiguity hindsight

The 'detection' step could not tell the head from the tail of a fly due to the low resolution of the video. Thus, the orientation of the fly computed online was only known modulo π; it was not known whether the orientation is θ_t or $\theta_t + \pi$. To resolve this ambiguity, at each frame our tracker determined whether to add 180° to the orientation of each fly. Using a variation of the Viterbi algorithm (Cormen, 2001), the sequence of orientation offsets was computed that minimized the change in orientation between consecutive frames and the difference between orientation and velocity direction when the fly was moving. To use this method, we made the following assumptions. First, when a fly was walking quickly, its head would point forward, i.e., the orientation of its body and the direction of the fly's velocity would approximately match. Second, we assumed that the fly's orientation did not change much from one frame to the next. In this section, we define a criterion that combined these two assumptions, then show how to minimize this criterion.

Let θ_t be the orientation of the fly at frame t, ϕ_t be the velocity direction at frame t, v_t be the speed of the fly at time t, and T be the number of frames in the entire video. We were searching for the binary values $s_t \in \{0, 1\}$ that indicated whether we

[18] $\leq$ 50 frames = 2.5 s

would add π to the orientation: $\theta'_t = \theta_t + \pi s_t$. We found the sequence of states $\mathbf{s}_{1:T}$ that minimized the following criterion:

$$J(\mathbf{s}_{1:T}) = \sum_{t=1}^{T} [J^1(s_t) + J^2(s_t, s_{t-1})],$$

$$J^1(s_t) = w(v_t)|(\theta_t + \pi s_t - \phi_t)_{(-\pi,\pi]}|,$$

$$J^2(s_t, s_{t-1}) = (1 - w(v_t))|(\theta_t + \pi s_t - \theta_{t-1} - \pi s_{t-1})_{(-\pi,\pi]}|.$$

The first term $J^1(s_t)$ penalized the orientation $\theta_t + \pi s_t$ differing from the velocity direction ϕ_t. When the fly was sitting still, it might still have a non-zero velocity. However, the direction of this velocity was not related to the orientation of the fly. Thus, we weighted this error term proportional to the magnitude of the velocity of the fly. We used the weight function

$$w(v) = \min\{w_{max}, \lambda v^2\},$$

where λ and w_{max} were constants[19]. The second term $J^2(s_t, s_{t-1})$ penalized the orientation at frame t, $\theta_t + \pi s_t$, differing from the orientation at frame $t-1$, $\theta_{t-1} + \pi s_{t-1}$.

The global optimum of this criterion could be found efficiently (space and time $O(T)$) using dynamic programming (Cormen, 2001). In order to do so, $J_t(s_{1:t})$ needed

[19] We used $\lambda = 0.05(px/fr)^{-2} = 1.12mm/s$ and $w_{max} = 0.25$.

to be rewritten recursively as

$$\begin{aligned}
[C_t(s_t), p_t(s_t)] &\triangleq \min_{s_{1:t-1}} J_t(s_{1:t-1}, s_t) \\
&= \min_{s_{t-1}}[\min_{s_{1:t-2}} J_{t-1}(s_{1:t-2}, s_{t-1}) + \\
&\qquad J^1(s_t) + J^2(s_t, s_{t-1})] \\
&= \min_{s_{t-1}}[C_{t-1}(s_{t-1}) + J^1(s_t) + J^2(s_t, s_{t-1})].
\end{aligned}$$

$C_t(s_t)$ was the minimum cost of a sequence ending in state s_t, and $p(s_t)$ stored the s_{t-1} that resulted in this minimum.

A.1.5 System evaluation

We measured the quality of our tracker by comparing its measurements with groundtruth on a set of benchmark videos. We distinguished identity, position, and sex assignment errors. Identity errors included swapping flies' identities, losing flies' tracks, flies that were split into two detections, flies that were merged into a single detection, and spurious detections that did not correspond to flies (Fig. 4.2b). Position errors were inaccuracies, usually subpixel, in the estimated position and orientation of a fly (Fig. 4.2c). Sex assignment errors were mistakes in determining whether a fly was male or female.

A.1.5.1 Identity errors

We evaluated the frequency of identity errors made by our system on 18 manually annotated video sequences, each containing 10, 20, or 50 wild type flies, which were either all female, all male, or half male, half female. Two 5-min videos were used as benchmarks for each condition. Each video was about 5 minutes long and recorded at 20 fps. For ease of counting, we began by putting 10 flies in the arena then captured the 10-fly video. We then added 10 more flies and captured the 20-fly video. Finally, we added 30 more flies and captured the 50-fly video. We show example identity errors in Figure 4.2b.

To detect identity errors made by the tracker, we would ideally watch each video multiple times in slow-motion. In each viewing, the video would be zoomed in on a different fly. As this would have been extremely time-consuming, a trained operator instead examined those video frames in which tracking was the hardest: When flies were near each other, there were large differences between predicted and measured positions, or at the births and deaths of trajectories. These frames were inspected in slow motion, zoomed in on the difficult-to-follow flies. Tracking was easy when the flies were separated and their motion was well-predicted by the constant velocity model. It was more difficult when flies were close together or were jumping. For each video, we selected each frame and pair of flies that were touching (i.e., were part of the same connected component of foreground pixels, as described in Appendix A.1.2.2). We also selected all pairs of frames, in which swapping the identities of the pair of flies increased the error by less than a threshold. We set this threshold to 100. The

units of this threshold was pixels squared, thus this was $(2.5\text{mm})^2$. In addition, we selected each frame and fly that did not move according to the assumed motion model (see Appendix A.1.3.1). In particular, we watched the frame and fly if the error of the center prediction was greater than a threshold (we chose 20 pixels = 5 mm). Finally, we watched the birth and death of each track. Most of the frames watched contained no errors. We classified each error we observed into one of five types: lost fly, swapped identities, spurious track, merged flies, and split fly. Table A.1 lists the number of each type of error observed in each video we evaluated. The scoring took approximately 0.5 hours for each 10-fly video, 2 hours for each 20-fly video, and 8 hours for each 50-fly video. On average, we observed an identity error once every 5 fly-hours in the 10-fly videos, once every 1.5 fly-hours in the 20-fly videos, and once every 40 fly-minutes in the 50-fly videos. Example tracking errors are shown in Figure 4.2d.

Lost fly errors occured when the tracking system did not detect a fly in the arena. This would occur when both (1) the background subtraction step failed to classify enough pixels on the fly as foreground (Appendix A.1.2.1) and (2) the hindsight step was not able to connect the two track pieces because the number of consecutive frames in which background subtraction failed was too large or the motion of the fly was too erratic during these frames. In our videos, all occurrences of this type of error were caused by errors in the background modeling when a fly spent more than half the video in the same position and became part of the background. The lack of motion of some of the flies only occurred in the 20- and 50-fly videos. In these videos, some

of the flies had been in the arena for over 5 or 10 minutes, as discussed above. As the flies were in the arena longer, they seemed to grow accustomed to their environment and became less active. This suggests that it is best to collect video when the flies are first introduced to the arena and use this to estimate the background model. An explicit foreground model would also help prevent this type of error.

Table A.1: Identity errors. Number of each type of identity error for each video evaluated. Each row corresponds to a different video. The first two columns show the number of female and male flies in the video. The third column shows the number of frames in the video. The fourth column shows the number of times a pair of flies was close (note that this number can be greater than the number of frames in the video, as multiple pairs of flies may be close in a single frame). The next five columns show the number of errors of each type: *Swap* identity, *Lost* fly, *Spurious* track, *Merged* fly, and *Split* fly. The *Swap/Close* column shows the ratio of number of identity swaps to frames in which the flies are close, and the *Errors/Fly/Frame* column shows the ratio of errors to flies per frame.

Fly Sex		N. Frames		N. Errors					Error Freq	
♀*	♂	Total	Close	Swap	Lost	Spurious	Merged	Split	Swaps/ Close	Errors/Fly/ Frame
10	0	6364	42	0	0	0	0	0	0	0
10	0	6118	67	1	0	0	0	0	1.5e-2	1.9e-05
20	0	6221	261	0	1	0	0	0	0	9.4e-06
20	0	6206	358	0	1	0	0	0	0	8.5e-06
50	0	6123	2135	0	2	0	0	0	0	7.3e-06
50	0	6587	4545	1	0	0	0	0	2.2e-4	7.1e-06
0	10	6106	268	0	0	0	0	0	0	0
0	10	6133	316	0	0	0	0	0	0	0
0	20	6169	1237	0	1	0	0	0	0	8.1e-06
0	20	6118	1029	0	1	0	0	0	0	8.8e-06
0	50	8696	9765	4	0	1	0	0	4.1e-4	1.2e-05
0	50	6088	4855	7	1	0	0	0	1.4e-3	3.0e-05
5	5	6268	499	0	0	0	0	0	0	0
5	5	7859	753	0	0	0	0	0	0	0
10	10	6121	2050	1	1	0	0	0	4.9e-3	1.9e-05
10	10	6104	1460	0	1	0	0	0	0	8.9e-06
25	25	6220	9843	1	3	0	0	0	1.0e-4	1.4e-05
25	25	6536	9902	1	1	1	0	0	1.0e-4	9.6e-06

Swapped identity errors occured when the identity of two flies returned by the tracker swapped at some point during the video sequence. This would occur when the motion model failed to predict the motion of at least one of the pair of flies, and the relative positions of the pair of flies was such that the error of swapping identities was smaller than not. We noted three situations in which this occurred. First, identities may have been swapped if two flies jumped at the same time in close proximity to one another. Second, consider a case in which one fly sat still and another fly jumped over it. As the tracker computed the error as the sum of squared distances for each matching of identity to observation, it preferred that each fly make a small jump rather than that one fly sit still and another fly make a large jump. This type of error could be prevented by modifying the hindsight step (Appendix A.1.4.1), and we plan to do this in the future. Third, a swap could occur if the splitting of a large connected component into multiple detections failed (Appendix A.1.2.3). For instance, suppose one fly was actually just to the left of another fly. Occasionally, the clustering computed would actually split a connected component vertically rather than horizontally. In future work, we plan to address this issue as by incorporating a prior on the desired shape of the clusters into the clustering algorithm.

Spurious track errors occurred when something that was not a fly was detected as a fly for a sequence of frames and was detected for enough frames so that the hindsight step did not correct the error. This type of error occurred twice in the videos. In the first case, a relatively large piece of debris in the arena at some point stuck to/was picked up by a fly walking over it. This piece of debris was therefore

visible for less than half of the video and therefore was classified as foreground. In the second case, the spurious detection occurred in the last frame of the video, thus it could not be resolved by the hindsight step.

We did not observe the other two types of errors: 'merged' or 'split.' Before annotating the videos, we hypothesized the following definitions. *Merged* fly errors would occur when two flies were detected as one for a sequence of frames long enough that the hindsight step could not fix it. Similarly, *split* fly errors would occur when a single fly was detected as two for a sequence of frames long enough that the hindsight step could not fix it.

A.1.5.2 Fixing identity errors manually

Using simple heuristics, a small number of suspicious frames and flies were automatically flagged. An operator could then inspect these frames and manually fix any errors using our GUI. It was possible to detect identity errors automatically and fix them manually in a matter of minutes. A user can therefore observe the small set of suspicious frames and manually fix any observed gross errors with a minimal amount of work. All manually determined identity errors in the benchmark sequences were also flagged automatically, and thus, error detection was 100% accurate with this limited supervision.

A.1.5.3 Position errors

We developed two methods for evaluating errors made in estimating the position of each fly in two different ways. The first involved simultaneously recording a HR video

of a portion of the arena and comparing the manually labeled fly positions in the HR data to the positions returned by the tracker on the standard LR video of the entire arena. Appendix A.1.5.4 describes this evaluation. The second involved manually selecting tracks in which the fly looked to be moving with an approximately constant velocity. We then compared the tracks returned by the tracker to a very smoothed version of these tracks. Appendix A.1.5.5 describes this evaluation. Both of these techniques resulted in qualitatively similar estimates of position error.

A.1.5.4 Comparing to high-resolution groundtruth

We captured nine videos simultaneously with the original camera viewing the entire arena and with camera of the same model as the original fitted with a lens that zoomed in a small portion of the arena (15x higher magnification than the standard lens, corresponding to fly lengths of 120 pixels). Figure A.1 shows frames of the same flies captured by each camera.

We manually labeled a random sample of 100 flies in the HR video that were (1) fully visible and (2) not near another fly. For each sample, we drew the bounding box of the fly to estimate the center position and orientation of the fly. In addition, we also clicked on five points visible on each fly: the tip of the left antenna, the tip of the right antenna, the start of the left front leg, the start of the right front leg, and the scutellum. Figure A.1 shows examples of the labels for some random samples.

To compare the HR labels and the LR tracks, we need to know the 2D projective transform P taking coordinates in the HR video (x_h, y_h) to coordinates in the LR

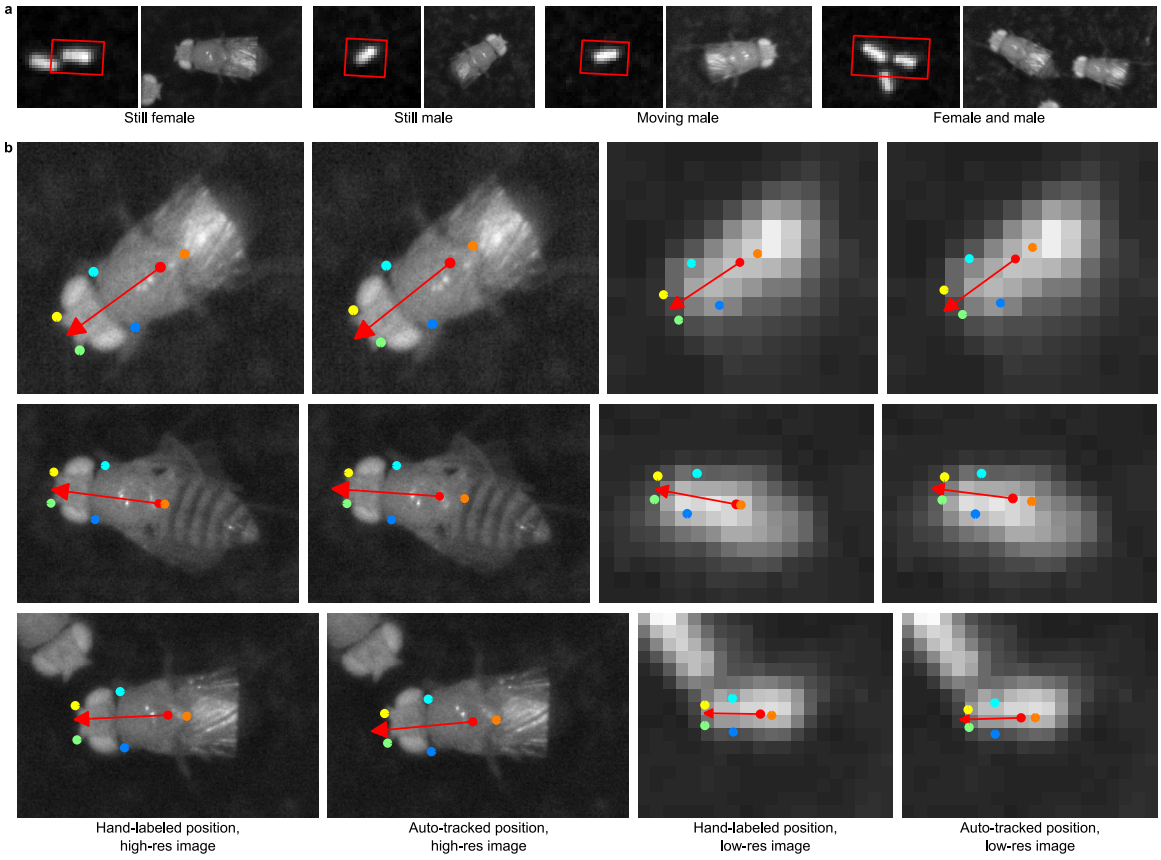

Figure A.1: Illustration of groundtruthing using high-resolution video. (**a**) Example images of the same flies captured by the low-resolution (LR) and high-resolution (HR) cameras. The left image of each pair is from the LR camera, the right image is from the HR camera. The red box in the LR images indicates the location of the adjacent HR image. The last pair of frames shows a male and female fly near each other. (**b**) Examples of HR labels and corresponding LR tracks. Each row shows the manually labeled HR image and the positions estimated by the tracker for a different example. The first column shows the true labels plotted on the HR frame. The second column shows the projection of the positions estimated by the tracker on the HR frame. The third column shows the projection of the true labels on the LR frame. The last column shows the positions estimated by the tracker on the LR frame. The last row shows touching flies. The red circle and arrow show the bounding box-based center position and orientation. The colored circles indicate the positions of the five parts.

video (x_l, y_l). This was a linear transformation with 8 degrees of freedom:

$$(cx_l, cy_l, c) = (x_h, y_h, 1)P,$$

where P was an arbitrary 3×3 matrix with $P_{33} \neq 0$. We approximated the projective transform P using a few manually and automatically selected correspondence points on a grid. However, the projective transform computed in this way was inaccurate because (1) the number of correspondence points available was small and (2) the flies had some depth. Thus, we used the center positions of the labels and the center positions of the tracks to refine the projective transform. We found matches between flies in the LR and HR videos using the initial transform. Then, we updated P to minimize the error in predicting the center positions of the flies. Note that we used the same P matrix for all frames in all videos, as the two cameras did not move with respect to each other.

We used this same projective transform to compute error in orientation and labeled parts as well. As the tracker outputs the center position and orientation, not the locations of the predicted parts, for a given part we computed the average offset of the part along the major axis, normalized by major axis length, and the average offset of the part along the minor axis, normalized by the minor axis length. We used these values to predict the position of the part given just the tracked center position and orientation.

Figure A.2 shows the cumulative distribution of errors in estimating the center position, labeled part positions, and orientation. The median error in estimating the

center was 0.0292 mm, equivalent to 2% of a fly's body length. The median error in estimating the orientation was 3.14°. The median error in estimating the part positions varied between 0.10 and 0.16 mm.

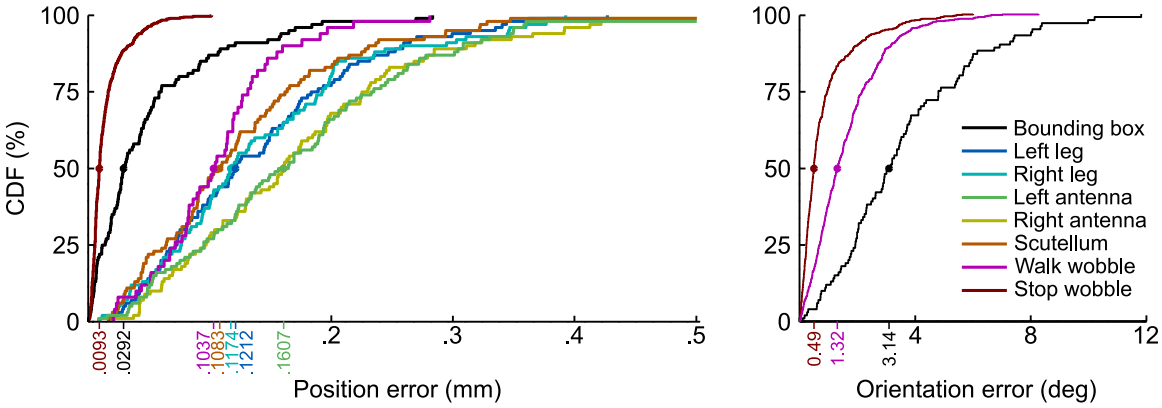

Figure A.2: Cumulative distribution of position errors. We plot the cumulative distribution of position errors for each of the methods of estimating error. On the left, we plot error in estimating point locations. On the right, we plot error in estimating the orientation of the fly. The line labeled 'Bounding box' corresponds to errors in estimating the center and orientation of the fly by manually drawing a bounding box on the HR images. The next five lines correspond to errors in estimating the positions of the parts manually labeled on the HR images. The 'Walk wobble' line corresponds to estimates of the center and orientation error computed by smoothing the velocity and orientation during walks. The 'Stop wobble' line corresponds to estimates of the center and orientation computed from the variance in position of a stopped fly. On the x-axes, the colored ticks mark the median values.

We repeated the above experiment on 50 samples in which the chosen fly was close to another fly. Example labels for this test are shown in Figure A.1b. The mean and standard deviation of the errors are shown in Table A.2. As expected, the error when the flies were close was slightly larger: 0.0461 mm for the center position and 10.61 for the orientation.

Table A.2: Each row of this table corresponds to a different error measure computed from the HR groundtruth samples in which another fly was near the labeled fly. The *Type* column describes the measure, the *Median* column lists the median error in the estimate and the *Std* column lists the standard deviation of the error of the estimate. The first two rows show the error for the center position and orientation estimates, computed from the bounding box labels. The last five rows show the error estimates for the labeled parts.

Type	Median	Std
Center	0.046 mm	0.090 mm
Orientation	2.8°	2.0°
Left Antenna	0.18 mm	0.09 mm
Right Antenna	0.19 mm	0.09 mm
Left Leg	0.21 mm	0.09 mm
Right Leg	0.21 mm	0.09 mm
Scutellum	0.14 mm	0.10 mm

A.1.5.5 Estimating error from fly "wobble"

As it is difficult to set up a synchronized additional HR camera and time-consuming to capture and label data from it, we evaluated a simpler, though possibly less accurate algorithm for estimating the amount of fine error. In a standard LR video, we manually selected 10 sequences each of length 50 frames (2.5 seconds) in which the chosen fly appeared to be moving with an approximately constant velocity. As we believed in this sequence the fly's velocity was fairly constant, smoothing should not effect the true velocity too much. We smoothed six times with the filter $[1, 2, 1]/4$. We then computed the error between the raw track and the smoothed track for the center position and the orientation. The cumulative distribution of errors is plotted in Figure A.2. The distribution of center position error estimated from wobble during walks closely matches the distributions of part location errors computed from the HR video. The orientation error estimated from wobble during walks was smaller than

that measured from the HR video. We hypothesized that this was because of variance in manual labeling of the orientation. Still, these error measures were qualitatively similar to those computed from the HR groundtruth data. Therefore, we found this second method appropriate for estimating position errors.

For comparison, we performed a similar evaluation using a fly that seemed to be static, following (Valente et al., 2007). Again, we used 10 tracks of length 50 frames. Instead of smoothing the trajectory, we assumed that the position was static, thus computed the error to the mean center position and orientation (Fig. A.2). The errors estimated in this manner underestimated the true amount of error. We hypothesized that this was because pixelation effects did not occur when the fly was still.

A.1.5.6 Gender assignment

As female flies were slightly larger than male flies, a fly's sex could be automatically predicted from its image area. For each trajectory, the median area was computed and sex was assigned by comparing this area to a threshold estimated from single-sex experiments (correcting for biases from lighting variations in different parts of the arena). The hold-one-out error rate was $4/77 = 0.0519$ for females and $3/106 = 0.0283$ for males.

A.2 Behavior definitions

All our behavior definitions had the following structure. The fly was performing the defined behavior from frames t_1 to t_2 if all of the following apply. (i) In each frame

$t_1, ..., t_2$, properties of the fly (for example, speed or distance to another fly) were within given ranges. (ii) In each frame $t_1, ..., t_2$ properties of the fly were temporally near (within a given number of frames) frames in which the properties were within tighter ranges. (iii) The summed properties (for example, total distance traveled) of the fly's trajectory in $t_1 \ldots t_2$ were within given ranges. (iv) The mean value of properties of the fly were within given ranges. Social behaviors operate on properties of pairs of flies rather than individuals. Parameters of each behavior, including the properties and ranges for each of the above rules, are given in Table A.3.

Table A.3: Parameters for each of the eight behaviors. Each row for a behavior corresponds to a different property that is computed at every time instant. The 'Property' column gives this property an abbreviated name; the exact definitions are described below the table. The four Property columns show the ranges the property is allowed to take for each of the four conditions enumerated in the Methods section. The 'Min Length' column shows the minimum length of the sequence. The 'Radius' column shows the definition of 'near' for property (2): frame t_1 is near frame t_2 if t_1 is within Rad seconds of t_2.

Behavior	Property	Parameter ranges				Min Length (s)	Radius (s)
		Per-frame (1)	Near frame (2)	Sum (3)	Mean (4)		
walking	speed (mm/s)	$[9.9, \infty)$	$[11.9, \infty)$	$[2.4, \infty)$	$[10.6, \infty)$	.25	.2
	$\lvert\dot{\theta}\rvert$ (°/.05s)	$[0, 31.3]$	$[0, 19.8]$		$[0, 5.2]$		
	acc (mm/(.05 s)^2)	$[0, 2.0]$	$[0, 0.8]$		$[0, 1.1]$		
	$\lvert smth(\theta)\rvert$ (°/.05s)	$[0, 12.9]$	$[0, 10.5]$				
stopped	speed (mm/s)	$[0, 4.8]$	$[0, 1.7]$	$[0, 2.6]$	$[0, 3.1]$	.35s	.1
	$\lvert\dot{\theta}\rvert$ (°/.05s)	$[0, 5.7]$	$[0, 2.3]$	$[0, 9.7]$	$[0, 3.1]$		
	acc (mm/(.05s)^2)	$[0, 1.00]$	$[0, 0.80]$		$[0, 0.88]$		
sharp turn	$\lvert\dot{\theta}\rvert$ (°/.05s)	$[4.0, \infty)$	$[6.6, \infty)$	$[27.6, \infty)$	$[9.3, \infty)$	.35	.1
	speed (mm/s)	$[0, 27.2]$	$[0, 9.2]$	$[0, 4.5]$	$[0, 13.6]$		
	acc (mm/(.05s)^2)	$[0, 1.4]$	$[0, 1.2]$		$[0, 1.2]$		
crabwalk	$\lvert\phi - \theta\rvert$ (°/.05s)	$[7.1, \infty)$	$[26.8, \infty)$	$[99.7, \infty)$	$[18.9, \infty)$	.5	.1
	$\lvert\dot{\theta}\rvert$ (°/.05s)	$[0, 21.6]$	$[0, 3.9]$	$[0, 151.8]$	$[0, 7.7]$		
	$\lvert smth(\theta)\rvert$ (°/.05s)	$[0, 16.9]$	$[0, 12.6]$		$[0, 6.7]$		
	$\perp$ tail vel (mm/s)			$[1.54, \infty)$	$[0.54, \infty)$		
backing up	fwd vel (mm/s)	$(-\infty, 0]$	$(-\infty, -0.50]$	$(-\infty, .08]$	$(-\infty, 0.50]$	.15	.15
chasing	min speed (mm/s)		$[9.9, \infty)$		$[8.5, \infty)$	.55	.55
	vel twd (mm/s)	$[-18.6, \infty)$	$[-6.5, \infty)$	$[-5.0, \infty)$	$[3.0, \infty)$		
	max speed (mm/s)		$[3.3, \infty)$		$[14.3, \infty)$		
	dist btn (mm)	$[0, 26.1]$	$[0, 12.1]$		$[0, 7.8]$		
	speed apt (mm/s)	$[0, 41.2]$	$[0, 37.7]$		$[0, 14.7]$		
	angle btn (°)	$[0, 79.0]$	$[0, 62.9]$		$[0, 61.7]$		
	θ diff (°)	$[0, 180.5]$	$[0, 120.3]$		$[0, 98.4]$		
	ϕ (°)	$[0, 173.7]$	$[0, 108.2]$		$[0, 40.9]$		
jumping	speed (mm/s)		$[48.1, \infty)$			0	.05
touching	dist btn (mm)		$[0, 2.5]$			.25	.05
	ang btn (°)		[0,0]				

- **Table A.3 Property key**:
- **speed**: Magnitude of the vector between the fly's centroids in frames $t-1$ to t, normalized by the frame rate. The integral of speed (column 3) is the total distance traveled during the segment, measured in mm.
- $|\dot{\theta}|$: Absolute value of change in orientation from frame $t-1$ to t, normalized by the frame rate. The integral of $|\dot{\theta}|$ is the absolute value of the total change in orientation during the segment, measured in degrees.
- **acc**: Absolute change in velocity between frames $t-1$ and $t+1$, measured in mm per frame^2 $= (0.05s)^2$
- $|\dot{smth}(\theta)|$: Absolute change in the smoothed orientation from frame $t-1$ to t, normalized by frame rate $= 0.05s/frame$.
- $|\phi - \theta|$: Absolute difference between orientation at frame t and velocity direction from frames t to $t+1$.
- $\perp$ **tail vel**: Change in position of tail of fly from frames t to $t+1$, projected onto the direction orthoganal to the fly's orientation in frame t.
- **fwd vel**: Dot product of orientation vector at frame t and vector connecting centroids in frames t to $t+1$, normalized by frame rate.
- **min speed**: Minimum speed of either fly involved in the chase.
- **vel twd**: Dot product of direction of chased fly from chasing fly and vector connecting centroids of chasing fly in frames t to $t+1$, normalized by frame.
- **max speed**: Maximum speed of either fly involved in the chase.
- **dist btn**: Distance between the head of the chasing fly and any point on the boundary ellipse of the chased fly
- **speed apt** Magnitude of the difference vector between the velocity vectors of each fly from frames $t-1$ to t, normalized by frame rate.
- **angle btn** Absolute difference between angle from chasing fly to chased fly and chasing fly's orientation.
- θ **diff** Absolute difference between flies' orientations.
- ϕ **diff** Absolute difference between flies' velocity directions.
- **ang btn**: Minimum absolute angle between touching fly's orientation and direction to any point on other fly.

For each behavior, each trajectory was segmented into intervals in which the fly was and was not performing the behavior by maximizing the sum-squared lengths of the positive sequences using a globally optimal, dynamic programming algorithm. Note that this one-versus-all set of behavior detectors resulted in some frames of the trajectory not being labeled at all (our behavior vocabulary is incomplete), and that a fly may have been engaged in multiple behaviors at the same time (for example, chasing and walking).

Our software allowed us to define behavior detectors in two ways. The quickest way was direct manual selection of the ranges of property values defining a behavior. We found this approach intuitive and easy for a couple of behaviors ('back up' and 'touch'). In all other cases we used example-based training to learn the ranges. Using the latter approach, a user manually segments sample trajectories to create training data. The parameter ranges were then computed automatically so that the detected segmentations agree with the manual segmentations. In both cases, no new computer code was required. In both cases, other scientists may inspect the parameter ranges defining specific behaviors and thus reproduce exactly a given experiment.

Below, we describe how we chose the quantitative definitions of the behaviors analyzed in the Results section. We also provide a table with the properties and precise thresholds we used (Table A.3). Additionally, we provide code for automatically detecting these behaviors online (`http://dickinson.caltech.edu/ctrax`).

Six of our behaviors (walk, stop, sharp turn, crabwalk, backup, and jump) involved basic locomotor actions. The majority of the time, the flies either walked at

a relatively constant velocity or stopped in place. The next-most common behavior was 'sharp turn,' in which a fly makes a large and rapid change in orientation. Sharp turns usually occurred in response to the arena wall or another fly. Most commonly, the fly pivoted around its hind end, though occasionally it pivoted around its center or front end. These front-end pivots primarily occurred during 'encounters' with another fly (see below). Other locomotor classifications included 'crabwalks,' in which the fly walked with a substantial sideways component, and 'backups,' in which the flies' translational velocity was negative. Both crabwalks and backups were often exhibited as a result of encounters with other flies. Jumps consisted of rapid translations within the arena, often as a consequence of encounters with other flies. Our two remaining behaviors (touch and chase) related to social interactions between flies. A touch occurred when the head of one fly came in contact with another fly. Chases were cases in which one fly (always a male) followed another across the arena.

For 6/8 behaviors (walking, stopping, making sharp turns, jumping, crabwalking, and chasing), it was time-consuming and non-intuitive to manually examine the parameter space for the precise set of parameters that best fit our intuition about the behavior definitions. Thus, we chose the parameters by manually labeling a number of trajectories. These labeled trajectories were the training examples used to learn the parameter intervals. The advantage of this learning-based approach is that to obtain an automatic behavior classifier a behavior expert can simply specify segmented training trajectories for a behavior of interest. He/she does not need to write any code. We chose the structure of our classifier so that the training examples were

converted into 'characteristic' parameter ranges for each behavior. We thus ended up with a clear and concise definition of each behavior that is open to inspection and criticism and makes experiments easily reproducible.

Given the segmented example trajectories, we then manually chose which properties the classifier would depend on, and whether it would be bounded from above, below, or both for each of the four rules enumerated above. We used a genetic algorithm (de Boer et al., 2005) to find the ranges that produced segmentations closest to the labeled trajectories. Our cost function for comparing a proposed segmentation and the groundtruth segmentation was

$$cost = (\#\text{ spurious detections}) + (\#\text{ missed detections}). + 0.2(\#\text{ mislabeled frames})$$

Spurious detections were detected sequences that do not match any labeled sequence, and missed detections were labeled sequences that do not match any detected sequence. We said that two segments matched if the proposed segmentation could be made identical to the groundtruth by relabeling at most 5 frames = .25 seconds at the beginning, end, or middle. We made the definition of matching tolerant to small errors because the exact frame a behavior began on was subject to interpretation. The exact details of the scoring function are shown in Algorithm 1.

To find the behavior definition parameters that minimize the cost criterion described above, we used the cross-entropy method (de Boer et al., 2005). The cross-entropy method was initialized with hyperparameters that described the prior dis-

Algorithm 1 Score an automatically detected behavior labeling $x_{1:T}$ against the groundtruth $y_{1:T}$.

Input: Proposed labeling $x_{1:T}$ and groundtruth labeling $y_{1:T}$.
Output: Measure of the number of errors in the labeling *cost*.

```
cost ← 0
for t1, t2: y_{t1:t2} ≠ x_{t1:t2}, x_{t1−1} = y_{t1−1}, x_{t2+1} = y_{t2+1} do
  length ← t2 − t1 + 1
  if length > 5 then
    cost ← cost + 1
  end if
  cost ← cost + length/5
end for
```

tribution on the parameters[20]. It then generated a set of N joint samples of all parameters[21] according to this prior. The cost criterion was evaluated for each sample. The M 'elite' samples with the highest scores were chosen[22]. The hyperparameters defining the prior were reset to those which maximize the likelihood of these elite samples. These steps were iterated until there was no decrease in the highest cost elite sample over a span of d iterations[23].

We observed holistically that the segmentations produced by the learned classifiers match our intuitive definitions of the behaviors. In Supplementary Movie 4.7, we show examples of behaviors that were labeled manually, and of behaviors that were detected automatically.

[20]For all parameters, we assumed independent Gaussian prior distributions. To set the initial mean and variances of these prior distributions, for each positive training sequence, the system computed the most aggressive parameter values that would result in the sequence being classified as positive. The prior distribution mean was initialized to the average of the largest and smallest aggressive parameter values over all training examples. The prior standard deviation was initialized to one quarter of the difference between the largest and smallest aggressive parameter values.

[21]We set $N = 100$ samples

[22]We set $M = .25N = 25$

[23]We use $d = 5$

References

Al-Anzi B, Tracey WD Jr, Benzer S (2006) Response of *Drosophila* to wasabi is mediated by painless, the fly homolog of mammalian TRPA1/ANKTM1. Current Biology 16:1034–40.

Armstrong JD, Texada MJ, Munjaal R, Baker DA, Beckingham KM (2006) Gravitaxis in *Drosophila melanogaster*: A forward genetic screen. Genes, Brain and Behavior 5:222–239.

Baker DA, Beckingham KM, Armstrong JD (2007) Functional dissection of the neural substrates for gravitaxic maze behavior in *Drosophila melanogaster*. Journal of Comparative Neurology 501:756–64.

Beckingham KM, Texada MJ, Baker DA, Munjaal R, Armstrong JD (2005) Genetics of graviperception in animals. Advances in Genetics 55:105–145.

Bell WJ (1985) Sources of information controlling motor patterns in arthopod local search orientation. Journal of Insect Physiology 31:837–847.

Bell WJ (1991) Searching Behaviour: The Behavioural Ecology of Finding Resources. Chapman and Hall, New York.

Bender J, Frye M (2009) Invertebrate solutions for sensing gravity. Current Biology 19:R186–R190.

Benzer S (1967) Behavioral mutants of *Drosophila* isolated by countercurrent distribution. Proceedings of the National Academy of Sciences 58:1112–1119.

Borst A (2009) *Drosophila*'s view on insect vision. Current Biology 19:R36–R47.

Borst A, Haag J (2007) Optic flow processing in the cockpit of the fly. In G North, RJ Greenspan, eds., Invertebrate Neurobiology, 101–122. Cold Spring Harbor Laboratory Press, Cold Spring Harbor, NY.

Branson K, Belongie S (2005) Tracking multiple mouse contours (without too many samples). Proceedings of the IEEE Conference on Computer Vision and Pattern Recognition 1:1039–1046.

Branson K, Robie AA, Bender J, Perona P, Dickinson MH (2009) High-throughput ethomics in large groups of *Drosophila*. Nature Methods 6:451–457.

Budick SA, Reiser MB, Dickinson MH (2007) The role of visual and mechanosensory cues in structuring forward flight in *Drosophila melanogaster*. Journal of Experimental Biology 210:4092–4103.

Bulthoff H, Götz KG, Herre M (1982) Recurrent inversion of visual orientation in the walking fly, *Drosophila melanogaster*. Journal of Comparative Physiology 148:471–481.

Burkhardt D, Gewecke M (1965) Mechanoreception in Arthropoda: The chain from stimulus to behavioral pattern. Cold Spring Harbor Symposia on Quantative Biology 30:601–14.

Card G, Dickinson M (2008) Performance trade-offs in the flight initiation of *Drosophila*. Journal of Experimental Biology 211:341–53.

Carpenter F (1905) The reactions of the pomace fly, *Drosophila ampelophila* Loew, to light, gravity and mechanical stimulation. American Naturalist 39:157–171.

Cook R (1980) The extent of visual control in the courtship tracking of *D. melanogaster*. Biological Cybernetics 37:41–51.

Cormen T (2001) Introduction to Algorithms. MIT Press, Cambridge, Mass.

Coyne JA, Boussy I, Prout T (1982) Long-distance migration of *Drosophila*. American Naturalist 119:589–595.

Crocker J, Grier D (1996) Methods of digital video microscopy for colloidal studies. Journal of Colloid And Interface Science 179:298–310.

Dankert H, Wang L, Hoopfer E, Anderson D, Perona P (2009) Automated monitoring and analysis of social behavior in *Drosophila*. Nature Methods 6:297–303.

de Boer P, Kroese D, Mannor S, Rubinstein R (2005) A tutorial on the cross-entropy method. Annals of Operations Research 134:19–67.

Duistermars BJ, Chow DM, Frye MA (2009) Flies require bilateral sensory input to track odor gradients in flight. Current Biology 19:1301–1307.

Dusenbery D (1992) Sensory Ecology: How Organisms Acquire and Respond to Information. W. H. Freeman and Company, New York.

Eberl DF, Boekhoff-Falk G (2007) Development of Johnston's organ in *Drosophila*. International Journal of Developmental Biology 51:679–687.

Eberl DF, Hardy RW, Kernan MJ (2000) Genetically similar transduction mechanisms for touch and hearing in *Drosophila*. Journal of Neuroscience 20:5981–5988.

Ewing AW (1978) Antenna of *Drosophila* as a 'love song' receptor. Physiological Entomology 3:33–36.

Fraenkel GS, Gunn DL (1961) The Orientation of Animals: Kineses, Taxes and Compass Reactions. Dover Publications, Inc., New York.

Gong Z, Son W, Chung YD, Kim J, Shin DW, McClung CA, Lee Y, Lee HW, Chang DJ, Kaang BK, Cho H, Oh U, Hirsh J, Kernan MJ, Kim C (2004) Two interdependent TRPV channel subunits, inactive and Nanchung, mediate hearing in *Drosophila*. Journal of Neuroscience 24:9059–9066.

Gonzalez R, Woods R (2007) Digital Image Processing. Prentice Hall.

Göpfert MC, Robert D (2002) The mechanical basis of *Drosophila* audition. Journal of Experimental Biology 205:1199–1208.

Götz K (1968) Flight control in *Drosophila* by visual perception of motion. Biological Cybernetics 4:199–208.

Götz KG (1975) Optomotor equilibrium of *Drosophila* navigation system. Journal of Comparative Physiology 99:187–210.

Götz KG (1980) Visual Guidance in *Drosophila*. In Q Siddiqi, P Babu, L Hall, J Hall, eds., Development and Neurobiology of Drosophila, Basic Life Science, 391–407. Plenum Press, New York.

Götz KG (1987) Course-control, metabolism and wing interference during ultralong tethered flight in *Drosophila melanogaster*. Journal of Experimental Biology 128:35–46.

Götz KG (1989) Search and Choice in *Drosophila*. In RN Singh, NJ Strausfeld, eds., Neurobiology of Sensory Systems, 139–153. Plenum Publishing Corporation, New York.

Götz KG (1994) Exploratory strategies in *Drosophila*. In K Schildberger, N Elsner, eds., Neural Basis of Behavioral Adaptations, 47–59. G. Fischer, Stuttgart, Germany.

Götz KG, Biesinger R (1985a) Centrophobism in *Drosophila melanogaster*. 1. Behavioral-modification induced by ether. Journal of Comparative Physiology A, Sensory, Neural, and Behavioral Physiology 156:319–327.

Götz KG, Biesinger R (1985b) Centrophobism in *Drosophila melanogaster*. 2. Physiological approach to search and search control. Journal of Comparative Physiology A, Sensory, Neural, and Behavioral Physiology 156:329–337.

Götz KG, Wenking H (1973) Visual control of locomotion in walking fruitfly *Drosophila*. Journal of Comparative Physiology 85:235–266.

Greenspan RJ (2008) The origins of behavioral genetics. Current Biology 18:R192–198.

Grover D, Tower J, Tavaré S (2008) O fly, where art thou? Journal of the Royal Society Interface 5:1181–1191.

Hall J (1978) Courtship among males due to a male-sterile mutation in *Drosophila melanogaster*. Behavior Genetics 8:125–141.

Hastie T, Tibshirani R, Friedman J (2001) The Elements of Statistical Learning. Springer Series in Statistics. Springer, New York.

Hirsch J (1959) Studies in experimental behavior genetics. II. Individual differences in geotaxis as a function of chromosome variations in synthesized *Drosophila* populations. Journal of Comparative Physiology 52:304–8.

Hirsch J, Eerlenmeyer-Kimling L (1962) Studies in experimental behavior genetics: IV. Chromosome analyses for geotaxis. Journal of Comparative & Physiologcial Psychology 55:732–739.

Hirsch J, Ksander G (1969) Studies in experimental behavior genetics. V. Negative geotaxis and further chromosome analyses in *Drosophila melanogaster*. Journal of Comparative & Physiologcial Psychology 67:118–122.

Holmes T, Sheeba V, Mizrak D, Rubovsky B, Dahdal D (2007) Circuit-breaking and behavioral analysis by molecular genetic manipulation of neural activity in *Drosophila*. In Invertebrate Neurobiology, 19–52. Cold Spring Harbor Laboratory Press.

Homberg U (1989) Structure and functions of the central complex in insects. In AP Gupta, ed., Arthropod Brain: Its Development, Structure and Functions, 347–367. Wiley, New York.

Horn E (1978) The mechanism of object fixation and its relation to spontaneous pattern preferences in *Drosophila melanogaster*. Biological Cybernetics 31:145–158.

Horn E, Kessler W (1975) The control of antennae lift movements and its importance on gravity reception in walking blowfly, *Calliphora erythrocephla*. Journal of Comparative Physiology 97:189–203.

Horn E, Wehher R (1975) Mechanism of visual-pattern fixation in walking fly, *Drosophila melanogaster*. Journal of Comparative Physiology 101:39–56.

Hoyer S, Eckart A, Herrel A, Zars T, Fischer S, Hardie S, Heisenberg M (2008) Octopamine in male aggression of *Drosophila*. Current Biology 18:159–167.

Inagaki HK, Kamikouchi A, Ito K (2010) Methods for quantifying simple gravity sensing in *Drosophila melanogaster*. Nature Protocols 5:20–25.

Kalmus H (1964) Animals as mathematicans. Nature 202:1156–1160.

Kamikouchi A, Inagaki HK, Effertz T, Hendrich O, Fiala A, Göpfert MC, Ito K (2009) The neural basis of *Drosophila* gravity-sensing and hearing. Nature 458:165–171.

Kamikouchi A, Shimada T, Ito K (2006) Comprehensive classification of the auditory sensory projections in the brain of the fruit fly *Drosophila melanogaster*. The Journal of Comparative Neurology 499:317–356.

Katsov AY, Clandinin TR (2008) Motion processing streams in *Drosophila* are behaviorally specialized. Neuron 59:322–335.

Khan Z, Balch T, Dellaert F (2005) MCMC-based particle filtering for tracking a variable number of interacting targets. IEEE Transactions on Pattern Analysis and Machine Intelligence 27:1805–1819.

Kim J, Chung YD, Park DY, Choi S, Shin DW, Soh H, Lee HW, Son W, Yim J, Park CS, Kernan MJ, Kim C (2003) A TRPV family ion channel required for hearing in *Drosophila*. Nature 424:81–84.

Kimme C, Ballard D, Sklansky J (1975) Finding circles by an array of accumulators. Communications of the Association for Computing Machinery 18:120–122.

Konooka R, Benzer S (1971) Clock mutants of *Drosophila melanogaster*. Proceedings of the National Academy of Sciences 9:2112–2116.

Krapp HG (2010) Sensorimotor transformation: From visual responses to motor commands. Current Biology 20:R236–R239.

Maimon G, Straw AD, Dickinson MH (2010) Active flight increases the gain of visual motion processing in *Drosophila*. Nature Neuroscience 13:393–399.

Mamiya A, Beshel J, Xu C, Zhong Y (2008) Neural representations of airflow in *Drosophila* mushroom body. PLoS One 3:e4063. doi:10.1371/journal.pone.0004063.

Manning A (1967) Antennae and sexual receptivity in *Drosophila* melanogaster females. Science 158:136–137.

Martin JR (2004) A portrait of locomotor behaviour in *Drosophila* determined by a video-tracking paradigm. Behavioural Processes 67:207–219.

Martin JR, Raabe T, Heisenberg M (1999) Central complex substructures are required for the maintenance of locomotor activity in *Drosophila melanogaster*. Journal of Comparative Physiology A, Sensory, Neural, and Behavioral Physiology 185:277–288.

Nation JL (2008) Insect Physiology and Biochemistry. CRC Press, Boca Raton, Fl.

Neuser K, Triphan T, Mronz M, Poeck B, Strauss R (2008) Analysis of a spatial orientation memory in *Drosophila*. Nature 453:1244–1248.

Otsuna H, Ito K (2006) Systematic analysis of the visual projection neurons of *Drosophila melanogaster*. I. Lobula-specific pathways. Journal of Comparative Neurology 497:928–958.

Papadimitriou C, Steiglitz K (1998) Combinatorial Optimization: Algorithms and Complexity. Dover Publications, Mineola, New York.

Parsons MM, Krapp HG, Laughlin SB (2010) Sensor fusion in identified visual interneurons. Current Biology 20:624–8.

Perera A, Srinivas C, Hoogs A, Brooksby G (2006) Multi-object tracking through simultaneous long occlusions and split-merge conditions. Proceedings of the IEEE Conference on Computer Vision and Pattern Recognition 1:666–673.

Piccardi M (2004) Background subtraction techniques: A review. Proceedings of the IEEE International Conference on Systems, Man, and Cybernetics 4:3099–3104.

Pick S, Strauss R (2005) Goal-driven behavioral adaptations in gap-climbing *Drosophila*. Current Biology 15:1473–1478.

Pringle JWS (1938) Proprioception in insects: III. The function of the hair sensilla at the joints. Journal of Experimental Biology 15:467–473.

Ramazani R, Krishnan H, Bergeson S, Atkinson N (2007) Computer automated movement detection for the analysis of behavior. Journal of Neuroscience Methods 162:171–179.

Ramot D, Johnson B, Berry Jr T, Carnell L, Goodman M (2008) The parallel worm tracker: A platform for measuring average speed and drug-induced paralysis in nematodes. PLoS ONE 3:e2208. doi:10.1371/journal.pone.0002208.

Reichardt W, Poggio T (1975) Theory of pattern induced flight orientation of fly *Musca domestica*. 2. Biological Cybernetics 18:69–80.

Reiser M, Dickinson M (2008) A modular display system for insect behavioral neuroscience. Neuroscience Methods 167:127–139.

Reynolds AM, Frye MA (2007) Free-flight odor tracking in *Drosophila* is consistent with an optimal intermittent scale-free search. PLoS One 2:e354. doi:10.1371/journal.pone.0000354.

Ridgel AL, Ritzmann RE (2005) Effects of neck and circumoesophageal connective lesions on posture and locomotion in the cockroach. Journal of Comparative Physiology A: Neuroethology, Sensory, Neural, and Behavioral Physiology 191:559–573.

Ritchie MG (2008) Behavioural genetics: The social fly. Current Biology 18:R862–R864.

Ritzmann R, Büschges A (2007) Insect Walking: From reduced preparations to natural terrain. In G North, RJ Greenspan, eds., Invertebrate Neurobiology, 229–250. Cold Spring Harbor Laboratory Press.

Ryu W, Samuel A (2002) Thermotaxis in *Caenorhabditis elegans* analyzed by measuring responses to defined thermal stimuli. Journal of Neuroscience 22:5727–5733.

Sanes JR, Zipursky SL (2010) Design principles of insect and vertebrate visual systems. Neuron 66:15–36.

Schaeffer (1928) Spiral movement in man. Journal of Morphology 45:293–398.

Schneider D (1964) Insect antennae. Annual Review of Entomology 9:103–122.

Schuppe HC, Hengstenberg R (1993) Optical-properties of the ocelli in *Calliphora erythocephala* and their role in the dorsal light response. Journal of Comparative Physiology A, Sensory, Neural, and Behavioral Physiology 173:143–149.

Schuster S, Strauss R, Götz KG (2002) Virtual-reality techniques resolve the visual cues used by fruit flies to evaluate object distances. Current Biology 12:1591–1594.

Shafer O, Levine J, Truman J, Hall J (2004) Flies by night: Effects of changing day length on *Drosophila*'s circadian clock. Current Biology 14:424–432.

Sherman A, Dickinson MH (2003) A comparison of visual and haltere-mediated equilibrium reflexes in the fruit fly *Drosophila melanogaster*. Journal of Experimental Biology 206:295–302.

Siegel R, Hall J (1979) Conditioned responses in courtship behavior of normal and mutant *Drosophila*. Proceedings of the National Academy of Sciences 76:3430–3434.

Simon JC, Dickinson MH (2010) A new chamber for studying the behavior of *Drosophila*. PLoS ONE 5:e8793. doi:10.1371/journal.pone.0008793.

Simpson JH (2009) Mapping and manipulating neural circuits in the fly brain. Advances in Genetics 65:79–143.

Sokol RR, Rohlf FJ (1995) Biometry. Freeman, New York.

Soll D, Voss E (1997) Two- and three-dimensional computer systems for analyzing how animal cells crawl. In D Soll, E Voss, eds., Motion analysis of living cells, 25–52. Wiley-Liss, New York.

Srinivasan MV, Zhang S, Altwein M, Tautz J (2000) Honeybee navigation: Nature and calibration of the "odometer". Science 287:851–853.

Strausfeld NJ, Okamura JY (2007) Visual system of calliphorid flies: Organization of optic glomeruli and their lobula complex efferents. The Journal of Comparative Neurology 500:166–188.

Strauss R (2002) The central complex and the genetic dissection of locomotor behaviour. Current Opinion in Neurobiology 12:633–638.

Strauss R, Heisenberg M (1991) Altered patterns of walking in *Drosophila* central complex mutants central-body-defect. Journal of Neurogenetics 7:147–147.

Strauss R, Heisenberg M (1993) A higher control center of locomotor behavior in the *Drosophila* brain. Journal of Neuroscience 13:1852–1861.

Strauss R, Pichler J (1998) Persistence of orientation toward a temporarily invisible landmark in *Drosophila melanogaster*. Journal of Comparative Physiology A, Sensory, Neural, and Behavioral Physiology 182:411–23.

Strauss R, Schuster S, Götz KG (1997) Processing of artificial visual feedback in the walking fruit fly *Drosophila melanogaster*. Journal of Experimental Biology 200:1281–1296.

Straw AD, Dickinson MH (2009) Motmot, an open-source toolkit for realtime video acquisition and analysis. Source Code for Biology and Medicine 4. doi: 10.1186/1751-0473-4-5.

Sun Y, Liu L, Ben-Shahar Y, Jacobs JS, Eberl DF, Welsh MJ (2009) *TRPA* channels distinguish gravity sensing from hearing in Johnston's organ. Proceedings of the National Academy of Sciences 106:13606–13611.

Taylor G, Krapp HG (2008) Sensory systems and flight stability: What do insects measure and why? Advances in Insect Physiology 34:231–316.

Todi SV, Sharma Y, Eberl DF (2004) Anatomical and molecular design of the *Drosophila* antenna as a flagellar auditory organ. Microscopy Research and Technique 63:388–99.

Tompkins L, Gross AC, Hall JC, Gailey DA, Siegel RW (1982) The role of female movement in the sexual behavior of *Drosophila melanogaster*. Behavior Genetics 12:295–307.

Tsunozaki M, Chalasani S, Bargmann C (2008) A behavioral switch: cGMP and PKC signaling in olfactory neurons reverses odor preference in *C. elegans*. Neuron 59:959–971.

Valente D, Golani I, Mitra P (2007) Analysis of the trajectory of *Drosophila melanogaster* in a circular open field arena. PLoS ONE 2:e1083. doi:10.1371/journal.pone.0001083.

Veeraraghavan A, Chellappa R, Srinivasan M (2008) Shape-and-behavior-encoded tracking of bee dances. IEEE Transactions on Pattern Analysis and Machine Intelligence 30:463–476.

Venkatachalam K, Montell C (2007) TRP channels. Annual Review of Biochemistry 76:387–417.

Walker RG, Willingham AT, Zuker CS (2000) A *Drosophila* mechanosensory transduction channel. Science 287:2229–2234.

Wallace GK (1959) Visual scanning in the desert locust *Schistocerca gregaria* Forskål. Journal of Experimental Biology 36:512–525.

Wehner R (1981) Spatial vision in arthropods. In H Autrum, R Jung, WR Loewenstein, DM Mackay, HL Teuber, eds., Handbook of Sensory Physiology, volume 7/6C, 287–616. Springer Verlag, New York.

Wilson RI, Turner GC, Laurent G (2004) Transformation of olfactory representations in the *Drosophila* antennal lobe. Science 303:366–70.

Wittlinger M, Wehher R, Wolf H (2006) The ant odometer: Stepping on stilts and stumps. Science 312:1965–1967.

Wolf F, Rodan A, Tsai L, Heberlein U (2002) High-resolution analysis of ethanol-induced locomotor stimulation in *Drosophila*. Journal of Neuroscience 22:11035–11044.

Yorozu S, Wong A, Fischer BJ, Dankert H, Kernan MJ, Kamikouchi A, Ito K, Anderson DJ (2009) Distinct sensory representations of wind and near-field sound in the *Drosophila* brain. Nature 458:201–5.

Young JM, Armstrong JD (2010) Structure of the adult central complex in *Drosophila*: organization of distinct neuronal subsets. Journal of Comparative Neurology 518:1500–1524.

Zhang F, Aravanis A, Adamantidis A, de Lecea L, Deisseroth K, et al. (2007) Circuit-breakers: Optical technologies for probing neural signals and systems. Nature Reviews Neuroscience 8:577–581.

Zhu Y, Nern A, Zipursky SL, Frye MA (2009) Peripheral visual circuits functionally segregate motion and phototaxis behaviors in the fly. Current Biology 19:613–619.